CBPF - CENTRO BRASILEIRO DE PESQUISAS FÍSICAS

Aspects of Field Theory:
Monopoles, Vortices, and all that

Philipe de Fabritiis

Supervisor: José Abdalla Helayël-Neto

RIO DE JANEIRO
2023

CBPF
Centro Brasileiro de Pesquisas Físicas
SUBORDINADA AO MCTI

MINISTÉRIO DA CIÊNCIA, TECNOLOGIA E INOVAÇÕES

"ASPECTS OF FIELD THEORY: MONOPOLES, VORTICES, AND ALL THAT"

PHILIPE OSÓRIO DE FABRITIIS

Tese de Doutorado em Física apresentada no Centro Brasileiro de Pesquisas Físicas do Ministério da Ciência Tecnologia e Inovação. Fazendo parte da banca examinadora os seguintes professores:

José Abdalla Helayël-Neto - Orientador/CBPF

Patrício Alfredo Gaete Durán - CCTVaL (CHILE)

Mário Jr. de Oliveira Neves - UFRRJ

Sebastião Alves Dias - CBPF

Sérgio Barbosa Duarte - CBPF

Rio de Janeiro, 18 de janeiro de 2023.

Abstract

In the first part of this thesis, we present a finite-energy electroweak monopole solution obtained by considering non-linear extensions in the electroweak sector. We find constraints for a class of non-linear extensions and work out an estimate for the monopole mass. We also derive a lower bound for the monopole energy and discuss the case of a Dirac monopole. Furthermore, we study the phenomenological consequences of this non-linear extension through high-energy processes. Using experimental data, we investigate viable lower bounds on the non-linear parameter. We also discuss gauge-boson scatterings, contextualizing our findings with recent results on anomalous gauge couplings.

In the second part of this thesis, we propose a parity-invariant Maxwell-Chern-Simons $U(1)\times U(1)$ model coupled with scalar matter. We describe its main properties, and show that it admits finite-energy topological vortices, exhibiting explicit numerical solutions and analyzing them. Moreover, we present a self-dual version of our model. We discuss in detail its main features, and exhibit explicit finite-energy topological vortices and non-topological solitons. The mixed Chern-Simons term plays an important role here, ensuring the main properties of the model and suggesting possible applications in condensed matter.

Key Words: Field Theory, Gauge Theories, Solitons in Field Theory, Magnetic Monopoles, Non-linear Electrodynamics, Abelian Vortices, Chern-Simons theories.

Resumo

Na primeira parte dessa tese, apresentamos uma solução de monopólo eletrofraco com energia finita, obtida considerando extensões não-lineares do setor eletrofraco. Obtemos vínculos para uma classe de extensões não-lineares e fazemos uma estimativa para a massa do monopólo. Derivamos também um limite inferior para a energia do monopólo e discutimos o caso mais simples de um monopólo de Dirac. Em seguida, estudamos as consequências fenomenológicas dessa extensão não-linear, através de processos em altas energias. Usando dados experimentais, investigamos possíveis limites inferiores para o parâmetro não-linear. Discutimos também espalhamentos de bósons de gauge, contextualizando nossos resultados com resultados recentes em acoplamentos anômalos de gauge.

Na segunda parte dessa tese, apresentamos um modelo de Maxwell-Chern-Simons $U(1) \times U(1)$ invariante por paridade acoplado com matéria escalar. Descrevemos suas principais propriedades e mostramos que ele admite vórtices topológicos com energia finita, exibindo soluções numéricas explícitas e analisando-as. Na sequência, apresentamos uma versão auto-dual do nosso modelo. Discutimos em detalhe suas principais características e exibimos vórtices topológicos e sólitons não-topológicos com energia finita. O termo de Chern-Simons misto tem um papel fundamental aqui, garantindo as principais propriedades do modelo e sugerindo possíveis aplicações em matéria condensada.

Palavras-Chave: Teoria de Campos, Teorias de Calibre, Sólitons em Teoria de Campos, Monopólos Magnéticos, Eletrodinâmica Não-Linear, Vórtices Abelianos, Teoria de Chern-Simons.

Acknowledgements

Scientific research is somehow an endless search for the truth. In Physics, the goal is to understand Nature in its most intimate details. Scientists must be independent, creative, and hard-working to carry out their research in a satisfactory level, but they can certainly count on more experienced scientists to point them in the right direction.

In this sense, I would like to thank my supervisor, Prof. Helayël, for being like a father to me. He taught me how to be a Scientist and is an outstanding example of Researcher, Professor, and Human being. For those who say that he's the Jesus of Physics, I say with pleasure that I'm one of his Apostles, and I'll preach his word wherever I am. Prof. Tião also had a very important role in my scientific education and is like that cool uncle: helps me whenever I need it, and always brings me joy. Thank you very much for everything.

In the same vein, I would like to thank all my collaborators: Wellisson de Lima, Pedro Malta, Mário Neves, Gustavo de Brito and Antônio Duarte. These guys are much more than co-workers, they are my personal friends and helped me a countless number of times.

Its a great pleasure to live in *Diracstão*, and I thank all its inhabitants for their company in this journey (Gustavo, Pedro, Yuri, Judismar, Fábio, André + Wellisson, Matheus, João Paulo, Bernard, Henrique). From the old generation, I especially thank Guga for being always present in my life and also Pedruxo for his support. From the new generation, I especially thank Well, we found a very nice equilibrium together.

I thank all the people from CBPF: cleaning staff, security guards, secretaries, etc. Especially Bete and Ricardo for the patience and help with important burocratic stuff. I decided to anticipate my Ph.D. thesis for January during the week between Christmas and New Year, thus I thank COEDU for allowing me to schedule in such a short time.

Finally, I would like to thank all scientists, professors, and students, who in their daily struggle contribute to the advance of knowledge and therefore of humanity as a whole.

The author thanks the Brazilian scientific support agencies, Fundação Carlos Chagas Filho de Amparo à Pesquisa do Estado do Rio de Janeiro (FAPERJ) and Conselho Nacional de Desenvolvimento Científico e Tecnológico (CNPq), for financial support.

About this Ph.D. thesis

The content of this Ph.D. thesis is organized in two parts, based on two different projects developed during my Ph.D.. Project A is about extensions of the electroweak sector of the Standard Model. We mainly investigated the possibility of a finite-energy magnetic monopole in the electroweak sector and the effects of a non-linear extension of this sector. This project was done in collaboration with my supervisor, José Helayël, and with a collaborator, Pedro Malta. The publications associated with this project are [1] and [2]. Project B is about vortices in Maxwell-Chern-Simons theories. The main line of investigation was related with the possibility of charged vortices in a parity-invariant version of these models. This project was done in collaboration with Wellisson De Lima, another Ph.D. student of our group. The publications associated with this project are [4] and [5]. Besides these works, I also published a paper on Lorentz symmetry violation with the external collaborators Pedro Malta and Mario Neves [3].

The projects covered in this thesis are still on progress. On the Project B, we are developing the supersymmetric extension of our parity-invariant Maxwell-Chern-Simons model. In fact, our self-dual model can be seen as the bosonic part of a $\mathcal{N} = 2$ supersymmetric model, thus providing a natural origin for the self-dual potential that we adopted. This is work in progress and I believe that we will be able to publish our results soon. On the Project A, we plan to perform a non-linear extension encompassing the entire electroweak gauge group, analyzing the possibility of a monopole solution in this scenario, as well as the phenomenological consequences of this extension in high-energy processes.

Finally, there is a very interesting work in progress about matter in the Refined Gribov-Zwanziger framework, in collaboration with Antônio Duarte and Gustavo de Brito [6].

1. P. De Fabritiis, J.A. Helayël-Neto, *Electroweak monopoles with a non-linearly realized weak hypercharge*, Eur. Phys. J. C **81**, 788 (2021).

2. P. De Fabritiis, P.C. Malta, and J.A. Helayël-Neto, *Phenomenology of a Born-Infeld extension of the $U(1)_Y$ sector at lepton colliders*, Phys. Rev. D **105**, 016007 (2022)

3. P. De Fabritiis, P.C. Malta, and M.J. Neves, *Lorentz-symmetry violation in the electroweak sector: Scattering processes in future e^+e^- colliders*, Nucl. Phys. B **974**, 115628 (2022).

4. W.B. De Lima and P. De Fabritiis, *Self-dual Maxwell-Chern-Simons solitons in a parity-invariant scenario*, Phys. Lett. B **833**, 137326 (2022).

5. W.B. De Lima and P. De Fabritiis, *Vortices in a parity-invariant Maxwell-Chern-Simons model*, arXiv: 2205.10427 [hep-th]. Submitted for publication.

6. G.P. de Brito, P. De Fabritiis and A.D. Pereira, *Refined Gribov-Zwanziger theory coupled to scalar fields in the Landau gauge*. To be submitted soon.

Contents

I Magnetic monopoles and non-linear extensions in the electroweak sector **1**

1 Introduction **2**

2 Electroweak monopoles **6**

2.1 The original electroweak monopole solution 6

2.2 A finite-energy monopole solution 12

2.3 Non-linear extensions of $U(1)_Y$ 15

2.4 Lower bounds for the monopole energy 18

2.5 A non-linear Dirac monopole 20

3 Phenomenology of the non-linear extension **22**

3.1 Theoretical setup 22

3.2 Experimental limits 26

3.2.1 $Z \to 3\,\gamma$ 26

3.2.2 $e^-\,e^+ \to 3\,\gamma$ 30

3.2.3 Pure gauge-boson scatterings 39

4 Concluding remarks **47**

II Abelian vortices in parity-invariant Maxwell-Chern-Simons models **49**

5 Introduction **50**

6 Vortices in a parity-invariant scenario **53**

6.1 Theoretical setup 53

6.2 Topological configurations 57

6.2.1 Asymptotic conditions 58

6.2.2 The vortex *ansatz* 59

6.3 Explicit vortex solutions 63

6.3.1 m=0, n=1 64
6.3.2 m=n=1 65
6.3.3 m=2, n=1 67
6.3.4 Vortex solutions for different K_i's 69
6.4 Vortices in limiting cases 70

7 A self-dual regime **75**
7.1 Theoretical setup 75
7.2 Self-duality equations 79
7.3 Explicit solutions and discussion 85

8 Concluding remarks **91**

Presentation and General Framework

The Standard Model of Particle Physics (SM) is one of the most successful theories in human history, providing a framework that allows us to describe almost all observed phenomena in Nature in a remarkably simple and precise form. The fundamental interactions of the SM are described by gauge theories, a beautiful class of quantum field theories where the symmetry dictates the form of the interactions. Gauge symmetry naturally plays a key role in the description of the building blocks of Nature, allowing us to perform the drama with the minimum number of actors, while respecting the Poincaré symmetry of Minkowski spacetime, the stage for quantum field theory. This thesis is about two interesting subjects in gauge theories: magnetic monopoles and abelian vortices.

Magnetic monopoles, introduced by Dirac in 1931, have so far shied away from experimental discovery, despite all efforts put into their search in all these years. For a long time, it was believed that the SM did not admit magnetic monopoles due to the topological structure of its gauge group. However, Cho and Maison have shown in 1997 that this is not true, describing a way to accommodate a magnetic monopole in the electroweak sector. A possible way to regularize the monopole energy, achieving a finite and calculable mass that can be reached in particle accelerators, is to perform a non-linear extension in the gauge sector, a subject that has become popular after the measurement of light-by-light scattering in heavy-ion collisions. Nowadays, there is a real chance of detection of magnetic monopoles in experiments like MoEDAL at CERN, after so many years of fruitless searches. Such a discovery could have immeasurable practical implications, and theoretical studies that help in its search and understanding of its properties are an urgent matter. This is the background for the first part of this thesis.

Abelian vortices were first discussed in the context of superconductivity by Abrikosov in 1957, and in high-energy physics by Nielsen and Olesen in 1972. In the Abelian-Higgs model, these vortices have finite energy, are electrically neutral and have a quantized magnetic flux, but in the presence of a Chern-Simons (CS) term, the property of flux attachment relating the electric charge with the magnetic flux allows for the existence of electrically charged vortices with finite energy. Interestingly, these objects can play an important role, for example, in the fractional quantum Hall effect, high-T_c superconductors, and superfluids. The presence of a CS term usually comes with the violation of parity symmetry, but this is not always true, as Hagen showed in 1992. Gauge theories with a CS term have been used in condensed matter physics, and since the role of parity and time-reversal symmetry has been attracting much interest recently, theoretical studies of charged vortices in a parity-invariant scenario could be useful for the description of condensed matter systems. This is the background for the second part of this thesis.

Part I

Magnetic monopoles and non-linear extensions in the electroweak sector

Chapter 1

Introduction

In 1931, Dirac showed [1] that the existence of a magnetic monopole is not only consistent with the laws of Quantum Mechanics, but can provide an explanation for the quantization of electric charge and also render Maxwell equations more symmetric, realizing in an elegant way the duality symmetry. Since the groundbreaking work of Dirac, this fascinating subject has been theoretically explored in different circumstances, but despite the huge efforts to search for them experimentally, they remain undetected.

In Dirac's work, it is not possible to predict what the monopole mass would be, since its classical energy is infinite by virtue of its singularity. Wu and Yang [2] generalized the concept for non-Abelian gauge theories showing that a pure SU(2) Yang-Mills theory also allows a point-like magnetic monopole, but also here the energy is infinite. 't Hooft and Polyakov [3, 4] made a breakthrough discovery, finding a finite-energy monopole solution as a topological soliton in a SO(3) gauge theory with a scalar field in the adjoint representation, the so-called Georgi-Glashow model [5]. Here, for the first time, the monopole appears as a necessary prediction of the model instead of being only a consistent possibility and, remarkably, with a finite calculable mass.

Julia and Zee [6] extended the 't Hooft and Polyakov's solution by introducing a Coulombic part in the *ansatz*, and therefore finding a dyon solution, a particle with both electric and magnetic charges as introduced by Schwinger [7]. Bogomol'nyi [8] and also Prasad and Sommerfield [9] found a special limit, nowadays called BPS limit, such that there is an analytical solution for the monopole (and dyon) and a lower bound for its energy. The monopole solution was constructed in Grand-Unified Theories by Dokos and Tomaras [10], and it's also relevant in the context of Supersymmetry and Dualities [11, 12].

The Electroweak (EW) Theory by Glashow, Salam and Weinberg [13, 14, 15] provides an extremely successful description for the unification of electromagnetic and weak interactions, and after the Higgs discovery in 2012 [16], and all the others experimental tests in which it was successful, we can say that the Standard Model (SM) is in a very good shape. It's a very important question, therefore, to investigate if there exists an electroweak generalization of the 't Hooft-Polyakov monopole solution.

It was generally believed that such a solution would not be possible in the EW theory because the spontaneous symmetry breaking pattern of the EW gauge group $G = SU(2)_L \,\mathrm{x}\, U(1)_Y \rightarrow H = U(1)_{em}$ does not allow a non-trivial second homotopy group, that is, we have $\pi_2(G/H) = 0$. Nevertheless, there is an alternative topological scenario showing that the Standard Model admits an electroweak monopole solution. In fact, it was originally shown by Cho and Maison [17] that, if we interpret the normalized Higgs doublet as a CP^1 field, we find the necessary topology to have a monopole solution since $\pi_2(CP^1) = \pi_2(S^2) = \mathbb{Z}$. It is sometimes said that this topologically stable EW monopole is somehow a non-trivial hybrid between the abelian Dirac monopole and the non-abelian 't Hooft-Polyakov monopole.

In their original work, Cho and Maison [17] present not only the topological scenario for the existence of electroweak monopoles, but also provide an explicit numerical solution for them, by assuming a spherically symmetric *ansatz*. The authors actually proved the existence of a more general electroweak dyon solution in the SM, and it is important to notice that an analytical existence theorem for such a solution can also be established [18]. Unfortunately, this object suffers from a singularity in the origin, which yields an infinite energy at the classical level. A priori, there is nothing wrong with this, because the electron itself has an infinite electrostatic energy in Maxwell's Electrodynamics, though its mass is finite. This does not allow us to predict the mass of the monopole and, if we have a hope to find it experimentally, this becomes a non-trivial issue. Therefore, it is the purpose of this work to find a way to regularize the energy of the monopole solution and, then, infer about its mass.

There are already proposals of SM extensions giving regularized monopole solutions. One of them was proposed by Cho, Kimm, and Yoon [19], basically consisting in modifying the $U(1)_Y$ sector introducing a function depending on the magnitude of Higgs field in the usual hypercharge field strength $-\frac{1}{4}\epsilon\left(|H|/v\right) B_{\mu\nu}B^{\mu\nu}$. It is possible to choose conditions on this ϵ such that we recover the usual SM in the standard electroweak vacuum and such that the energy integral is regularized at the origin, giving a finite-energy dyon solution. Roughly speaking they found a way to give an effective running to the $U(1)_Y$ coupling such that it can compensate the singularity present at the origin an therefore give a finite-energy dyon solution. The simple solution presented by the authors was latter shown by Ellis, Mavromatos and You [20] to be incompatible with the LHC Data from the Higgs decay in two photons, but these authors were able to adjust their solution in a phenomenological consistent way, giving a family of possible solutions.

Following this line, Blaschke and Beneš [21] were able to find a lower bound for the EW monopole mass by constructing a family of effective theories that have a BPS limit, in a way that the monopole mass can be found analytically and determined by the asymptotic behavior of the fields. Recently, Cho, Zhang and Zou [22] shown that is possible to regularize the energy by electric charge renormalization, founding a new BPS bound.

Another interesting solution was proposed by Arunasalam and Kobakhidze [23], where they considered an extension of the usual $U(1)_Y$ kinetic term to a non-linear Born-Infeld (BI) [24] Lagrangian. With this extension in the same way that the electron energy is regularized in the original BI Electrodynamics, the monopole energy here gets also regularized and its mass turns out to be proportional to the BI mass parameter β, that somehow controls the $U(1)_Y$ field non-linearity and can be constrained considering light-by-light scattering as was shown by Ellis, Mavromatos and You [25]. The authors in [23] showed that a finite-energy monopole solution exists with this non-linear BI extension, and considered some consequences for the EW phase transition. Other interesting recent works are [26, 27, 28]. Therefore, the non-linear extension of the hypercharge sector can lead to a finite-energy electroweak monopole solution. This gives us a good motivation for considering non-linear models, because nowadays there is hope to finally find a monopole in dedicated experiments, such as MoEDAL at CERN [29, 30]. Furthermore, it is imperative to understand the phenomenological implications of such an extension.

The subject of non-linear extensions of Electrodynamics is a very rich research topic. The idea of non-linear electromagnetic responses of the vacuum was first suggested by Halpern [31] and one year later by Heisenberg [32], where he proposed that virtual electron-positron pairs could be at the origin of photon-photon collisions. Soon thereafter, actions with non-linear electrodynamics were introduced by Born and Infeld [24] and also Euler and Heisenberg [33] in the 1930's to deal with the classical problem of the infinite self-energy of a point charge. These extensions, which have been also explored in areas as diverse as black-hole physics, superconductors, and cosmology [34, 35, 36, 37, 38, 39, 40, 41, 42], can display interesting features, such as vacuum birefringence and dichroism [43, 44, 45]. For recent developments, see refs. [46, 47, 48].

Perhaps the most striking prediction of these models is the occurrence of light-by-light scattering already at tree-level. This extremely rare process was recently observed by the ATLAS and CMS collaborations in heavy-ion collisions at the LHC [49, 50, 51]. The perspective to test effects of non-linear extensions of the Standard Model (SM) in high-energy experiments – in lepton and hadron accelerators or potentially in photon colliders – motivates us to search for possible phenomenological consequences.

The non-linear extension of traditional Maxwell electrodynamics modifies photon-photon interactions by introducing higher-order terms in the Lagrangian. Here, we are interested in extending the whole hypercharge sector of the electroweak gauge group, thus giving rise to other interesting phenomena. In fact, besides reproducing the already known non-linear effects in standard electrodynamics (corrected by a factor involving the Weinberg angle), this extension induces anomalous quartic couplings between the Z-boson and the photon. This in turn theoretically allows for rare processes to take place already at tree-level, as for example the creation of a Z-boson pair from the collision of two photons.

Non-linear effects have not been observed at low energies. This means that the parameter controlling the non-linearity of the fields is expected to be large in comparison to other relevant energy scales. The parameters in non-linear theories may be constrained in different ways, *e.g.*, via hydrogen spectroscopy or interferometry [52, 53]. A more stringent bound is obtained using LHC data on light-by-light scattering in heavy-ion collisions [25]. The lower bound reported there is $\sim 100\,\mathrm{GeV}$, but it could reach $\sim 200\,\mathrm{GeV}$ under less restrictive assumptions. The ATLAS data on $gg \to \gamma\gamma$ can enhance this sensitivity by one order of magnitude in a BI extension of SM [54], reaching the TeV scale as in brane-inspired models.

Part I is organized in 4 Chapters, being the first one given by this Introduction. Chapter 2 is organized as follows: in Sec. 2.1, we make a short review of the original EW monopole solution. In Sec. 2.2, we propose a regularization of the monopole solution, by adopting a non-linear extension of the hypercharge sector. Next, we analyze our results in some special cases, and estimate the respective masses. This is done in Sec. 2.3. Sec. 2.4 is devoted to finding a lower bound for the energy; finally, in Sec. 2.5, we analyze the simpler case of a Dirac magnetic charge. Chapter 3 is organized as follows: in Sec. 3.1 we present the theoretical setup of our model. In Sec. 3.2 we discuss options to constrain the expansion parameter β, in particular through the decay $Z \to 3\,\gamma$ in Sec. 3.2.1 and the scattering $e^-\,e^+ \to 3\,\gamma$ in Sec. 3.2.2, respectively. In Sec. 3.2.3 we discuss neutral gauge-boson scattering processes and contextualize our discussion with recent results in anomalous quartic gauge couplings. Finally, in Chapter 4, we state our concluding remarks for the first part of this thesis.

Chapter 2

Electroweak monopoles

In this Chapter we introduce the original electroweak monopole solution [17]. We discuss the issue of infinite energy and a class of extensions that could regularize it, giving a finite-energy monopole solution. We analyze some special cases inspired by non-linear extensions of electrodynamics and obtain the respective masses. After that, we discuss a lower bound for the monopole energy and an interesting Dirac's magnetic charge solution in this non-linear scenario. We suggest the recent reviews [55, 56] for more details.[1]

2.1 The original electroweak monopole solution

Let us consider the bosonic sector of the Electroweak Lagrangian in the Standard Model:

$$\mathcal{L}_0 = |D_\mu H|^2 - \frac{\lambda}{2}\left(H^\dagger H - \frac{\mu^2}{\lambda}\right)^2 - \frac{1}{4}F^a_{\mu\nu}F^{\mu\nu}_a - \frac{1}{4}B_{\mu\nu}B^{\mu\nu}, \tag{2.1}$$

where we are using

$$\begin{aligned} F^a_{\mu\nu} &= \partial_\mu A^a_\nu - \partial_\nu A^a_\mu + g f^{abc} A^b_\mu A^c_\nu, \\ B_{\mu\nu} &= \partial_\mu B_\nu - \partial_\nu B_\mu. \end{aligned} \tag{2.2}$$

The covariant derivative with respect to the $SU(2)_L$ x $U(1)_Y$ gauge group is defined by,

$$D_\mu H = \left(\partial_\mu - i\frac{g}{2}A^a_\mu \sigma^a - i\frac{g'}{2}B_\mu\right) H, \tag{2.3}$$

[1] This Chapter is based on Eur. Phys. J. C **81**, 788 (2021).

and H is the SM Higgs doublet. Given the above Lagrangian, one can obtain the equations of motion, given by

$$\begin{aligned} D_\mu D^\mu H &= -\lambda \left(H^\dagger H - \frac{\mu^2}{\lambda} \right) H, \\ D_\mu F_a^{\mu\nu} &= -i\frac{g}{2} \left(H^\dagger \sigma_a D^\nu H - D^\nu H^\dagger \sigma_a H \right), \\ \partial_\mu B^{\mu\nu} &= -i\frac{g'}{2} \left(H^\dagger D^\nu H - D^\nu H^\dagger H \right), \end{aligned} \tag{2.4}$$

where we used $D_\mu F^{\mu\nu a} = \partial_\mu F^{\mu\nu a} - g f^{abc} A_\mu^c F^{\mu\nu b}$.

Let us introduce the following parametrization for the Higgs field, without loss of generality,

$$H = \frac{1}{\sqrt{2}} \rho \, \xi, \quad \text{with} \;\; \xi^\dagger \xi = 1. \tag{2.5}$$

Here the doublet structure is carried by the field ξ as well as the Higgs hypercharge. Therefore, ξ carries the Higgs field quantum numbers, and we would like to emphasize that the presence of the hypercharge quantum number in the field ξ is extremely important to discuss the existence of the monopole solution. In fact, taking into account the $U(1)_Y$, we can interpret the unit doublet ξ as a $CP(1)$ field, and therefore find the non-trivial topology that we need to discuss monopole solutions, since $\pi_2\left(CP(1)\right) = \pi^2\left(S^2\right) = \mathbb{Z}$. Note that there is no loss of generality in the parametrization of the Higgs given above. The Higgs doublet has 2 complex degrees of freedom (d.o.f.), and in this parametrization we have in principle 2 complex d.o.f in ξ, but the constraint $\xi^\dagger \xi = 1$ removes 1 real d.o.f., that is moved to the real field ρ, that does not have any charge under the gauge group. Using this parametrization, and defining $\rho_0^2 = \frac{2\mu^2}{\lambda}$, we can rewrite,

$$\begin{aligned} \mathcal{L}_0 = &\frac{1}{2}(\partial_\mu \rho)^2 + \frac{\rho^2}{2} |D_\mu \xi|^2 - \frac{\lambda}{8} \left(\rho^2 - \rho_0^2 \right)^2 + \\ &- \frac{1}{4} F^a_{\mu\nu} F_a^{\mu\nu} - \frac{1}{4} B_{\mu\nu} B^{\mu\nu}. \end{aligned} \tag{2.6}$$

The equations of motion written in terms of the new parametrization are,

$$\partial^2 \rho = \rho |D_\mu \xi|^2 - \frac{\lambda}{2} \left(\rho^2 - \rho_0^2 \right) \rho, \tag{2.7}$$

$$\rho D^2 \xi = -2 \, \partial_\mu \rho \, D_\mu \xi, \tag{2.8}$$

$$D_\mu F^{\mu\nu a} = -i\frac{g}{4} \rho^2 \left(\xi^\dagger \sigma^a D^\nu \xi - D^\nu \xi^\dagger \sigma^a \xi \right), \tag{2.9}$$

$$\partial_\mu B^{\mu\nu} = -i\frac{g'}{4} \rho^2 \left(\xi^\dagger D^\nu \xi - D^\nu \xi^\dagger \xi \right). \tag{2.10}$$

Let us consider the spherically symmetric *ansatz*, proposed in [17], with spherical coordi-

nates (t, r, θ, φ):

$$\begin{aligned}
&\rho = \rho(r), \quad \xi = i \begin{pmatrix} \sin(\theta/2)\, e^{-i\varphi} \\ -\cos(\theta/2) \end{pmatrix}, \\
&\vec{A}_\mu = \frac{1}{g} A(r)\, \partial_\mu t\, \hat{r} + \frac{1}{g}(f(r)-1)\, \hat{r} \times \partial_\mu \hat{r}, \\
&B_\mu = \frac{1}{g'} B(r)\, \partial_\mu t - \frac{1}{g'}(1-\cos\theta)\, \partial_\mu \varphi.
\end{aligned} \tag{2.11}$$

For the benefit of the reader, we will write the gauge field $\vec{A}_\mu$ in components:

$$\vec{A}_\mu = \begin{pmatrix} \frac{1}{g}A(r)\partial_\mu t\; s_\theta c_\varphi + \frac{1}{g}(f(r)-1)(-s_\varphi \partial_\mu \theta - s_\theta c_\theta c_\varphi \partial_\mu \varphi) \\ \frac{1}{g}A(r)\partial_\mu t\; s_\theta s_\varphi + \frac{1}{g}(f(r)-1)(c_\varphi \partial_\mu \theta - s_\theta c_\theta s_\varphi \partial_\mu \varphi) \\ \frac{1}{g}A(r)\partial_\mu t\; c_\theta + \frac{1}{g}(f(r)-1)(s_\theta^2 \partial_\mu \varphi) \end{pmatrix}. \tag{2.12}$$

First of all, notice that we have, $\hat{r} = -\xi^\dagger \vec{\sigma}\, \xi$, what in an abelian decomposition would define the abelian direction in the gauge space. Care should be paid to not confuse the coordinates in the field space with the spacetime coordinates in this spherically symmetric *ansatz*, where the interplay between both is important as usually happens in this subject. We also remark that again the $U(1)_Y$ is extremely important for these considerations, and without it the Higgs doublet would not allow a spherically symmetric *ansatz*, besides not having the correct topology to admit a monopole solution. Looking more closely to this *ansatz*, we can see that when we take $A(r) = B(r) = f(r) = 0$, we obtain a term like a magnetic potential for the field $\vec{A}_\mu$ that could describe a non-abelian monopole in the $SU(2)_L$ sector, and the field B_μ would give an abelian monopole in the $U(1)_Y$ sector. There is an apparent string singularity in ξ and B_μ along the negative z-axis, but this is only a gauge artifact, and can be removed. Therefore this *ansatz* is in the right direction to search for monopoles, and it is sometimes said that the Cho-Maison monopole is somehow an hybrid between the abelian and non-abelian monopoles.

Let us introduce the physical fields to understand better the content of the *ansatz*. To define the mass eigenstates in the gauge sector, we will choose the unitary gauge using a gauge transformation U that puts the doublet in the usual form, that is $\xi \to (U\xi)^a = \delta^{a2}$, with $a = 1, 2$,

$$\xi \to U\xi = \begin{pmatrix} 0 \\ 1 \end{pmatrix}. \tag{2.13}$$

The transformation U that does the job is

$$U = i \begin{pmatrix} \cos(\theta/2) & \sin(\theta/2) e^{-i\varphi} \\ -\sin(\theta/2) e^{i\varphi} & \cos(\theta/2) \end{pmatrix}. \tag{2.14}$$

When we do such a gauge transformation, remembering that we have $\hat{r} = -\xi^\dagger \vec{\sigma}\, \xi$, we transform this abelian direction to $\hat{r}^a \to \delta^{a3}$, with $a = 1, 2, 3$, that is,

$$\hat{r} = \begin{pmatrix} \sin\theta\cos\varphi \\ \sin\theta\sin\varphi \\ \cos\theta \end{pmatrix} \to \begin{pmatrix} 0 \\ 0 \\ 1 \end{pmatrix}. \tag{2.15}$$

Also the gauge fields have to change under this gauge transformation as usual, by

$$A'_\mu = U A_\mu U^{-1} - \frac{i}{g}\,\partial_\mu U\, U^{-1}. \tag{2.16}$$

One can open the Lie-algebra valued field as $A_\mu = A^a_\mu \frac{\sigma^a}{2}$, and using this specific form of gauge transformation U, obtain the expression for the transformation of each component of the field A_μ given in the *ansatz* comparing both sides of the above expression,

$$A^{1'}_\mu = A^1_\mu[1-(1-c_\theta)c^2_\varphi] - A^2_\mu[(1-c_\theta)s_\varphi c_\varphi] - A^3_\mu[s_\theta c_\varphi] - \frac{1}{g}[s_\theta c_\varphi \partial_\mu\varphi + s_\varphi \partial_\mu\theta], \tag{2.17}$$

$$A^{2'}_\mu = -A^1_\mu[(1-c_\theta)c_\varphi s_\varphi] + A^2_\mu[1-(1-c_\theta)s^2_\varphi] - A^3_\mu[s_\theta s_\varphi] - \frac{1}{g}[s_\theta s_\varphi \partial_\mu\varphi - c_\varphi \partial_\mu\theta], \tag{2.18}$$

$$A^{3'}_\mu = A^1_\mu[s_\theta c_\varphi] + A^2_\mu[s_\theta s_\varphi] + A^3_\mu[c_\theta] - \frac{1}{g}[(1-c_\theta)\partial_\mu\varphi]. \tag{2.19}$$

Therefore, in the unitary gauge, we have

$$\vec{A}_\mu = \frac{1}{g}\begin{pmatrix} -f(r)\,(\sin\varphi\partial_\mu\theta + \sin\theta\cos\varphi\partial_\mu\varphi) \\ f(r)\,(\cos\varphi\partial_\mu\theta - \sin\theta\sin\varphi\partial_\mu\varphi) \\ A(r)\partial_\mu t - (1-\cos\theta)\partial_\mu\varphi \end{pmatrix}. \tag{2.20}$$

We define the physical fields A_μ and Z_μ through the rotation with the Weinberg angle, that is, $Z_\mu = \cos\theta_W A^3_\mu - \sin\theta_W B_\mu$ and $A_\mu = \sin\theta_W A^3_\mu + \cos\theta_W B_\mu$, that is,

$$\begin{pmatrix} Z_\mu \\ A_\mu \end{pmatrix} = \begin{pmatrix} \cos\theta_W & -\sin\theta_W \\ \sin\theta_W & \cos\theta_W \end{pmatrix}\begin{pmatrix} A^3_\mu \\ B_\mu \end{pmatrix}, \tag{2.21}$$

and we define also the W-bosons through $W^\pm_\mu = \frac{1}{\sqrt{2}}\left(A^1_\mu \mp i A^2_\mu\right)$. Plugging the *ansatz*, we obtain

$$\begin{aligned} A^{\rm em}_\mu &= e\left(\frac{1}{g^2}A(r) + \frac{1}{g'^2}B(r)\right)\partial_\mu t - \frac{1}{e}(1-\cos\theta)\partial_\mu\varphi; \\ Z_\mu &= \frac{e}{gg'}(A(r)-B(r))\partial_\mu t; \\ W^-_\mu &= \frac{i}{g}\frac{f(r)}{\sqrt{2}}e^{i\varphi}(\partial_\mu\theta + i\sin\theta\partial_\mu\varphi), \end{aligned} \tag{2.22}$$

where we defined $e = g\sin\theta_W = g'\cos\theta_W$. Therefore, we have our *ansatz* written in terms of the physical fields, and we can begin to search for solutions of the equations of motion.

The equations of motion will give us a set of coupled differential equations in the radial variable for the fields $(A(r), B(r), f(r), \rho(r))$. We point out that we are considering here only static and spherically symmetric solutions, therefore, the derivatives are taken with respect to the variable r. The spherical symmetry of the *ansatz* simplifies considerably the equations of motion, and one can show that these equations admit a general dyon solution if we impose certain boundary conditions [17]. Therefore, the equations of motion in the spherically symmetric *ansatz* read:

$$\begin{aligned}
&\ddot{\rho} + \frac{2}{r}\dot{\rho} - \frac{f^2}{2r^2}\rho = -\frac{(A-B)^2}{4}\rho + \frac{\lambda}{2}\left(\rho^2 - \frac{2\mu^2}{\lambda}\right)\rho, \\
&\ddot{f} - \frac{(f^2-1)}{r^2}f = \left(\frac{g^2}{4}\rho^2 - A^2\right)f, \\
&\ddot{A} + \frac{2}{r}\dot{A} - \frac{2f^2}{r^2}A = \frac{g^2}{4}\rho^2(A-B), \\
&\ddot{B} + \frac{2}{r}\dot{B} = -\frac{g'^2}{4}\rho^2(A-B).
\end{aligned} \tag{2.23}$$

In the original work [17], the authors showed that these equations admit a general dyon solution if we impose the following boundary conditions:

$$\begin{aligned}
&\rho(0) = 0, \quad f(0) = 1, \quad A(0) = 0, \quad B(0) = b_0, \\
&\rho(\infty) = \rho_0, \quad f(\infty) = 0, \quad A(\infty) = B(\infty) = A_0.
\end{aligned} \tag{2.24}$$

More precisely, with these boundary conditions, they showed that the equations of motion taken in the *ansatz* configuration admit a family of solutions labeled by the real parameter A_0 lying in the range $0 \leq A_0 < min\left(e\rho_0, \frac{g}{2}\rho_0\right)$, and represent a dyon in the SM. Here we are interested in the simpler case of a monopole solution, since it is lighter than the dyon and more easily accessible in a experimental sense. Therefore we will take in our analysis the simplifying assumption $A(r) = B(r) = 0$, that is, we will turn off the Coulombic part of the *ansatz*, to investigate the electroweak monopole solutions. We would like to mention that even if this is not the more complete picture of the topological objects that we could find in the SM, it is still an absolutely non-trivial solution since we are taking a non-zero $f(r)$ that will bring the effects of weak bosons and give us a topologically stable electroweak monopole.

Given the Lagrangian and the equations of motion, one can find the canonical energy-momentum tensor associated with the translation symmetry of the system, obtained by

the Nöether procedure, as:

$$\begin{aligned}\hat{T}_0^{\mu\nu} =& - F_a^{\mu\rho}\partial^\nu A_\rho^a - B^{\mu\rho}\partial^\nu B_\rho - \eta^{\mu\nu}\mathcal{L} + \\ &+ D^\mu H^\dagger \partial^\nu H + \partial^\nu H^\dagger D^\mu H. \end{aligned} \tag{2.25}$$

The canonical energy-momentum tensor is clearly not gauge-invariant, but we can improve it as usual, summing total derivatives that will not alter the physics of the system. Therefore, we can sum the quantity $\delta T^{\mu\nu}$, given by,

$$\delta T^{\mu\nu} = \partial_\rho (F_a^{\mu\rho} A_a^\nu) + \partial_\rho (B^{\mu\rho} B^\nu), \tag{2.26}$$

and therefore, summing this quantity and using the equations of motion, we can obtain an improved gauge-invariant energy-momentum tensor, that is given by:

$$\begin{aligned} T_0^{\mu\nu} =& F_a^{\mu\rho}\, F_\rho^{a\,\nu} + B^{\mu\rho} B_\rho{}^\nu - \eta^{\mu\nu}\mathcal{L}_0 + \\ &+ D^\mu H^\dagger D^\nu H + D^\nu H^\dagger D^\mu H. \end{aligned} \tag{2.27}$$

To find the Hamiltonian of this system, we only need to consider the component T^{00} integrated in all space, and therefore, we can obtain,

$$\begin{aligned} H = \int d^3x \left[\frac{1}{2}\left(F_{0i}^a\right)^2 + \frac{1}{2}\left(B_{0i}\right)^2 + |D_0 H|^2\right] + \\ \left[\frac{1}{4}\left(F_{ij}^a\right)^2 + \frac{1}{4}\left(B_{ij}\right)^2 + |D_i H|^2 + \frac{\lambda}{2}\left(H^\dagger H - \frac{\mu^2}{\lambda}\right)^2\right]. \end{aligned} \tag{2.28}$$

Therefore, the energy functional for the *ansatz* 2.11 is

$$\begin{aligned} E = 4\pi \int_0^\infty dr\, r^2 \Bigg[& \frac{\rho^2}{8}(A-B)^2 + \frac{\dot{\rho}^2}{2} + \frac{\rho^2 f^2}{4}\frac{1}{r^2} \\ & + \frac{\dot{A}^2}{2g^2} + \frac{A^2 f^2}{g^2}\frac{1}{r^2} + \frac{\dot{f}^2}{g^2}\frac{1}{r^2} + \frac{(f^2-1)^2}{2g^2}\frac{1}{r^4} \\ & + \frac{\lambda}{8}(\rho^2 - \frac{2\mu^2}{\lambda})^2 + \frac{\dot{B}^2}{2g'^2} + \frac{1}{2g'^2}\frac{1}{r^4}\Bigg]. \end{aligned} \tag{2.29}$$

Using the appropriate boundary conditions for the functions $\rho(r), f(r), A(r), B(r)$, one can show that most of the terms above give a finite result, but the last term in the above expression will become infinite, and we will call this contribution E^*, that is,

$$E^* = 4\pi \int_0^\infty dr\, \frac{1}{2\, g'^2\, r^2}. \tag{2.30}$$

This is exactly the origin of the infinite energy of the monopole solution at the classical

level, a singularity at the origin. Because of this problem, we cannot predict the monopole mass, and we will propose in the following a solution to this issue, finding a finite-energy monopole. It is important to note that these are classical considerations, and one could consider extensions of the SM that can regularize this divergence, paying special attention to the $U(1)_Y$ sector where it appears.

2.2 A finite-energy monopole solution

Let us consider now the simpler case of a monopole solution, since it is lighter than the dyon and more easily accessible in an experimental sense. That is, we will consider the simplified version of the more general *ansatz* 2.11 where we turn off the Coulombic part taking $A(r) = B(r) = 0$. The EW monopole *ansatz* will therefore be given by

$$\begin{aligned}
&\rho = \rho(r), \quad \xi = i \begin{pmatrix} \sin(\theta/2)\, e^{-i\varphi} \\ -\cos(\theta/2) \end{pmatrix} \\
&\vec{A}_\mu = \frac{1}{g}(f(r) - 1)\, \hat{r} \times \partial_\mu \hat{r}; \\
&B_\mu = -\frac{1}{g'}(1 - \cos\theta)\, \partial_\mu \varphi.
\end{aligned} \tag{2.31}$$

The equations of motion are simplified in this case to

$$\begin{aligned}
&\ddot{\rho} + \frac{2}{r}\dot{\rho} - \frac{f^2}{2r^2}\rho = \frac{\lambda}{2}\left(\rho^2 - \frac{2\mu^2}{\lambda}\right)\rho; \\
&\ddot{f} - \frac{(f^2-1)}{r^2} f = \frac{f g^2}{4}\rho^2.
\end{aligned} \tag{2.32}$$

The monopole *ansatz* 2.31 provides a solution to the equations of motion if we adopt the following boundary conditions [17]:

$$\rho(0) = 0,\ \rho(\infty) = \rho_0,\ f(0) = 1,\ f(\infty) = 0, \tag{2.33}$$

where we defined $\rho_0 = \sqrt{\frac{2\mu^2}{\lambda}}$. The energy functional for the monopole configuration is also simplified, giving us

$$\begin{aligned}
E = 4\pi \int_0^\infty dr\, r^2 \Bigg[&\frac{\dot{\rho}^2}{2} + \frac{\rho^2 f^2}{4}\frac{1}{r^2} + \frac{\lambda}{8}(\rho^2 - \rho_0^2)^2 \\
&+ \frac{\dot{f}^2}{g^2}\frac{1}{r^2} + \frac{(f^2-1)^2}{2g^2}\frac{1}{r^4} + \frac{1}{2g'^2}\frac{1}{r^4}\Bigg],
\end{aligned} \tag{2.34}$$

such that one can write for simplicity in the following,

$$E = E_1 + E^*. \tag{2.35}$$

We remark that the problematic term E^* is still here, as one can see in the last term of the above expression.

Let us propose a general extension of the $U(1)_Y$ sector in the EW Lagrangian $\mathcal{L}_0$:

$$\mathcal{L} = \mathcal{L}_0 + f\left(\mathcal{F}, \mathcal{G}\right), \tag{2.36}$$

where we define $\mathcal{F} = \frac{1}{4} B_{\mu\nu} B^{\mu\nu}$, and $\mathcal{G} = \frac{1}{4} B_{\mu\nu} \tilde{B}^{\mu\nu}$, the $U(1)_Y$ Lorentz and gauge-invariant basic objects, where $\tilde{B}^{\mu\nu} = \frac{1}{2} \epsilon^{\mu\nu\rho\sigma} B_{\rho\sigma}$. In this case, the equations of motion for the $U(1)_Y$ sector will become

$$\partial_\mu B^{\mu\nu} = \frac{J^\nu + B^{\mu\nu} \partial_\mu \partial_{\mathcal{F}} f + \tilde{B}^{\mu\nu} \partial_\mu \partial_{\mathcal{G}} f + \partial_\mu \tilde{B}^{\mu\nu} \partial_{\mathcal{G}} f}{1 - \partial_{\mathcal{F}} f}, \tag{2.37}$$

where we defined $\partial_{\mathcal{F}} f = \frac{\partial f}{\partial \mathcal{F}}$, $\partial_{\mathcal{G}} f = \frac{\partial f}{\partial \mathcal{G}}$, and we defined also the hypercharge matter current $J^\nu = -i \frac{g'}{2} \left(H^\dagger D^\nu H - D^\nu H^\dagger H \right)$. Now, we can plug the *ansatz* in this equation of motion to see which constraints we obtain. Notice that here we have $\partial_0 = 0$, and $B_0 = 0$, and thus immediately we obtain $B_{i0} = 0$, $\tilde{B}_{ij} = 0$. After some algebraic manipulations, we can also obtain

$$\begin{aligned} \left(\xi^\dagger D_\mu \xi - D_\mu \xi^\dagger \xi \right) &= i \left[g A^1_\mu \sin\theta \cos\varphi + g A^2_\mu \sin\theta \sin\varphi \right. \\ &\left. + g A^3_\mu \cos\theta - g' B_\mu - (1 - \cos\theta) \partial_\mu \varphi \right] \\ &= 0, \end{aligned} \tag{2.38}$$

and thus, $J^\nu = 0$. We can write $B^{ij} \propto \epsilon^{ijk} \mathcal{B}_k(r)$, where $\vec{\mathcal{B}}(r)$ is the radial hypercharge magnetic field associated with the $U(1)_Y$ gauge potential, and thus one can find $\partial_i B^{ij} = 0$.

The equation of motion, after these considerations, can be written as

$$B^{i\nu} \partial_i \partial_{\mathcal{F}} f + \tilde{B}^{i\nu} \partial_i \partial_{\mathcal{G}} f + \partial_i \tilde{B}^{i\nu} \partial_{\mathcal{G}} f = 0. \tag{2.39}$$

Therefore, given our proposal of extending the hypercharge sector adding a generic function $f\left(\mathcal{F}, \mathcal{G}\right)$, we conclude that the monopole *ansatz* will satisfy the modified $U(1)_Y$ equation of motion if the function $f(\mathcal{F}, \mathcal{G})$ satisfies the following conditions:

$$\begin{aligned} \partial_i \left(B^{ij} \partial_{\mathcal{F}} f \right) |_{ansatz} &= 0, \\ \partial_i \left(\tilde{B}^{i0} \partial_{\mathcal{G}} f \right) |_{ansatz} &= 0. \end{aligned} \tag{2.40}$$

Now, let us study the energy of the monopole configuration in this extended model.

One can obtain the following energy-momentum tensor:

$$\tilde{T}^{\mu\nu} = T_0^{\mu\nu} + B^{\mu\rho}\partial^\nu B_\rho\,\partial_{\mathcal{F}} f + \tilde{B}^{\mu\rho}\partial^\nu B_\rho\,\partial_{\mathcal{G}} f - \eta^{\mu\nu} f + \\ - \left(\frac{J^\mu + B^{\rho\mu}\partial_\rho \partial_{\mathcal{F}} f + \partial_\rho \left(\tilde{B}^{\rho\mu}\partial_{\mathcal{G}} f \right)}{1 - \partial_{\mathcal{F}} f} \right) B^\nu + J^\mu B^\nu, \tag{2.41}$$

where $T_0^{\mu\nu}$ is the usual energy-momentum tensor. Now we can take the Hamiltonian and calculate the monopole energy, by simply plugging our *ansatz* into this expression. In the monopole *ansatz*, we remember again that $\partial_0 = 0$ and $B_0 = 0$, giving us a huge simplification. In fact, since we have $B_{0i} = \tilde{B}_{ij} = 0$, we can immediately obtain $B_{\mu\nu}B^{\mu\nu} \propto \vec{\mathcal{B}}(r)^2$ and also $B_{\mu\nu}\tilde{B}^{\mu\nu} = 0$, giving us

$$\mathcal{F}|_{ansatz} = \frac{1}{2g'^2}\frac{1}{r^4}, \\ \mathcal{G}|_{ansatz} = 0. \tag{2.42}$$

Thus, the monopole energy in this extended model is

$$E = E_1 + \int_0^\infty dr 4\pi r^2 \left[\frac{1}{2g'^2}\frac{1}{r^4} - f\left(\mathcal{F}|_{ansatz}; \mathcal{G}|_{ansatz}\right) \right]. \tag{2.43}$$

Notice that we can easily handle the infinite energy coming from E^* simply taking $f(\mathcal{F}, \mathcal{G}) = \mathcal{F} + \phi(\mathcal{F}, \mathcal{G})$. Therefore, we can use the expressions 2.40 and 2.43 to search for extensions of the $U(1)_Y$ sector of the Electroweak Lagrangian such that the monopole *ansatz* is a finite energy solution for the equation of motion.

In fact, let us impose that this function $\phi(\mathcal{F}, \mathcal{G})$, that will represent our generalized $U(1)_Y$ kinetic term, depends non-trivially on $\mathcal{F}$ and only on the square of $\mathcal{G} = \frac{1}{4}B_{\mu\nu}\tilde{B}^{\mu\nu}$, that is, ϕ is a generic function of $\mathcal{F}$ and $\mathcal{G}^2$. The physical reason for this assumption is to not have a parity violating term in the gauge kinetic sector of the photon after the EW symmetry breaking. One can show that, only imposing this physical assumption, the conditions 2.40 will be trivially satisfied for any reasonable function ϕ, that is, the monopole *ansatz* will satisfy the equation of motion coming from the extended $U(1)_Y$ sector. We remark here that this is a sufficient condition to solve the constraints 2.40, but it is not necessary.

Therefore, the most general extension of the hypercharge sector for which the monopole *ansatz* 2.31 is a solution of the equations of motion, and consistent with the above physical assumption is any reasonable function $\phi(\mathcal{F}, \mathcal{G}^2)$ such that the energy integral is finite, *i.e.*,

$$-\int_0^\infty dr 4\pi r^2 \left[\phi\left(\mathcal{F} = \frac{1}{2g'^2 r^4}; \mathcal{G}^2 = 0 \right) \right] = \text{Finite}. \tag{2.44}$$

In particular, since we want to reproduce the usual $-\frac{1}{4}B_{\mu\nu}B^{\mu\nu}$ term in first approximation to recover the SM results at first order, we will study a restricted class of possible extensions considering that ϕ depends on $\mathcal{F}$ and $\mathcal{G}$ through the particular combination $X = \frac{\mathcal{F}}{\beta^2} - \frac{\mathcal{G}^2}{2\beta^4}$, where β is a parameter with dimensions of Mass^2. As we already know, the conditions 2.40 are trivially satisfied, and we need only to care about the finiteness of the energy integral. What we are doing here is to improve the hypercharge sector to a non-linear version, and we will consider three physically interesting cases, corresponding to $\phi_1 = -\beta^2 \log[1+X]$, $\phi_2 = \beta^2\left[e^{-X}-1\right]$ and finally, $\phi_3 = \beta^2\left[1-\sqrt{1+2X}\right]$, that respectively will give us the $U(1)_Y$ version of the Logarithmic [43], Exponential [44], and Born-Infeld [24] non-linear Electrodynamics.

2.3 Non-linear extensions of $U(1)_Y$

The subject of non-linear Electrodynamics was introduced in the thirties by Euler and Heisenberg [33] after the Nature's paper by Born and Infeld [24], to remove the singularities associated with charged point-like particles, and it has ever since attracted the interest of physicists due to its interesting features. For example, non-linear Electrodynamics predicts light-by-light scattering in vacuum and such phenomenon is being tested experimentally nowadays [49, 50, 51]. Interestingly, some non-linear models emerge naturally from the low-energy limit of string theory, and this has been applied in very different contexts as, for example, black hole physics [34, 35, 36], holographic superconductivity [37, 38, 39], and cosmology [40, 41, 42]. There are, nowadays, many different proposals of non-linear Electrodynamics [46, 47, 48], exhibiting not only finite energy for the point-like charge, but also properties like vacuum birefringence and dichroism.

In this Section, we shall consider three possible non-linear extensions of the hypercharge sector, calculate the monopole energy for each of them, and compare the respective results. We remark that the Born-Infeld case was already studied in [23], and we are considering these results here only for the sake of comparison. In each of the following cases, what we will do is to consider different functions $\phi = \mathcal{L}_Y$, that extends the hypercharge sector to a non-linear theory, state its equation of motion, and compute the corresponding monopole energy for it. The right-hand side of the equation of motion will be given by the usual matter current $J^\nu = -\frac{ig'}{2}\left(H^\dagger D^\nu H - D^\nu H^\dagger H\right)$. All of them have a factor E_1 in common, since this is the contribution to the energy that comes from all the other terms except the $U(1)_Y$ kinetic term. As we already remarked before, this contribution E_1 is finite, and its value was calculated by [19], giving approximately $E_1 \approx 4.1\,\text{TeV}$.

Let us consider first the Logarithmic $U(1)_Y$ Electrodynamics, introduced few years

ago [43]. The Lagrangian for the hypercharge sector will be

$$\mathcal{L}_Y = -\beta^2 \log\left[1 + \frac{\mathcal{F}}{\beta^2} - \frac{\mathcal{G}^2}{2\beta^4}\right], \tag{2.45}$$

where as before, $\mathcal{F} = \frac{1}{4}B_{\mu\nu}B^{\mu\nu}$ and $\mathcal{G} = \frac{1}{4}B_{\mu\nu}\tilde{B}^{\mu\nu}$, and β is a parameter with dimensions of Mass^2. The $U(1)_Y$ equation of motion for our extended theory is

$$\partial_\mu\left[\frac{B^{\mu\nu} - \frac{1}{\beta^2}\mathcal{G}\tilde{B}^{\mu\nu}}{\left(1 + \frac{\mathcal{F}}{\beta^2} - \frac{\mathcal{G}^2}{2\beta^4}\right)}\right] = J^\nu, \tag{2.46}$$

The monopole energy here is given by

$$E = E_1 + \int_0^\infty dr\left[\beta^2 \log\left(1 + \frac{1}{2\beta^2 g'^2 r^4}\right) 4\pi r^2\right]. \tag{2.47}$$

Doing this integral we obtain

$$E = E_1 + \frac{2}{3}2^{3/4}\pi^2\frac{\sqrt{\beta}}{(g')^{3/2}}. \tag{2.48}$$

To estimate the energy, we will consider here $g' = 0.357$, that is approximately the value of the $U(1)_Y$ coupling at the EW scale. Thus, we obtain

$$E \approx 4.1\,\text{TeV} + 51.87\sqrt{\beta}. \tag{2.49}$$

Now, let us consider the Exponential $U(1)_Y$ Electrodynamics [44]. Here we have the following Lagrangian:

$$\mathcal{L}_Y = \beta^2\left[-1 + \exp^{\left(-\frac{\mathcal{F}}{\beta^2} + \frac{\mathcal{G}^2}{2\beta^4}\right)}\right]. \tag{2.50}$$

The equation of motion follows immediately,

$$\partial_\mu\left[\left(B^{\mu\nu} - \frac{1}{\beta^2}\mathcal{G}\tilde{B}^{\mu\nu}\right)\exp^{\left(-\frac{\mathcal{F}}{\beta^2} + \frac{\mathcal{G}^2}{2\beta^4}\right)}\right] = J^\nu. \tag{2.51}$$

Repeating the same steps, we can find the energy integral,

$$E = E_1 + \int_0^\infty dr 4\pi r^2\beta^2\left[1 - \exp^{\left(-\frac{\mathcal{F}}{\beta^2} + \frac{\mathcal{G}^2}{2\beta^4}\right)}\right]. \tag{2.52}$$

Doing this integral, we obtain

$$E = E_1 - \frac{\pi}{2^{3/4}}\Gamma(-3/4)\frac{\sqrt{\beta}}{(g')^{3/2}}. \tag{2.53}$$

Using as before $g' = 0.357$, we obtain

$$E \approx 4.1\,\text{TeV} + 42.33\,\sqrt{\beta}. \tag{2.54}$$

Last, but not least, we introduce the well-known Born-Infeld case, that have the following Lagrangian:

$$\mathcal{L}_Y = \beta^2 \left[1 - \sqrt{1 + \frac{2}{\beta^2}\mathcal{F} - \frac{1}{\beta^4}\mathcal{G}^2}\right]. \tag{2.55}$$

The equation of motion here is

$$\partial_\mu \left[\frac{B^{\mu\nu} - \frac{1}{\beta^2}\mathcal{G}\tilde{B}^{\mu\nu}}{\sqrt{1 + \frac{2}{\beta^2}\mathcal{F} - \frac{1}{\beta^4}\mathcal{G}^2}}\right] = J^\nu, \tag{2.56}$$

and the energy integral is given by

$$E = E_1 + \int_0^\infty dr 4\pi r^2 (-\beta^2)\left[1 - \sqrt{1 + \frac{2}{\beta^2}\mathcal{F} - \frac{1}{\beta^4}\mathcal{G}^2}\right]. \tag{2.57}$$

Solving this integral, we obtain

$$E = E_1 + \frac{3\sqrt{\pi}\,\Gamma(-3/4)^2}{8\,(g')^{3/4}}\sqrt{\beta} \tag{2.58}$$

Taking $g' = 0.357$, we have

$$E \approx 4.1\,\text{TeV} + 72.81\sqrt{\beta}. \tag{2.59}$$

Now that we already have the expressions for the energy, let us briefly discuss these $U(1)_Y$ extensions, leaving a more detailed analysis for the next Chapter. First of all, we can see that if we perform a Taylor expansion of them in the parameter $1/\beta^2$, we obtain at first non-trivial order,

$$\begin{aligned}\mathcal{L}_Y &= -\mathcal{F} + \frac{1}{2\beta^2}\left[\mathcal{F}^2 + \mathcal{G}^2\right] + O\left(1/\beta^4\right) \\ &= -\frac{1}{4}B_{\mu\nu}B^{\mu\nu} + \frac{1}{2\beta^2}\left[\left(\frac{1}{4}B_{\mu\nu}B^{\mu\nu}\right)^2 + \left(\frac{1}{4}B_{\mu\nu}\tilde{B}^{\mu\nu}\right)^2\right]\end{aligned} \tag{2.60}$$

Notice that they reproduce the usual kinetic term at first order, and exactly agree at order $O(1/\beta^2)$. This $\sqrt{\beta}$ parameter with dimensions of energy controls somehow the non-linearity of the fields, and can be obtained from experiments, but we notice that it should be large in comparison to our scales of energy since we do not observe non-linear effects at low energy. The best known bound for the β parameter nowadays is given by the work [25]

considering Data from light-by-light scattering measurements in LHC Pb-Pb collisions by ATLAS, and gives a lower bound for the Born-Infeld parameter in Electrodynamics given by $\sqrt{\beta} \geq 100\,\text{GeV}$. Here, we are doing a non-linear extension in the hypercharge sector instead of directly in the Electrodynamics, therefore, we should take a factor of $\cos\theta_W$ into account, obtaining the bound $\sqrt{\beta} \geq 90\,\text{GeV}$. In principle, one should take for each non-linear $U(1)_Y$ extension a different bound for the corresponding β parameter, but we can argue that we can consider all of them approximately equal with a good approximation. In fact, as the bound was obtained considering light-by-light scattering, the relevant term is the one with 4 photons in it, coming from the terms $(F_{\mu\nu}F^{\mu\nu})^2$ and $\left(F_{\mu\nu}\tilde{F}^{\mu\nu}\right)^2$. But by dimensional analysis, they should appear at order $O(1/\beta^2)$ in a Taylor expansion, and as we already remarked, the three non-linear extensions exactly agree at this order, therefore we can take the same bound for the β parameter in the three cases considered here with a good approximation.

Therefore, considering $\sqrt{\beta} \geq 90\,\text{GeV}$, we can obtain the estimated mass for the monopole configuration. Summarizing, considering these three different non-linear extensions we have:

$$E \approx 4,1 + 51,87\sqrt{\beta} \approx 8.7\ \text{TeV} \quad (\text{Logarithmic})\,, \tag{2.61a}$$

$$E \approx 4,1 + 42,33\sqrt{\beta} \approx 7.9\ \text{TeV} \quad (\text{Exponential})\,, \tag{2.61b}$$

$$E \approx 4,1 + 72,81\sqrt{\beta} \approx 11.6\ \text{TeV} \quad (\text{Born-Infeld})\,. \tag{2.61c}$$

We remark here that our Logarithmic and Exponential non-linear extensions give a lower mass for the monopole solution than the one obtained with Born-Infeld, but unfortunately it is still above the threshold energy for pair production of this object at the present LHC. In the following, we will consider a simplified setup to discuss a lower bound for the monopole energy in each case of interest.

2.4 Lower bounds for the monopole energy

The energy functional for the EW monopole *ansatz* is

$$E = \int_0^\infty dr\, 4\pi r^2 \left[\frac{\dot{\rho}^2}{2} + \frac{\rho^2 f^2}{4}\frac{1}{r^2} + \frac{\lambda}{8}(\rho^2 - \rho_0^2)^2 + \right.$$
$$\left. + \frac{\dot{f}^2}{g^2}\frac{1}{r^2} + \frac{(f^2-1)^2}{2g^2}\frac{1}{r^4} + \frac{1}{2g'^2}\frac{1}{r^4}\right]. \tag{2.62}$$

Taking the so-called BPS limit [8, 9], that is, taking the limit $\lambda \to 0$ but keeping the asymptotic condition $\rho \to \rho_0$, and also doing the improvement of the $U(1)_Y$ kinetic term

for a non-linear version, we can rewrite the above expression as

$$E = \int_0^\infty dr\, 4\pi r^2 \left[\left(\frac{\dot{\rho}}{\sqrt{2}} + \frac{(f^2-1)}{\sqrt{2} g r^2} \right)^2 + \left(\frac{\dot{f}}{gr} + \frac{f\rho}{2r} \right)^2 \right.$$
$$\left. - \frac{\dot{\rho}(f^2-1)}{gr^2} - \frac{\dot{f} f \rho}{gr^2} - \phi\left(\mathcal{F}|_{ansatz}\,,\, \mathcal{G}|_{ansatz}\right) \right]. \tag{2.63}$$

The last term is the contribution of the non-linearly extended hypercharge kinetic term, it was already computed and is completely independent of ρ and f, therefore we will omit it in our analysis. The terms in the first line are clearly non-negative, and therefore we can write a lower bound for the energy functional in this BPS limit,

$$E \geq -\frac{4\pi}{g} \int_0^\infty dr\, \left[\dot{\rho}(f^2-1) + \dot{f} f \rho \right]. \tag{2.64}$$

To saturate the bound and obtain the configurations that minimize the energy in this setup, we need to consider configurations that solve the following equations:

$$\dot{\rho}(r) + \frac{(f(r)^2-1)}{gr^2} = 0,$$
$$\dot{f}(r) + \frac{g f(r) \rho(r)}{2} = 0. \tag{2.65}$$

Interestingly, we would like to point out that if we didn't have a factor 2 in the denominator of the second equation, we would be able to find an analytical solution for these equations, as found by Bogomol'nyi [8], Prasad and Sommerfield [9] for the 'tHooft-Polyakov monopole. Such analytical solution would be

$$f(r) = \frac{g\rho_0 r}{\sinh(g\rho_0 r)}; \quad \rho(r) = \frac{\rho_0}{\tanh(g\rho_0 r)} - \frac{1}{gr}. \tag{2.66}$$

Unfortunately, we were not able to find an analytic solution for our case, but even though, we can search for a numerical solution to these equations, only to be capable of estimating a lower bound to the monopole mass. We remark that once again, a factor 2 prevents us from obtaining a total derivative in the expression 2.64, resulting in an analytical and elegant result. Considering configurations that solve the above equations and therefore saturate the energy bound, we can rewrite the lower bound,

$$E \geq \int_0^\infty dr\, 4\pi \left(\frac{\rho^2 f^2}{2} + \frac{(f^2-1)^2}{g^2 r^2} \right). \tag{2.67}$$

In the recent work [22], even though the authors used a different setup for the regularization of the monopole energy, when considering the BPS limit they obtained exactly the same expression for the equations that saturate the energy 2.65, as well as the same inte-

gral for the energy lower bound 2.67 that comes as consequence, and the result obtained there for such integral is given by

$$E \geq 2.98\,\text{TeV}. \tag{2.68}$$

We remark for the sake of comparison that another BPS bound was already obtained in [21], giving a lower bound of 2.37 TeV. In our case, the result obtained above is a lower bound for the EW monopole energy ignoring not only the scalar potential contribution, but also the hypercharge kinetic term ones. Taking in consideration now the result obtained for the hypercharge sector in each of the non-linear extensions that we did before, we find an estimate for the more realistic setup of a EW monopole,

$$E \geq 7.6 \text{ TeV} \quad \text{(Logarithmic)}, \tag{2.69a}$$

$$E \geq 6.8 \text{ TeV} \quad \text{(Exponential)}, \tag{2.69b}$$

$$E \geq 10.5 \text{ TeV} \quad \text{(Born-Infeld)}. \tag{2.69c}$$

Therefore, we conclude from our estimate that our non-linear extensions (i.e., Logarithmic and Exponential) give us a lower bound for the monopole mass that could be eventually found at the LHC, since the necessary energy to pair produce the monopole is nearby the present achievable energies. Therefore, even if our solutions have energy above the threshold for pair production at LHC, with these lower bounds we can have hope of some modification of our solution, that can give a monopole mass achievable at the present colliders.

2.5 A non-linear Dirac monopole

To conclude this Chapter, let us consider the simpler case of pure Electromagnetism and, following the same procedure as previously shown, let us find what the answer for a Dirac-like monopole would be. In fact, let us consider here the following Lagrangian:

$$\mathcal{L}_{\text{EM}} = -\frac{1}{4}F_{\mu\nu}F^{\mu\nu} + f\left(\mathcal{F}, \mathcal{G}\right), \tag{2.70}$$

where now we will do the non-linear extension directly on the Electromagnetism, and we are defining here the invariants as $\mathcal{F} = \frac{1}{4}F_{\mu\nu}F^{\mu\nu}$ and $\mathcal{G} = \frac{1}{4}F_{\mu\nu}\tilde{F}^{\mu\nu}$.

Following the same steps as before, we will find

$$\partial_\mu F^{\mu\nu} = \frac{F^{\mu\nu}\partial_\mu\partial_{\mathcal{F}}f + \tilde{F}^{\mu\nu}\partial_\mu\partial_{\mathcal{G}}f + \partial_\mu\tilde{F}^{\mu\nu}\partial_{\mathcal{G}}f}{1 - \partial_{\mathcal{F}}f}. \tag{2.71}$$

Consider now the *ansatz* for a Dirac-like monopole,

$$A_\mu = -\frac{1}{2e}(1-\cos\theta)\partial_\mu\varphi. \tag{2.72}$$

In the static regime we have $\partial_0 \equiv 0$, and therefore $A_0 = 0$, giving also $F_{0i} = 0$, and $\tilde{F}_{ij} = 0$ immediately. Therefore, we will obtain the following energy functional:

$$E = \int_0^\infty dr 4\pi r^2 \left[\frac{1}{8e^2r^4} - f\left(\mathcal{F} = \frac{1}{8e^2r^4}, \mathcal{G} = 0\right)\right]. \tag{2.73}$$

We already saw that the monopole *ansatz* gives a solution for the $U(1)$ equations of motion in the non-linear extensions that we considered here, and the same reasoning used before works for this case. Considering here the Logarithmic, Exponential and Born-Infeld Electrodynamics respectively, we obtain for the monopole energy,

$$\begin{aligned} E_{\text{Log}} &= \frac{2^{1/4}\,\pi^2}{2e^{3/2}}\sqrt{\beta}, \\ E_{\text{Exp}} &= \frac{\pi\,\Gamma(1/4)}{3\,2^{1/4}e^{3/2}}\sqrt{\beta}, \\ E_{\text{BI}} &= \frac{3\sqrt{\pi/2}\,\Gamma(-3/4)^2}{16e^{3/2}}\sqrt{\beta}. \end{aligned} \tag{2.74}$$

Taking $e = 0.303$ and considering the bound obtained in [25] that gives $\sqrt{\beta} \geq 100\text{GeV}$ for the nonlinear extension directly in the Electromagnetism, we obtain

$$E_{\text{Log}} \approx 2.3\,\text{TeV}, \tag{2.75a}$$

$$E_{\text{Exp}} \approx 1.9\,\text{TeV}, \tag{2.75b}$$

$$E_{\text{BI}} \approx 3.3\,\text{TeV}. \tag{2.75c}$$

Therefore, we can see what is the mass of a Dirac monopole if we consider only the Electromagnetism with a non-linear extension. This is a simplified scenario, but even though, it can give us a lower bound for the monopole mass, in a scale achievable at LHC.

Chapter 3

Phenomenology of the non-linear extension

In this Chapter, we analyze the non-linear extension of the hypercharge sector used in Chapter 2. This gives rise to quartic effective interactions between the neutral gauge bosons absent in the SM at tree-level. These novel operators contribute to decay and scattering processes and we explore existing experimental data to place lower bounds on the non-linear parameter. We discuss recent results constraining anomalous gauge couplings and briefly consider possible improvements on these bounds in future experiments.[1]

3.1 Theoretical setup

The bosonic part of the Electroweak Lagrangian was introduced in the beginning of the last Chapter. Let us repeat it here for the convenience of the reader:

$$\mathcal{L}_{\text{EW}} = \mathcal{L}_{\text{Gauge}} + \mathcal{L}_{\text{Higgs}}, \tag{3.1}$$

where

$$\mathcal{L}_{\text{Gauge}} = -\frac{1}{4}F^a_{\mu\nu}F^{\mu\nu a} - \frac{1}{4}B_{\mu\nu}B^{\mu\nu}, \tag{3.2}$$

$$\mathcal{L}_{\text{Higgs}} = |D_\mu H|^2 - \lambda\left(H^\dagger H - \frac{m^2}{2\lambda}\right)^2. \tag{3.3}$$

Here we defined the covariant derivative as

$$D_\mu = \partial_\mu - igA^a_\mu T^a - ig'YB_\mu. \tag{3.4}$$

[1] This Chapter is based on Phys. Rev. D **105**, 016007 (2022).

In the equations above, A^a_μ and B_μ are the gauge fields associated with the gauge group $SU(2)_{\rm L} \times U(1)_{\rm Y}$, $F^a_{\mu\nu} = \partial_\mu A^a_\nu - \partial_\nu A^a_\mu + g\epsilon_{abc} A^b_\mu A^c_\nu$ and $B_{\mu\nu} = \partial_\mu B_\nu - \partial_\nu B_\mu$ are the respective field strengths, g and g' are the couplings. Here T^a are the generators of $SU(2)_{\rm L}$ satisfying $\left[T^a, T^b\right] = i\epsilon^{abc}T^c$ and Y is the weak hypercharge. Note that there is a slight difference in the normalization conventions for the scalar potential in comparison with the last Chapter.

The Higgs field H is a $SU(2)_{\rm L}$ doublet with hypercharge $Y(H) = +1/2$. The scalar potential induces a non-trivial vacuum expectation value given by $|\langle H\rangle|^2 = v^2/2 = m^2/2\lambda$. Below this energy scale, the theory is cast into the Higgs phase with three massive vector bosons $W^\pm_\mu$, Z_μ, a massive scalar h and a massless photon A_μ (γ) in the spectrum. The physical fields can be written using the Weinberg angle θ_W: the neutral vector bosons are defined by $Z_\mu = \cos\theta_W\, A^3_\mu - \sin\theta_W\, B_\mu$ and $A_\mu = \sin\theta_W\, A^3_\mu + \cos\theta_W\, B_\mu$, whereas the charged vector fields are defined by $W^\pm_\mu = \left(A^1_\mu \mp i A^2_\mu\right)/\sqrt{2}$.

The masses of the vector bosons can be precisely measured and are $m_W = gv/2 = 80.4$ GeV and $m_Z = m_W/\cos\theta_W = 91.2$ GeV. The Weinberg angle can be experimentally determined and satisfies $\sin^2\theta_W = 0.23$. After symmetry breaking, the kinetic part of the gauge Lagrangian (omitting mass terms) reads

$$\mathcal{L}^{\rm Kin}_{\rm Gauge} = -\frac{1}{4}\, F_{\mu\nu}F^{\mu\nu} - \frac{1}{4}\, Z_{\mu\nu}Z^{\mu\nu} - \frac{1}{2}\, W^+_{\mu\nu}W^{\mu\nu-}\,, \tag{3.5}$$

where the field-strength tensors are defined as usual.

We may now introduce the leptons through the following Lagrangian:

$$\mathcal{L}_{\rm Leptons} = i\,\bar{L}_i\gamma^\mu D_\mu L_i + i\,\bar{\ell}_{iR}\gamma^\mu D_\mu \ell_{iR}\,, \tag{3.6}$$

where L_i denotes the lepton doublets $L_i = (\nu_{iL}\ \ \ell_{iL})^t$ with ν_{iL}, ℓ_{iL} and ℓ_{iR} representing the left-handed neutrinos, the left-handed charged leptons and the right-handed lepton fields, respectively. Here i is a flavor index to distinguish between the three generations of leptons. The hypercharge assignment adopted here is: $Y(L_i) = -1/2$ and $Y(\ell_{iR}) = -1$. Taking Eq. (3.6) with Eq. (3.4) including the gauge fields after symmetry breaking we obtain the interactions between matter and gauge fields. In what follows only two such interaction terms will be relevant, namely,

$$\mathcal{L}_{ee\gamma} = -e\bar{\ell}_i\gamma_\mu\ell_i A^\mu\,, \tag{3.7}$$

$$\mathcal{L}_{eeZ} = \frac{g}{4\cos\theta_W}\bar{\ell}_i\gamma_\mu\left(-1 + 4\sin^2\theta_W + \gamma^5\right)\ell_i Z^\mu\,. \tag{3.8}$$

Here we propose a general extension of the weak hypercharge sector of the EW La-

grangian, in the same spirit that we considered in the last Chapter:

$$\mathcal{L} = -\frac{1}{4} B_{\mu\nu} B^{\mu\nu} \quad \longrightarrow \quad \mathcal{L}_{\rm Y} = f\left(\mathcal{F}, \mathcal{G}\right) , \tag{3.9}$$

where we defined the Lorentz and gauge-invariant objects as usual

$$\mathcal{F} = \frac{1}{4} B_{\mu\nu} B^{\mu\nu} \qquad \text{and} \qquad \mathcal{G} = \frac{1}{4} B_{\mu\nu} \tilde{B}^{\mu\nu} \tag{3.10}$$

with the dual field-strength tensor given by $\tilde{B}^{\mu\nu} = \frac{1}{2}\epsilon^{\mu\nu\rho\sigma} B_{\rho\sigma}$. This type of non-linear extension was already discussed in the last Chapter, where it was shown that under certain conditions, it allows a finite-energy electroweak monopole solution.

The SM predictions are so far in excellent agreement with experiment and, in order to recover the usual SM results, we demand that our general extension $f\left(\mathcal{F}, \mathcal{G}\right)$ reproduces the usual term $-\frac{1}{4} B_{\mu\nu} B^{\mu\nu}$ in some appropriate limit. Since we do not want to have a parity-violating term in the photon sector after spontaneous symmetry breaking, we impose the assumption that $f\left(\mathcal{F}, \mathcal{G}\right)$ depends on $\mathcal{G}$ only through $\mathcal{G}^2$. These physically motivated assumptions were also adopted in the last Chapter.

Let us consider, for instance, a Born-Infeld (BI) extension of the hypercharge sector [24] given by

$$\mathcal{L}_{\rm Y}^{\rm BI} = \beta^2 \left[1 - \sqrt{1 + 2\left(\frac{\mathcal{F}}{\beta^2} - \frac{\mathcal{G}^2}{2\beta^4} \right)} \right] , \tag{3.11}$$

where β is a parameter with dimension of mass squared. This non-linear extension has been extensively studied in the context of electrodynamics, with applications in a range of subjects, and has attracted a lot of interest in the recent years after the observation of light-by-light scattering at the LHC [49, 50, 51]. Interestingly enough, the BI action can be derived from String Theory [57] and also appears in the dynamics of D-branes [58].

Our goal is to study the phenomenological consequences of the non-linear extension in high-energy processes. To accomplish this, we need to obtain the induced operators written in terms of the physical fields after symmetry breaking. The mass scale set by $\sqrt{\beta}$ is expected to be large in comparison with the typical energies of the processes considered, motivating us to perform a Taylor expansion of Eq. (3.11) in powers of $X = \frac{\mathcal{F}}{\beta^2} - \frac{\mathcal{G}^2}{2\beta^4}$:

$$\mathcal{L}_{\rm Y} = -\mathcal{F} + \frac{1}{2\beta^2}\left[\mathcal{F}^2 + \mathcal{G}^2\right] + \mathcal{O}\left(1/\beta^4\right) . \tag{3.12}$$

We will only consider tree-level processes with at most four gauge bosons in each vertex, so we can safely restrict ourselves to leading non-trivial order. It is important to keep in mind that this perturbative approach can only be trusted as long as the energy of the process is lower than the mass scale set by $\sqrt{\beta}$, as this guarantees that the next terms in

the expansion provide increasingly negligible corrections to the leading-order terms.

Furthermore, taking into consideration the recent interest in different versions of non-linear electrodynamics, we could also consider other interesting extensions that would give rise to the same physical effects in the approximation considered here. In fact, using X defined above, we could as well have considered here the other extensions that we used in the last Chapter, given by $\mathcal{L}_{\rm Y}^{\rm Log} = -\beta^2 \log\left[1+X\right]$ and $\mathcal{L}_{\rm Y}^{\rm Exp} = \beta^2\left[e^{-X}-1\right]$ giving us the $U(1)_{\rm Y}$ version of the logarithmic [43] and exponential [44, 45] non-linear electrodynamics. The three extensions agree up to leading non-trivial order and we will restrict ourselves to tree-level processes with at most four gauge bosons interactions, so we may safely consider the β parameters as being equal with a good approximation and use Eq. (3.12) to describe their common effects.

The Lagrangian above is a function of the $U(1)_{\rm Y}$ gauge field, B_μ, but after symmetry breaking we can write it in terms of the physical fields, A_μ and Z_μ, retrieving the usual SM kinetic terms at zeroth order. At first order we have ($s_\theta \equiv \sin\theta_W, c_\theta \equiv \cos\theta_W$)

$$\begin{aligned}
\mathcal{L}_{\rm Y}^{(1/\beta^2)} &= \frac{1}{32\beta^2}\Big\{ s_\theta^4\left[(ZZ)(ZZ)+(Z\tilde{Z})(Z\tilde{Z})\right] \\
&+ c_\theta^4\left[(FF)(FF)+(F\tilde{F})(F\tilde{F})\right] \\
&+ 2s_\theta^2c_\theta^2\left[(FF)(ZZ)+(F\tilde{F})(Z\tilde{Z})\right] \\
&+ 4s_\theta^2c_\theta^2\left[(ZF)(ZF)+(Z\tilde{F})(Z\tilde{F})\right] \\
&- 4s_\theta^3c_\theta\left[(ZZ)(ZF)+(Z\tilde{Z})(Z\tilde{F})\right] \\
&- 4s_\theta c_\theta^3\left[(FF)(FZ)+(F\tilde{F})(F\tilde{Z})\right]\Big\}, \qquad (3.13)
\end{aligned}$$

where we defined $(ZZ) \equiv Z_{\mu\nu}Z^{\mu\nu}$ with an analogous definition for the dual versions. All non-linearly induced vertices above have the same momentum structure and very similar Feynman rules; this traces back to the common origin of such interactions.

In conclusion, we see that our non-linear extension in the hypercharge sector generates a series of dimension-eight effective operators generically suppressed by a factor $(\mathcal{E}/\Lambda)^4$, where $\mathcal{E}$ is a typical energy scale characteristic of the process and Λ is the mass scale set by $\sqrt{\beta}$. These effective operators will introduce new vertices, allowing processes that could only occur in the SM at loop-level to take place already at tree-level. In the next section we explore this fact and consider different high-energy processes to obtain lower bounds on β whenever experimental data are available. We also discuss the impact of our non-linear extension on scattering processes involving neutral gauge bosons.

3.2 Experimental limits

In the section above we have extracted quartic interaction vertices between the photon and Z-boson which are completely absent from the SM, thus opening up interesting possibilities to constrain the parameter β. In the following we explore a few of them.

3.2.1 $Z \to 3\,\gamma$

In the SM there is no tree-level $Z\gamma\gamma\gamma$ vertex, so the decay process $Z \to 3\,\gamma$ proceeds exclusively via fermion and W-boson loops [59, 60]. The theoretical prediction for the partial width is $\Gamma\left(Z \to 3\,\gamma\right)_{\rm SM} = 1.35$ eV [61] and, given the experimentally determined total width of the Z-boson $\Gamma^{\rm Z}_{\rm exp} = 2.49$ GeV [62], the expected branching ratio is $\mathrm{BR}\left(Z \to 3\,\gamma\right)_{\rm SM} = 5.4 \times 10^{-10}$. The currently best upper bound was obtained by the ATLAS collaboration using pp collisions at $\sqrt{s} = 8$ TeV and reads [63]

$$\mathrm{BR}\left(Z \to 3\,\gamma\right)_{\rm exp} < 2.2 \times 10^{-6}\,, \tag{3.14}$$

representing a five-fold improvement on the previous determination from LEP [64]. This process is clearly very rare and could not yet be measured directly. It is thus an ideal testing ground for new physics [65, 66].

The SM prediction is compatible with the best current experimental bound, but there is a vast gap between them. The non-linear extension can therefore be constrained by comparing its prediction to the experimental bound, cf. Eq. (3.14). The tree-level amplitude for a Z-boson with 4-momentum p decaying into three photons with 4-momenta q_k (k = 1,2,3) is

$$-i\mathcal{M} = \epsilon_\alpha(p) V^{\alpha\beta\gamma\delta}_{Z3\gamma}\left(\beta\right) \epsilon^*_\beta(q_1)\epsilon^*_\gamma(q_2)\epsilon^*_\delta(q_3)\,, \tag{3.15}$$

where the vertex factor

$$V^{\alpha\beta\gamma\delta}_{Z3\gamma}\left(\beta\right) = -i\frac{s_\theta c^3_\theta}{\beta^2} f^{\alpha\beta\gamma\delta} \tag{3.16}$$

may be read from the last line of Eq. (3.13). The momentum-dependent function $f^{\alpha\beta\gamma\delta}$

is given by

$$\begin{aligned}
-f^{\alpha\beta\gamma\delta} &= \Big[(q_1\cdot q_2)\eta^{\beta\gamma} - q_1^\gamma q_2^\beta\Big]\left[(p\cdot q_3)\eta^{\alpha\delta} - p^\delta q_3^\alpha\right] \\
&+ \Big[(q_1\cdot q_3)\eta^{\beta\delta} - q_1^\delta q_3^\beta\Big]\left[(p\cdot q_2)\eta^{\alpha\gamma} - p^\gamma q_2^\alpha\right] \\
&+ \left[(q_2\cdot q_3)\eta^{\gamma\delta} - q_2^\delta q_3^\gamma\right]\left[(p\cdot q_1)\eta^{\alpha\beta} - p^\beta q_1^\alpha\right] \\
&+ \epsilon^{\mu\beta\rho\gamma}\epsilon^{\nu\delta\kappa\alpha}p_\kappa q_{1\mu}q_{2\rho}q_{3\nu} \\
&+ \epsilon^{\mu\beta\rho\delta}\epsilon^{\nu\gamma\kappa\alpha}p_\kappa q_{1\mu}q_{2\nu}q_{3\rho} \\
&+ \epsilon^{\mu\gamma\rho\delta}\epsilon^{\nu\beta\kappa\alpha}p_\kappa q_{1\nu}q_{2\mu}q_{3\rho}\,. \qquad (3.17)
\end{aligned}$$

Here we have assumed that p flows into the vertex, whereas the q_k flow out of it. Incidentally, this momentum structure is the same for all vertices in Eq. (3.13).

From this point on, we neglect the loop-level SM amplitude so the tree-level result from Eq. (3.15) is essentially the only contribution to the decay. The unpolarized squared amplitude reads

$$\langle|\mathcal{M}|^2\rangle = \frac{8s_\theta^2 c_\theta^6}{3\beta^4}\Phi(p,q_1,q_2,q_3)\,, \qquad (3.18)$$

with the momentum factor given by

$$\Phi(p,q_1,q_2,q_3) = \frac{1}{2}\left(p\cdot q_1\right)^2\left(q_2\cdot q_3\right)^2 + \text{perm.}\,, \qquad (3.19)$$

where "perm." indicates all permutations of the q_k. In the rest frame of the decaying Z-boson, $p^\mu = (m_Z, 0)$, and the outgoing photons have $E_k = |\mathbf{q}_k|$. By applying the usual dispersion relations and momentum conservation, we find

$$p\cdot q_3 = m_Z E_3 \quad \text{and} \quad q_1\cdot q_2 = \frac{m_Z^2}{2} - m_Z E_3\,, \qquad (3.20)$$

with similar results for the other 4-momenta pairs. Therefore, we can rewrite $\Phi(p,q_1,q_2,q_3)$ as

$$\Phi(p,q_1,q_2,q_3) = \frac{m_Z^4}{4}\sum_{k=1,2,3} E_k^2(m_Z - 2E_k)^2\,. \qquad (3.21)$$

Notice that this expression is symmetric under the change of final photons, a reasonable behavior since there is no preferred photon in this decay. As the phase space integral also enjoys this symmetry, we can simply use one of the terms above to do the integration and multiply the output by three, since they will necessarily give the same result. The partial width is defined as

$$d\Gamma = \frac{1}{3!}\frac{1}{2m_Z}\langle|\mathcal{M}|^2\rangle d\Pi_3\,, \qquad (3.22)$$

where 1/3! is the the symmetry factor due to the identical photons in the final state. The

three-body phase-space function is

$$\begin{aligned} d\Pi_3 &= \frac{d^3\mathbf{q}_1}{(2\pi)^3\,2E_1}\frac{d^3\mathbf{q}_2}{(2\pi)^3\,2E_2}\frac{d^3\mathbf{q}_3}{(2\pi)^3\,2E_3} \\ &\times \ (2\pi)^4\delta^4\left(p-q_1-q_2-q_3\right)\,. \end{aligned} \tag{3.23}$$

We have then

$$\begin{aligned} d\Gamma &= K\frac{E_3(m_Z-2E_3)^2}{E_1E_2}d^3\mathbf{q}_1d^3\mathbf{q}_2d^3\mathbf{q}_3 \\ &\times \ \delta^4\left(p-q_1-q_2-q_3\right), \end{aligned} \tag{3.24}$$

where the constant K, already including the factor of three, is

$$K=\frac{s_\theta^2c_\theta^6m_Z^3}{1536\pi^5\beta^4}\,. \tag{3.25}$$

The rest of the calculation follows a path similar to the textbook calculation of muon decay [67]. The delta function may be split into two factors enforcing energy and 3-momentum conservation. The latter allows us to write $\mathbf{q}_2 \to -(\mathbf{q}_1+\mathbf{q}_3)$ and $E_2 \to |\mathbf{q}_1+\mathbf{q}_3|$. Let us take the polar axis along $\mathbf{q}_3$, which is held fixed, so that

$$\begin{aligned} E_2(\cos\theta) &= |\mathbf{q}_1+\mathbf{q}_3| \\ &= \sqrt{E_1^2+E_3^2+2E_1E_3\cos\theta}\,. \end{aligned} \tag{3.26}$$

We may then write $d^3\mathbf{q}_1 = 2\pi E_1^2 d|\mathbf{q}_1|d\cos\theta$ and we have

$$\begin{aligned} d\Gamma &= 2\pi K\frac{E_1E_3(m_Z-2E_3)^2}{|\mathbf{q}_1+\mathbf{q}_3|}d^3\mathbf{q}_3dE_1d\cos\theta \\ &\times \ \delta\left[g(\cos\theta)\right]\,, \end{aligned} \tag{3.27}$$

where $g(\cos\theta) = m_Z - E_1 - E_2(\cos\theta) - E_3$.

Now, the delta function cannot be directly integrated, so we need to change variables. This redefinition leads to

$$\delta\left[g(\cos\theta)\right] = \frac{E_2(\cos\theta)}{E_1E_3}\delta\left(\cos\theta-\cos\theta_0\right)\,, \tag{3.28}$$

where $\cos\theta_0$ is such that $g(\cos\theta_0)=0$. The delta function now implies that both the maximum energy of any individual photon and the minimum energy of any pair of photons are $m_Z/2$. Consequently, we have E_1 and E_3 limited to the ranges $(\frac{m_Z}{2}-E_3,\ \frac{m_Z}{2})$ and $(0,\ \frac{m_Z}{2})$, respectively. Performing the remaining integrations and dividing by the Z-boson

width we find that the branching ratio is given by

$$\begin{aligned} \mathrm{BR}\left(Z \to 3\,\gamma\right)_{\mathrm{Y}} &= \frac{s_\theta^2 c_\theta^6}{184320\,\pi^3\,\Gamma^{\mathrm{Z}}_{\mathrm{exp}}}\frac{m_Z^9}{\beta^4} \\ &= 6.7\times 10^{-7}\left(\frac{m_Z}{\sqrt{\beta}}\right)^8 . \end{aligned} \tag{3.29}$$

We are finally able to place an experimental bound on β. The branching ratio predicted by the SM is extremely small ($\sim 10^{-10}$), way below current experimental sensitivities. Allowing the result above to fully saturate the experimental upper limit, *i.e.*, $\mathrm{BR}\left(Z \to 3\,\gamma\right)_{\mathrm{Y}} \simeq \mathrm{BR}\left(Z \to 3\,\gamma\right)_{\mathrm{exp}}$, cf. Eq. (3.14). This implies that

$$\sqrt{\beta} \gtrsim 80\,\mathrm{GeV}\,, \tag{3.30}$$

which is slightly lower than the currently best bound [25]. In Ref. [68] the authors adopted the result of Eq. (3.30) above on the BI parameter to make estimates on the redshift and to discuss birefringence and dichroism in connection with a class of p-extended BI-type actions in the presence of an external uniform magnetic field.

Here we must add an important remark. The energy scale of a decay process is set by the mass of the decaying particle, here given by $m_Z = 91.2$ GeV. Therefore, the bound obtained above must be taken with a grain of salt since it represents a mass scale lower than the energy of the process, challenging the basic assumption behind our effective-theory approach. Nonetheless, it is worth noticing that this restriction is a matter of experimental limitation: the best bound on the Z-decay into three photons is still orders of magnitude away from the SM prediction, so we may confidently expect that future experiments will yield much more stringent bounds on it, therefore significantly improving on the result above.

The lower bound in Eq. (3.30) is clearly limited by the experimental sensitivity. If the current experimental upper bound on the branching ratio (cf. Eq. (3.14)) would be improved by a factor of ~ 3 – a smaller improvement than the one from ATLAS [63] relative to LEP [64] – we would be able to exclude the region $\sqrt{\beta} \lesssim m_Z$. Future lepton colliders, *e.g.*, ILC [69, 70, 71, 72] and FCC-ee [73, 74], whose main goal is precision Higgs physics, could operate at the Z-pole and produce a vast sample of Z-bosons: the ILC and the FCC-ee could produce respectively 10^2 and 10^5 times more Z-bosons than LEP. It is therefore possible, with much better statistics and improved detector capabilities, to improve the upper limit on $\mathrm{BR}\left(Z \to 3\gamma\right)$ enough to constrain $\sqrt{\beta}$ at or above m_Z.

In Fig. 3.1 we plot the lower bound on $\sqrt{\beta}$ as a function of the future improvement of the experimental sensitivity, $\mathrm{BR}\left(Z \to 3\,\gamma\right)_{\mathrm{exp}}$, relative to the currently best one [63]. The situation discussed in the paragraph above is illustrated by the area shaded in red: an improvement of at least ~ 3 would lead to viable bounds. The unfortunately weak

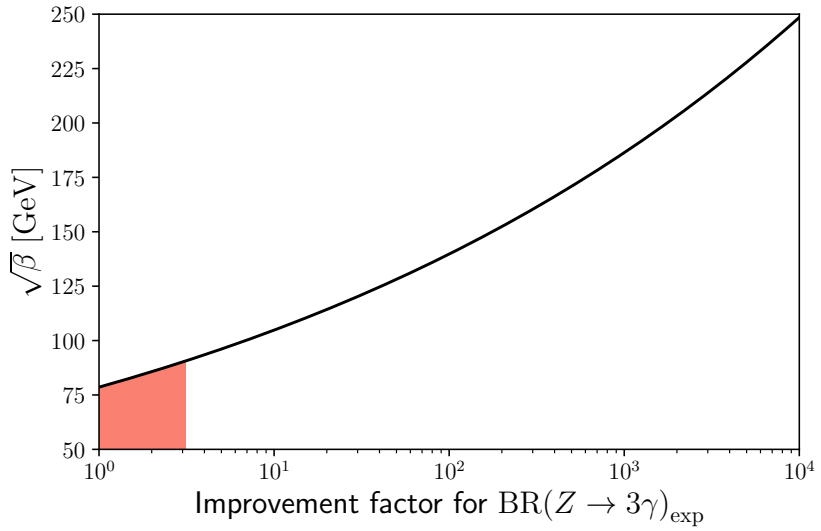

Figure 3.1: Projection for the lower bound on $\sqrt{\beta}$ as a function of the improvement factor of the experimental sensitivity relative to the currently best one, cf. Eq. (3.14) [63]. Incidentally, Eq. (3.29) reaches the order of magnitude of the SM prediction with $\sqrt{\beta} \sim$ 220 GeV. The region shaded in red is such that $\sqrt{\beta} < m_Z$, where our predictions are not accurate.

dependence of the expansion parameter on the experimental sensitivity is made explicit by the slope of the curve, meaning that only large improvements in sensitivity would lead to noticeable improvements in the lower bound on our non-linear extension.

As a final remark we note that the discussion above relies on the fact that, so far (and in the foreseeable future), only upper limits on the process $Z \to 3\,\gamma$ could be placed. The SM prediction is four orders of magnitude below the currently best upper bound, so we may also speculate about possible limits on the expansion parameter in case the SM expectation is eventually confirmed. In this scenario there is no tension between the SM and experiment, so we may assume that the non-standard result is responsible for a small correction of the SM prediction, being hidden under the (relative) experimental uncertainty, *i.e.*, $\mathrm{BR}_{\mathrm{Y}}(\beta)/\mathrm{BR}_{\mathrm{SM}} \lesssim \delta_{\mathrm{exp}}$. Conservatively assuming $\delta_{\mathrm{exp}} \sim 10\%$ would allow us to place the strong lower bound $\sqrt{\beta} \gtrsim 295$ GeV. For even better precisions of 1% and 0.1% we find $\sqrt{\beta} \gtrsim 395$ GeV and $\sqrt{\beta} \gtrsim 530$ GeV, respectively.

3.2.2 $e^-\,e^+ \to 3\,\gamma$

Hadron colliders have played a central role in the establishment of the SM as our best theory of elementary particles and their interactions; great examples are the discoveries of the W- and Z-bosons, as well as of the Higgs scalar. However, lepton colliders, such as LEP, were crucial in subsequent precision measurements, helping to probe not only

tree-level predictions, but also radiative corrections [75]. The next development is to achieve even higher precision in measurements of electroweak parameters, in particular those related to the Higgs and gauge bosons [76].

Lepton colliders represent optimal tools to this end and next-generation machines have been proposed, such as ILC [69, 70, 71, 72], FCC-ee [73, 74], CEPC [77] and CLIC [78]. These are designed to study the SM in great detail, but searching for deviations from the SM that could hint at new physics is an equally important goal. In this context, the process $e^- e^+ \to 3\,\gamma$ offers an interesting option to test modifications of the gauge couplings, in particular those involving photons and Z-bosons. From Eq. (3.13) we see that our non-linear extension induces precisely such anomalous couplings that could give rise to new contributions for processes with three photons in the final state. We note that the SM contribution is very well described by QED with negligible electroweak corrections.

The QED contribution to $e^- e^+ \to 3\,\gamma$ at tree-level is given by

$$\begin{aligned} - \quad & i\mathcal{M}_{\rm QED} = ie^3 \overline{v}(p_2) \Bigg[\gamma^\rho \frac{\not{p}_1 - \not{q}_1 - \not{q}_2}{(p_1 - q_1 - q_2)^2} \gamma^\nu \\ \times \quad & \frac{\not{p}_1 - \not{q}_1}{(p_1 - q_1)^2} \gamma^\mu \Bigg] u(p_1) \epsilon^*_\mu(q_1) \epsilon^*_\nu(q_2) \epsilon^*_\rho(q_3)\,, \end{aligned} \tag{3.31}$$

which must be added to the other five amplitudes obtained from this one by permutation of the external photons. We are considering high-energy scatterings, so the electron mass may be safely neglected. The non-linearly induced photon- and Z-mediated amplitudes are given by

$$\begin{aligned} -i\mathcal{M}_\gamma &= \frac{-e}{(p_1+p_2)^2} \overline{v}(p_2) \gamma_\mu u(p_1) \\ &\times \; V_{4\gamma}^{\mu\nu\beta\rho}(\beta)\, \epsilon^*_\nu(q_1) \epsilon^*_\beta(q_2) \epsilon^*_\rho(q_3)\,, \end{aligned} \tag{3.32}$$

$$\begin{aligned} -i\mathcal{M}_{\rm Z} &= \frac{g_Z}{(p_1+p_2)^2 - m_Z^2 + i m_Z \Gamma_Z} \\ &\times \; \overline{v}(p_2) \gamma_\mu \left(c_v - c_a \gamma^5 \right) u(p_1) \\ &\times \; V_{Z3\gamma}^{\mu\nu\beta\rho}(\beta)\, \epsilon^*_\nu(q_1) \epsilon^*_\beta(q_2) \epsilon^*_\rho(q_3)\,, \end{aligned} \tag{3.33}$$

where $g_Z = e/4 s_\theta c_\theta$, $c_v = -1 + 4 s_\theta^2$ and $c_a = -1$. The Z-width is $\Gamma_Z = 2.49$ GeV. The $Z\gamma\gamma\gamma$ vertex was defined in Eq. (3.16) and the four-photon vertex is analogous:

$$V_{4\gamma}^{\alpha\beta\gamma\delta}(\beta) = i \frac{c_\theta^4}{\beta^2} f^{\alpha\beta\gamma\delta}\,. \tag{3.34}$$

The function $f^{\alpha\beta\gamma\delta}$ is given by Eq. (3.17) with the appropriate relabelling of the 4-momenta.

The total tree-level amplitude for the process, $\mathcal{M}$, is $\mathcal{M} = \mathcal{M}_{\rm QED} + \mathcal{M}_\gamma + \mathcal{M}_{\rm Z}$ and

the total unpolarized cross section is given by

$$d\sigma = \frac{1}{3!}\frac{1}{2E_{\rm cm}^2}\langle|\mathcal{M}|^2\rangle d\Pi_3\,, \tag{3.35}$$

where 1/3! is the the symmetry factor due to the identical photons in the final state and the phase-space factor is the same as in Eq. (3.23). The squared amplitude is essentially the sum of three contributions: a pure QED part, an interference term between QED and the non-linear amplitudes, and a purely non-linear term.

Let us discuss first the tree-level QED results for $e^-e^+ \to \gamma\gamma(\gamma)$. The experimental results from LEP included cross sections with final states of two and three photons subjected to detector cuts in energy and scattering angle, namely, $E_\gamma > 5$ GeV and $|\cos\theta_\gamma| < 0.96$ [79, 80], so it is important to understand the tree-level expectation from QED to $e^-e^+ \to \gamma\gamma$ and $e^-e^+ \to \gamma\gamma\gamma$ under these conditions.

We start with the simplest case, $e^-e^+ \to \gamma\gamma$. Since there are two identical particles in the final state and the reaction takes place at the CM, the two photons carry the same energy as the colliding electron. Assuming monochromatic beams with energies $\mathcal{O}(100\,\text{GeV})$, the outgoing photons automatically satisfy the energy cut. The tree-level differential cross section is given by the well-known result

$$\frac{d\sigma^{2\gamma}_{\rm QED}}{d\cos\theta} = \frac{2\pi\alpha^2}{s}\left(\frac{1+\cos^2\theta}{1-\cos^2\theta}\right)\,. \tag{3.36}$$

For two identical particles, the polar angle is confined to the range $0 \leq \cos\theta_\gamma \leq 1 - c_{\rm cut}$ and, integrating Eq. (3.36) in this range, we find[2]

$$\sigma^{2\gamma}_{\rm QED} = \frac{2\pi\alpha^2}{s}\left[\log\left(\frac{2-c_{\rm cut}}{c_{\rm cut}}\right) + c_{\rm cut} - 1\right]\,. \tag{3.37}$$

For LEP at $\sqrt{s} = 207$ GeV with $c_{\rm cut} = 0.04$ we get 9.6 pb. It is worthwhile pointing out that the divergence in the forward-backward direction leads to a significant reduction of the total cross section even for small angular cuts.

Let us now move on to the more involved case of $e^-e^+ \to \gamma\gamma\gamma$. The typical amplitude is given in Eq. (3.31), which must be added to other five similar contributions with permutations of the photon 4-momenta. If we define $p_{ij} = p_i \cdot q_j$ and $q_{ij} = q_i \cdot q_j$, the squared and spin-averaged amplitude can be written as

$$\langle|\mathcal{M}_{3\gamma}|^2\rangle = \mathcal{Q}\left[p_{11}\sum_{n=0}^{3}(p_1\cdot p_2)^n Q_n + \text{perm.}\right] \tag{3.38}$$

where "perm." indicates that we must add the expression with the photon labels reshuf-

[2]In order to keep track of the forward-backward enhancement in the ultra-relativistic limit it is usually imposed that $c_{\rm cut} = 2m_e^2/s$.

fled. The pre-factor is

$$\mathcal{Q} = \frac{2e^6}{(p_{11})(p_{12})(p_{13})(p_{21})(p_{22})(p_{23})} \tag{3.39}$$

and the terms in the sum are

$$\begin{aligned}
Q_0 &= p_{12}\Big[p_{13}p_{21}p_{22} + p_{23}\big(p_{11}p_{22} + p_{23}(p_{22} - q_{12}) + p_{21}(p_{22} + q_{23})\big)\Big] - p_{11}p_{22}p_{23}q_{23}\,, \\
Q_1 &= p_{12}\Big[p_{13}p_{21} - p_{21}(p_{22} - 4p_{23}) + p_{23}(p_{23} - q_{23})\Big] \\
&+ p_{22}\Big[p_{11}(-p_{22} + p_{23} + q_{23}) - p_{23}q_{12} + p_{22}q_{13} + p_{21}p_{23}\Big]\,, \\
Q_2 &= -2p_{12}p_{21} - p_{22}(2p_{21} - q_{12} + q_{13} + q_{23})\,, \\
Q_3 &= p_{21}\,.
\end{aligned} \tag{3.40a}$$

The final averaged squared amplitude can be symbolically recast in the form

$$\langle|\mathcal{M}_{3\gamma}|^2\rangle = \frac{e^6}{E_{\rm cm}^2}\mathcal{C}(p_i, q_j)\,, \tag{3.41}$$

where we have expressed all dimensional parameters in terms of the CM energy – in this way $\mathcal{C}(p_i, q_j)$ is effectively dimensionless. Taking into account the phase-space volume, cf. Eq. (3.23), the integral to be solved is

$$\mathcal{I}_{\rm QED} = \int \mathcal{C}(p_i, q_j)\frac{d^3\mathbf{q}_1}{E_1}\frac{d^3\mathbf{q}_2}{E_2}\frac{d^3\mathbf{q}_3}{E_3}\delta^4\left(\Sigma p_i - \Sigma q_j\right), \tag{3.42}$$

but an analytical treatment is cumbersome, so we resort to numerical methods, which also facilitate the application of the detector cuts. The results of the Monte Carlo integral are listed in table 3.1 for a few interesting values of the CM energy. The tree-level cross section for $e^-e^+ \to \gamma\gamma\gamma$ is ($e^2 = 4\pi\alpha$)

$$\sigma_{\rm QED}^{3\gamma} = \frac{\alpha^3}{48\pi^2 s}\mathcal{I}_{\rm QED} \simeq 8\times 10^{-3}\cdot\mathcal{I}_{\rm QED}\left(\frac{200\,\text{GeV}}{\sqrt{s}}\right)^2 \text{fb}\,. \tag{3.43}$$

Using $\sqrt{s} = 207$ GeV as an example, we have 0.285 pb.

Let us now discuss the interference term, $\langle|\mathcal{M}|^2_{\rm QED-Y}\rangle$. The interference amplitude between pure QED and the non-linear contributions may be written as

$$\langle|\mathcal{M}_{\rm QED-Y}|^2\rangle = \mathcal{H}\left[\sum_{n=0}^{3}(p_1\cdot p_2)^n H_n + \text{perm.}\right] \tag{3.44}$$

with

$$\mathcal{H} = \frac{c_\theta^2 e^4}{2\beta^2 p_1\cdot p_2\,(p_{11}p_{12}p_{13}p_{21}p_{22}p_{23})}\frac{\mathcal{H}_{\rm num}}{\mathcal{H}_{\rm den}} \tag{3.45}$$

and

$$\mathcal{H}_{\rm num} = 2c_\theta^2 m_Z^2\left(\Gamma_Z^2+m_Z^2\right)-\left(4c_\theta^2+3\right)m_Z^2(p_1\cdot p_2)+6(p_1\cdot p_2)^2\,, \tag{3.46a}$$

$$\mathcal{H}_{\rm den} = m_Z^4+\Gamma_Z^2 m_Z^2-4m_Z^2(p_1\cdot p_2)+4(p_1\cdot p_2)^2\,. \tag{3.46b}$$

The coefficients in Eq. (3.44) are given by

$$\begin{aligned} H_0 &= 2p_{22}\Bigg[(p_{11})^2\Big[(p_{13})^3p_{21}p_{22} \\ &+ p_{12}(p_{23})^2(p_{21}q_{23}+p_{22}p_{23})-p_{12}p_{13}p_{23}\Big(p_{12}p_{21} \\ &+ p_{21}(q_{23}-2p_{23})+p_{22}(p_{23}-q_{13})\Big)\Big] \\ &- p_{11}p_{12}p_{13}p_{21}p_{23}(p_{21}q_{23}+p_{22}p_{23}) \\ &- (p_{12})^2(p_{13})^2(p_{21})^2p_{23}\Bigg]\,, \end{aligned} \tag{3.47a}$$

$$\begin{aligned} H_1 &= -p_{22}\Bigg\{2p_{12}p_{13}(p_{21})^2p_{22}q_{13} \\ &+ (p_{11})^2p_{23}\Big[2(p_{12})^2(p_{23}+q_{13}) \\ &+ p_{12}\Big(p_{13}(p_{21}+p_{22})-2p_{21}q_{23}\Big)+p_{13}p_{21}p_{22}\Big] \\ &+ p_{11}p_{21}\Big[2(p_{13})^2p_{21}p_{22}+p_{12}p_{13}\Big(2(p_{23}q_{12}+q_{13}q_{23}) \\ &+ p_{21}(p_{23}-2q_{23})\Big)+2p_{12}p_{23}q_{13}q_{23}\Big]\Bigg\}\,, \end{aligned} \tag{3.47b}$$

$$\begin{aligned} H_2 &= p_{11}p_{21}\Big[p_{13}p_{22}(2p_{11}q_{23}+p_{23}q_{12}) \\ &+ p_{12}p_{23}(p_{13}q_{12}+2p_{21}q_{23})\Big]\,. \end{aligned} \tag{3.47c}$$

To simplify matters, we may express all energies and 3-momenta in units of the CM energy, $E_{\rm cm}$, so that we can write it as

$$\langle|\mathcal{M}|^2_{\rm QED-Y}\rangle = \mathcal{X}_{\rm QED-Y}e^4c_\theta^2\frac{E_{\rm cm}^2}{\beta^2}\mathcal{A}(p_i,q_j)\,, \tag{3.48}$$

with $\mathcal{A}(p_i,q_j)$ representing a function of the now dimensionless energies and 3-momenta that the reader may obtain from Eq. (3.44). The pre-factor $\mathcal{X}_{\rm QED-Y}$ is given by ($x = m_Z^2/E_{\rm cm}^2$ and $y=\Gamma_Z^2/m_z^2$)

$$\mathcal{X}_{\rm QED-Y} = \frac{3-(3+4c_\theta^2)x+4c_\theta^2x^2(1+y)}{(1-x)^2+yx^2}\,. \tag{3.49}$$

From the phase-space volume we get another factor of $E_{\rm cm}^2$ that cancels the one present

in the denominator of Eq. (3.35), so that, putting all the numerical factors together, we finally obtain

$$\sigma\left(e^-e^+ \to 3\gamma\right)_{\mathrm{QED-Y}} = \mathcal{X}_{\mathrm{QED-Y}} \frac{\alpha^2 c_\theta^2}{384\pi^3} \frac{s}{\beta^2} \mathcal{I}_{\mathrm{QED-Y}} \tag{3.50}$$

with $s = E_{\mathrm{cm}}^2$, $e^2 = 4\pi\alpha$ and

$$\mathcal{I}_{\mathrm{QED-Y}} = \int \mathcal{A}(p_i, q_j) \frac{d^3\mathbf{q}_1}{E_1} \frac{d^3\mathbf{q}_2}{E_2} \frac{d^3\mathbf{q}_3}{E_3} \delta^4\left(\Sigma p_i - \Sigma q_j\right). \tag{3.51}$$

Note that the quantities in Eq. (3.51) are all expressed in units of $\sqrt{s} = E_{\mathrm{cm}}$, being therefore dimensionless.

Equation (3.51) cannot be easily evaluated analytically due to the complexity of the integrand, so we solve it numerically via standard Monte Carlo methods. The Dirac delta enforcing 4-momentum conservation severely constrains the phase-space volume available to the outgoing photons. In fact, their individual energies are bound to be at most 0.5 and the sum of any pair of energies must be larger than this value, allowing us to limit the range of the sampled 3-momentum components to the interval $[-0.5, 0.5]$. In what follows we use data from e^-e^+ collisions at LEP resulting in two or three photons and the cross sections quoted were obtained under the experimental conditions of the detector. That means that we have to impose similar cuts to our theoretical cross sections if we want to compare them to LEP data.

Particularly important are the angular and energy cuts imposed [79, 80]. Since the forward-backward direction along the beam is inaccessible, the range in polar angles is limited to $16^\circ \leq \theta_\gamma \leq 164^\circ$, *i.e.*, the detectable photons must satisfy $|\cos\theta_\gamma| \leq 0.96$ to be contained in the electromagnetic calorimeter. Furthermore, the individual photons must have an energy $E_\gamma > 5$ GeV. Even though Eq. (3.51) is written in terms of dimensionless quantities, the aforementioned lower threshold on the detectable energy of the single photons introduces an energy dependence, as the cut is expressed as $E_\gamma > 5/\sqrt{s}$. The values of the integral evaluated at selected energy values are quoted in table 3.1. For the sake of concreteness, the interference cross section at $\sqrt{s} = 207$ GeV is

$$\sigma_{\mathrm{QED-Y}}\left(\sqrt{s} = 207\,\mathrm{GeV}\right) \simeq 0.88 \left(\frac{250\,\mathrm{GeV}}{\sqrt{\beta}}\right)^4 \mathrm{fb}\,. \tag{3.52}$$

We now move on to the purely non-linear contribution, $\langle|\mathcal{M}|^2_{\mathrm{Y}}\rangle$, which is expected to be sub-dominant relative to the interference term discussed above. The purely non-linear amplitude is given by

$$\langle|\mathcal{M}_{\mathrm{Y}}|^2\rangle = \mathcal{J}\left[\sum_{n=0}^{3} (p_1 \cdot p_2)^n J_n + \mathrm{perm.}\right] \tag{3.53}$$

where

$$\mathcal{J} = \frac{c_\theta^4 e^2}{2\beta^4 (p_1 \cdot p_2)^2} \frac{\mathcal{J}_{\rm num}}{\mathcal{J}_{\rm den}}\,, \tag{3.54}$$

with

$$\begin{aligned} \mathcal{J}_{\rm num} &= 2c_\theta^4 m_Z^2 \left(\Gamma_Z^2 + m_Z^2\right) \\ &- 6c_\theta^2 m_Z^2 (p_1 \cdot p_2) + 5(p_1 \cdot p_2)^2\,, \qquad (3.55a) \\ \mathcal{J}_{\rm den} &= m_Z^4 + \Gamma_Z^2 m_Z^2 \\ &- 4m_Z^2 (p_1 \cdot p_2) + 4(p_1 \cdot p_2)^2\,. \qquad (3.55b) \end{aligned}$$

The coefficients in Eq. (3.53) are given by

$$\begin{aligned} J_0 &= 3(p_{11})^2 p_{22} p_{23} q_{23} - 6 p_{11} p_{12} p_{22} p_{23} q_{13} \\ &+ 3 p_{12} p_{13} (p_{21})^2 q_{23}\,, \qquad (3.56a) \\ J_1 &= 3 p_{11} q_{23} (p_{21} q_{23} - 2 p_{22} q_{13}) \\ &+ (p_{11})^2 (q_{23})^2 + (p_{21})^2 (q_{23})^2\,, \qquad (3.56b) \\ J_2 &= q_{12} q_{13} q_{23}\,. \qquad (3.56c) \end{aligned}$$

The unpolarized squared amplitude is stated in Eq. (3.53) and, after expressing the 4-momenta in units of $E_{\rm cm}$, we have

$$\langle |\mathcal{M}|^2_{\rm Y} \rangle = \mathcal{X}_{\rm Y} e^2 c_\theta^4 \frac{E_{\rm cm}^6}{\beta^4} \mathcal{B}(p_i, q_j)\,, \tag{3.57}$$

with $\mathcal{B}(p_i, q_j)$ represents a dimensionless function in analogy with $\mathcal{A}(p_i, q_j)$. The pre-factor is

$$\mathcal{X}_{\rm Y} = \frac{5 - 12c_\theta^2 x + 8c_\theta^4 x^2 (1+y)}{(1-x)^2 + y x^2}\,. \tag{3.58}$$

Equation (3.57) may be integrated analytically[3], but here we adopted the same Monte Carlo set-up employed in the calculation of the interference term. The cross section is then given by

$$\sigma\left(e^- e^+ \to 3\gamma\right)_{\rm Y} = \mathcal{X}_{\rm Y} \frac{\alpha c_\theta^4}{6144\pi^4} \frac{s^3}{\beta^4} \mathcal{I}_{\rm Y}\,, \tag{3.59}$$

where $\mathcal{I}_{\rm Y}$ is defined analogously to $\mathcal{I}_{\rm QED-Y}$, cf. Eq. (3.51). Specializing to $\sqrt{s} = 207$ GeV and using the numerical value of the integral including detector cuts from table 3.1, we have

$$\sigma_{\rm Y}\left(\sqrt{s} = 207\,{\rm GeV}\right) \simeq 0.01 \left(\frac{250\,{\rm GeV}}{\sqrt{\beta}}\right)^8 {\rm fb}\,. \tag{3.60}$$

In the discussion above we have obtained the total cross sections involving the novel

[3]The result without detector cuts is: $\sigma_{\rm Y} = \mathcal{X}_{\rm Y} \frac{\alpha c_\theta^4}{368640\pi^2} \frac{s^3}{\beta^4}$.

$\sqrt{s}$ [GeV]	91.2	207	250	350
$\mathcal{I}_{\mathrm{QED}}$	27006	37976	41796	45854
$\mathcal{I}_{\mathrm{QED-Y}}$	19.45	20.02	20.13	20.24
$\mathcal{I}_{\mathrm{Y}}$	0.138	0.139	0.139	0.139

Table 3.1: Values of the numerical integrals appearing in Eqs. (3.50), (3.59) and (3.42). The first two energy values are relevant in the context of existing LEP data [79, 80], whereas the last two are important for future e^-e^+ colliders, such as the ILC [69, 70, 71, 72, 82]. The following cuts were applied: $E_\gamma > 5$ GeV and $|\cos\theta_\gamma| < 0.96$ [79, 80].

neutral vertices originating in Eq. (3.13). The fact that only quartic vertices are produced implies that $e^-\,e^+ \to 2\,\gamma$ does not receive corrections, at least at tree-level, but $e^-\,e^+ \to 3\,\gamma$ does. From dimensional analysis alone we expect the number of events with two photons to be roughly two orders of magnitude times larger than with three photons, thus making dedicated searches for three-photon events harder. Therefore, more commonly, experiments look for multi-photon processes and the best available data to our knowledge were collected at LEP where the CM energy of the $e^-\,e^+$ pair was scanned passing by the Z-pole and reaching more than 200 GeV.

The L3 collaboration analyzed LEP data of events resulting in multiphoton final states [79, 80]. Since electroweak corrections are heavily suppressed, these measurements provide a clean test of QED, whose predictions were successfully confirmed. The calculations of the QED expectation were performed following ref. [81], where contributions up to $\mathcal{O}(\alpha^3)$ are considered, *i.e.*, the tree-level cross sections for two and three final photons plus radiative corrections. Here, however, we are working with an effective theory and we limit our analysis to tree-level and we refrain from employing their results.

The tree-level cross section for $e^-\,e^+ \to 2\,\gamma$ is well known, cf. Eq. (3.37). No closed form for the tree-level cross section for $e^-\,e^+ \to 3\,\gamma$ in the CM could be found, so we calculated the squared amplitude analytically and performed the phase-space integration numerically including the appropriate detector cuts; cf. eq (3.43). Let us consider concrete data to try to constrain $\sqrt{\beta}$. Since we are dealing with an effective theory whose effects grow with energy, we will ignore data at the Z-pole [79] and focus on the more promising high-energy results [80].

The L3 collaboration analyzed $e^-\,e^+ \to \gamma\gamma(\gamma)$ data in detail and indicates cross-section measurements for final states with two and three photons. The highest energy bin is 207 GeV (cf. table 3 of ref. [80]) and they quote the expected $\mathcal{O}(\alpha^3)$ cross section as 9.9 pb, whereas our tree-level result is 9.2 pb. Given that the difference includes radiative contributions deliberately unaccounted for here and possible effects from further selection criteria, we are confident that our calculation delivers a meaningful result for the QED prediction at tree-level.

Now, given that QED accurately describes the experimental data, we are only able to find lower bounds on $\sqrt{\beta}$. In fact, we may constrain it by demanding that the effects of

the non-linear extension hide under the relative experimental uncertainty

$$\frac{\sigma_{\text{QED}-\text{Y}} + \sigma_{\text{Y}}}{\sigma_{\text{QED}}} \lesssim \delta_{\text{exp}} \,, \tag{3.61}$$

with σ_{QED} being the tree-level expectation from QED. The cross sections for final states with two and three photons are respectively $\sigma^{2\gamma}_{\text{QED}}$, Eq. (3.37), and $\sigma^{3\gamma}_{\text{QED}}$, eq (3.43). For the sake of concreteness, we focus on the highest energy bin quoted in table 3 from ref. [80], $\sqrt{s} = 207$ GeV, for which the relative uncertainty of the measured cross section is $\delta_{\text{exp}} = 0.34/10.16 \simeq 0.034$. Plugging this and $\sigma^{2\gamma}_{\text{QED}} + \sigma^{3\gamma}_{\text{QED}} = 9.2$ pb into Eq. (3.61), we obtain $\sqrt{\beta} \gtrsim 73$ GeV.

The absolute number of $e^- e^+ \to 3\,\gamma$ events is also reported in ref. [80] for different energies, albeit without the respective experimental uncertainties. Focusing again on $\sqrt{s} = 207$ GeV, the expected tree-level cross section for pure QED is 0.29 pb. At this energy, 29 three-photon events were observed, so we may conservatively assume that the uncertainty is $\sim \sqrt{29} \simeq 5.4$ events. Taking into account the effective integrated luminosity, 87.8 pb^{-1}, this is equivalent to 0.06 pb, so that the relative uncertainty is $\delta_{\text{exp}} = 0.06/0.29 \simeq 0.21$. With $\sigma_{\text{QED}} = \sigma^{3\gamma}_{\text{QED}} = 0.29$ pb, Eq. (3.61) gives $\sqrt{\beta} \gtrsim 97$ GeV.

The bounds found above suffer from the same limitation as the one from the analysis of Z-decay: $\sqrt{\beta} < \sqrt{s}$. This is, however, not surprising, since the experimental uncertainties are orders of magnitude larger than the typical values expected from Eqs. (3.52) and (3.60). We are thus confronted with the fact that the currently available data on $e^- e^+ \to \gamma\gamma(\gamma)$ do not yield viable bounds on $\sqrt{\beta}$.

Despite being experimentally more challenging, measuring $e^- e^+ \to 3\,\gamma$ has the largest potential, as only the process directly affected by the non-linear effects is examined. We conclude, therefore, that a sensible lower limit on $\sqrt{\beta}$ could be placed if future $e^- e^+$ colliders would include measuring this process in their research programs. Let us take the ILC as an example, which targets a total integrated luminosity of 14 ab^{-1} over its full operation time [82]. For the sake of clarity, let us focus on the initial stage with $\sqrt{s} = 250$ GeV, where an integrated luminosity of ~ 500 fb^{-1} is planned to be attained in the first five years. Assuming similar detector cuts as at LEP and a (pessimistic) 1% effective luminosity[4], ~ 5 fb^{-1}, pure QED predicts 1073 three-photon events, whereas the non-linear terms would contribute with extra 3 events for $\sqrt{\beta} = 300$ GeV, *i.e.*, the level of precision required would be $3/1073 \sim 0.3\%$. A similar precision would be required at $\sqrt{s} = 350$ GeV with $\sqrt{\beta} = 400$ GeV.

[4]For comparison, the analysis of $e^- e^+ \to \gamma\gamma(\gamma)$ at LEP in the energy range 192 – 209 GeV contained 0.43 fb^{-1} of data, roughly ten times less.

3.2.3 Pure gauge-boson scatterings

The electroweak sector of the SM is based on the non-Abelian gauge group $SU(2)_{\rm L} \times U(1)_{\rm Y}$. This is manifest in the form of the covariant derivative, cf. Eq. (3.4), and the non-linear transformation properties of the gauge bosons. Particularly relevant is the presence of triple and quartic self-interaction couplings in the gauge sector. As a matter of fact, in a pure Yang-Mills theory, the quartic coupling is related to the triple one, even at the quantum level, as a consequence of gauge symmetry – this is a trade-mark feature of a non-Abelian gauge theory. Given that the structure of the gauge self-couplings in the electroweak sector is completely specified by construction, any deviations from this would suggest the presence of new physics.

Measurements of the gauge self-couplings are therefore especially interesting from both theoretical and experimental points of view. Particularly important are high-energy scattering processes involving the Z-boson and the photon, which could give a clear signal indicating SM extensions modifying the hypercharge sector like the one proposed here. With this in mind, we consider some of the possible scattering processes proceeding via the quartic couplings from Eq. (3.13) already at tree-level, instead of loop-level as predicted by the SM.

As mentioned in Sec. 3.2.2, e^-e^+ colliders offer clean conditions for precision tests of the SM. More interestingly, there are currently proposals of machines that can be adapted to work as linear photon colliders. Important sources of photons at a linear lepton collider include bremsstrahlung [83] and Compton laser back-scattering [84] (there is also beamstrahlung [85]). At LEP or LHC bremsstrahlung is the dominating form of radiation production, whereas at TESLA [86], ILC [69, 87] or CLIC [78, 88, 89], Compton back-scattering of electrons in intense lasers would be used to produce $\gamma\gamma$ or $e\gamma$ collisions. In this scenario, the photons created may carry a substantial amount of the electron energy [90].

Given that future linear e^-e^+ machines envision in their prospects the possibility of an extension to include photon colliders at relatively low cost, let us focus on $\gamma\gamma$ collisions producing exclusively vector bosons $V_i = \gamma,\, Z,\, W^\pm$. In this context, measuring *e.g.* the process $\gamma\gamma \to W^+W^-$ in a photon collider is an attractive option due to its large ($\sim$80 pb) cross section [91, 92]. The non-linear realization of the hypercharge sector proposed in this work, however, does not affect charged gauge bosons, so we shall focus on $\gamma\gamma$ fusion leading to neutral gauge bosons as final products: $\gamma\,\gamma \to \gamma\,Z$, $\gamma\,\gamma \to Z\,Z$ and $\gamma\,\gamma \to \gamma\,\gamma$. It is noteworthy that, within the SM framework, these processes receive only loop-level contributions, but here they will be induced at tree-level by the effective operators present in Eq. (3.13).

For the sake of concreteness, in the following we compute the non-linear contribution

to the unpolarized cross section of the process $\gamma\,\gamma \to \gamma\,Z$ at tree-level. Though we consider this particular process in more detail, all others may be analysed by similar means. From Eq. (3.13) we see that the relevant vertex factor is $V_{Z3\gamma}^{\alpha\beta\gamma\delta}$, cf. Eqs. (3.16) and (3.17), but with the substitutions: $p \to p_1$, $q_1 \to -p_2$, $q_2 \to q_1$ and $q_3 \to q_2$ appropriate for a 2-to-2 scattering.

The tree-level amplitude for this process is then

$$-i\mathcal{M} = \epsilon_\alpha(p_1)\epsilon_\beta(p_2)V_{Z3\gamma}^{\alpha\beta\gamma\delta}\left(\beta\right)\epsilon_\gamma^*(q_1)\epsilon_\delta^*(q_2) \tag{3.62}$$

Here we are assuming that the unpolarized photons are on-shell and monochromatic[5]. After summing and averaging over polarizations, the unpolarized squared amplitude becomes

$$\begin{aligned}\langle|\mathcal{M}|^2\rangle = \frac{c_\theta^6 s_\theta^2}{8\beta^4}\left[m_Z^4\left(s^2+t^2+u^2\right)\right.\\ \left.-2m_Z^2\left(s^3+t^3+u^3\right)+s^4+t^4+u^4\right],\end{aligned} \tag{3.63}$$

where the Mandelstam variables, expressed in terms of the CM energy $E_{\rm cm}$ of the incoming photons and the scattering angle θ, are

$$s = E_{\rm cm}^2\,, \tag{3.64a}$$

$$t = -\frac{1}{2}(E_{cm}^2 - m_Z^2)(1 - cos\theta)\,, \tag{3.64b}$$

$$u = -\frac{1}{2}(E_{cm}^2 - m_Z^2)(1 + cos\theta)\,. \tag{3.64c}$$

Setting $x = m_Z^2/s$, the unpolarized differential cross section for the scattering $\gamma\gamma \to \gamma Z$ reads

$$\begin{aligned}\frac{d\sigma}{d\Omega} = \frac{c_\theta^6 s_\theta^2}{4096\pi^2}\frac{s^3}{\beta^4}\left(1-x\right)^3\left[\left(6-2x^2\right)\cos^2\theta\right.\\ \left.+\left(1-x\right)^2\cos^4\theta+9+2x+x^2\right],\end{aligned} \tag{3.65}$$

which can be integrated to yield

$$\begin{aligned}\sigma\left(\gamma\gamma\to\gamma Z\right)_Y &= \frac{s_\theta^2 c_\theta^6}{1920\pi}\left(\frac{s^3}{\beta^4}\right)\left(1-x\right)^3\\ &\times\ \left(21+3x+x^2\right).\end{aligned} \tag{3.66}$$

This result is shown in blue in Fig. 3.2 for $\sqrt{\beta} = 250$ GeV. If the non-linear hypercharge sector is indeed realized in Nature, the expression above would provide the only tree-level

[5]This is a simplified scenario and a more detailed analysis would follow the strategy from ref. [25], for example.

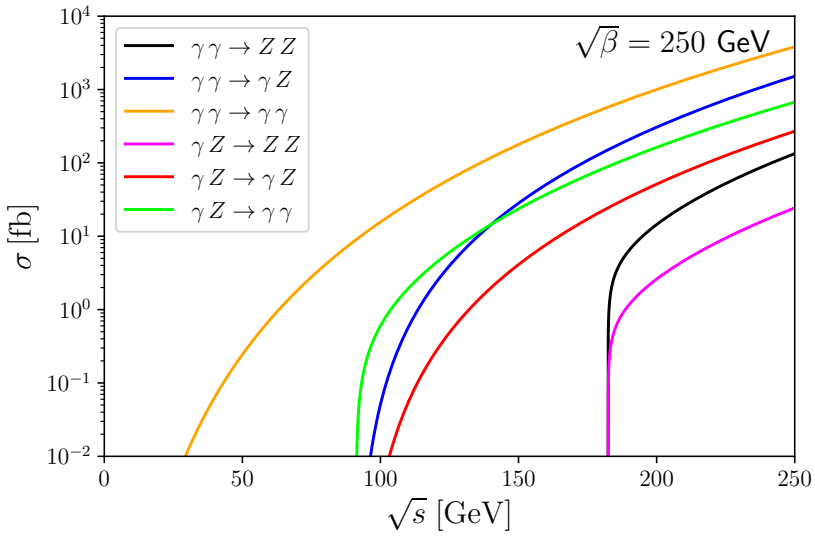

Figure 3.2: Unpolarized total cross sections for selected processes (no angular cuts applied; evaluated in the CM), cf. table 3.2. Here we set $\sqrt{\beta} = 250$ GeV for definiteness, but the scaling for other values can be easily performed via Eq. (3.73).

contribution to the cross section, since this process cannot take place in the SM at this order. In fact, the first SM contribution is generated via fermion and W-boson loops with a cross section of $\sim 3 \times 10^{-4}$ fb shortly above threshold and peaking at ~ 110 fb at ~ 750 GeV [93].

Another process of interest in a photon collider is $\gamma\,\gamma \to Z\,Z$ which, similar to $\gamma\,\gamma \to W^+\,W^-$, may be used to study the gauge structure of the SM as well as Higgs physics. As already mentioned, this process has no tree-level contribution in the SM – the first non-trival amplitude arises through fermion and W-boson loops with a cross section of ~ 20 fb immediately after threshold and roughly saturating at ~ 300 fb for CM energies $\gtrsim 800$ GeV [86, 94, 95]. In our non-linear extension the first non-zero contribution is at tree-level and the calculation of the (differential) cross section follows a similar rationale as the one leading to Eq. (3.66). The result is listed in table 3.2 and shown in black in Fig. 3.2.

Finally, let us briefly comment on $\gamma\,\gamma \to \gamma\,\gamma$, light-by-light (LbL) scattering. In Maxwell's linear electromagnetism this process is forbidden, but in the 1930's Heisenberg and Halpern [31, 32] realized that quantum effects could induce it. In the 1950's a full calculation was presented [96] and the cross section was found to be $\sim 10^{-34}$ pb for visible light [97, 98]. Only recently it was proposed that this elusive process could be observed at the LHC in Pb-Pb collisions [99] – in fact, strong evidence for it has been reported by the ATLAS [49] and CMS collaborations [50], being further confirmed by ATLAS [51]. The results are compatible with the SM prediction. As with the other photon-fusion processes previously discussed, LbL scattering takes place only at loop-level in the SM.

Process	N	$\kappa(x)$	$F(x)$
$\gamma\,\gamma \to \gamma\,\gamma$	$7c_\theta^8/1280\pi$	1	1
$\gamma\,\gamma \to \gamma\,Z$	$s_\theta^2 c_\theta^6/1920\pi$	$(1-x)^3$	$21+3x+x^2$
$\gamma\,\gamma \to Z\,Z$	$s_\theta^4 c_\theta^4/1280\pi$	$\sqrt{1-4x}$	$7-26x+27x^2$
$\gamma\,Z \to \gamma\,\gamma$	$s_\theta^2 c_\theta^6/5760\pi$	$(1-x)$	$21+3x+x^2$
$\gamma\,Z \to \gamma\,Z$	$s_\theta^4 c_\theta^4/2880\pi$	$(1-x)^4$	$21+6x+16x^2+6x^3+6x^4$
$\gamma\,Z \to Z\,Z$	$s_\theta^6 c_\theta^2/5760\pi$	$(1-x)\sqrt{1-4x}$	$21-75x+98x^2-20x^3+6x^4$

Table 3.2: Total cross sections for processes involving only quartic couplings of neutral gauge bosons, cf. Eq. (3.73) with $x = m_Z^2/s$. These results are shown in Fig. 3.2 for $\sqrt{\beta} = 250$ GeV.

Our non-linear extension, on the other hand, allows for it to proceed already at tree-level and with a potentially large cross section, cf. Fig. 3.2.

The quartic vertices in Eq. (3.13) allow for a few more tree-level scattering processes involving exclusively neutral gauge bosons than we have explicitly mentioned above. For the sake of completeness, the unpolarized differential cross-sections for the scattering of neutral gauge bosons in the non-linear extension considered in this work are given below, considering $\beta_Z \equiv \sqrt{1-4m_Z^2/E_{\rm cm}^2}$:

- $\gamma\gamma \to \gamma\gamma$

$$\frac{d\sigma}{d\Omega} = \frac{E_{\rm cm}^6 c_\theta^8 \left(3+\cos^2\theta\right)^2}{4096\pi^2\beta^4}. \tag{3.67}$$

- $\gamma\gamma \to \gamma Z$

$$\frac{d\sigma}{d\Omega} = \frac{c_\theta^6 s_\theta^2 \left(E_{\rm cm}^2 - m_Z^2\right)^3}{4096\pi^2\beta^4 E_{\rm cm}^4}\Big[\left(6E_{\rm cm}^4 - 2m_Z^4\right)\cos^2\theta + 9E_{\rm cm}^4 + \left(E_{\rm cm}^2 - m_Z^2\right)^2\cos^4\theta + 2E_{\rm cm}^2 m_Z^2 + m_Z^4\Big]. \tag{3.68}$$

- $\gamma\gamma \to ZZ$

$$\frac{d\sigma}{d\Omega} = \frac{c_\theta^4 s_\theta^4 E_{\rm cm}^2 \beta_Z}{4096\pi^2\beta^4}\Big[9E_{\rm cm}^4 + E_{\rm cm}^4\beta_Z^4\cos^4\theta + 6E_{\rm cm}^4\beta_Z^2\cos^2\theta - 32E_{\rm cm}^2 m_Z^2 + 40m_Z^4\Big]. \tag{3.69}$$

- $\gamma Z \to \gamma\gamma$

$$\frac{d\sigma}{d\Omega} = \frac{c_\theta^6 s_\theta^2 \left(E_{\rm cm}^2 - m_Z^2\right)}{6144\pi^2\beta^4}\Big[\left(6E_{\rm cm}^4 - 2m_Z^4\right)\cos^2\theta + 9E_{\rm cm}^4 + \left(E_{\rm cm}^2 - m_Z^2\right)^2\cos^4\theta + 2E_{\rm cm}^2 m_Z^2 + m_Z^4\Big]. \tag{3.70}$$

- $\gamma Z \to \gamma Z$

$$\begin{aligned}\frac{d\sigma}{d\Omega} = \frac{c_\theta^4 s_\theta^4 \left(E_{\rm cm}^2 - m_Z^2\right)^4}{49152\pi^2\beta^4 E_{\rm cm}^{10}} \Big[& 99E_{\rm cm}^8 + 20E_{\rm cm}^6 m_Z^2 \\ & + 74E_{\rm cm}^4 m_Z^4 + 20E_{\rm cm}^2 m_Z^6 + \left(E_{\rm cm}^2 - m_Z^2\right)^4 \cos 4\theta \\ & - 8m_Z^4 \left(E_{\rm cm}^2 - m_Z^2\right)^2 \cos 3\theta \\ & - 8m_Z^4 \left(11E_{\rm cm}^4 + 2E_{\rm cm}^2 m_Z^2 + 7m_Z^4\right) \cos\theta \\ & + 4\big(7E_{\rm cm}^8 - 4E_{\rm cm}^6 m_Z^2 + 4E_{\rm cm}^4 m_Z^4 \\ & - 4E_{\rm cm}^2 m_Z^6 + 7m_Z^8\big) \cos 2\theta + 35m_Z^8 \Big]. \end{aligned} \tag{3.71}$$

- $\gamma Z \to ZZ$

$$\begin{aligned}\frac{d\sigma}{d\Omega} = \frac{c_\theta^2 s_\theta^6 \beta_Z \left(E_{\rm cm}^2 - m_Z^2\right)}{6144\pi^2\beta^4 E_{\rm cm}^4} \big[& 9E_{\rm cm}^8 - 30E_{\rm cm}^6 m_Z^2 \\ & + 45E_{\rm cm}^4 m_Z^4 + \left(E_{\rm cm}^4 - 5E_{\rm cm}^2 m_Z^2 + 4m_Z^4\right)^2 \cos^4\theta \\ & + 2E_{\rm cm}^4 \beta_Z^2 \left(3E_{\rm cm}^4 + m_Z^4\right) \cos^2\theta \big]. \end{aligned} \tag{3.72}$$

The respective total cross sections, without any angular cuts, can be written in a systematic way as

$$\sigma \;=\; N\left(\frac{s^3}{\beta^4}\right)\kappa(x)F(x), \tag{3.73}$$

with $x = m_Z^2/s$. Here N is a numerical factor, $\kappa(x)$ is a kinematic and phase-space factor, and further energy-dependent contributions are contained in $F(x)$. These results are summarized in table 3.2 and shown in Fig. 3.2 for a reference value of $\sqrt{\beta} = 250$ GeV. The basic features are immediately salient: besides LbL scattering, all cross sections sharply rise after the respective thresholds and grow with increasing CM energy, as expected from the effective character of our hypercharge extension.

It is important at this point to contextualize our findings with recent results on anomalous quartic gauge couplings (aQGC). In fact, it is interesting to discuss experimental bounds and projected sensitivities on aQGC, as these may be translated into constraints on the parameter β from different, but complementary perspectives, ranging from past LHC runs to future lepton colliders. Particularly relevant is the discussion of recent results related to the anomalous vertices $\gamma\gamma\gamma Z$ and $\gamma\gamma\gamma\gamma$.

Anomalous quartic gauge couplings can be investigated with high precision at the LHC through $pp \to pXp$ processes, where X can be for instance $\gamma\gamma$ or γZ. In particular, it is interesting to focus on photon-induced processes in pp collisions since these processes are very sensitive to aQGC and therefore new physics beyond the SM (*e.g.*, extended Higgs sectors or extra-dimensions).

For instance, the $\gamma\gamma\gamma Z$ interaction appears in the SM through fermion and W-boson loops. This anomalous vertex induces the rare decay $Z \to \gamma\gamma\gamma$, contributes to $e^+e^- \to \gamma\gamma\gamma$ and allows also for the $\gamma\gamma \to \gamma Z$ scattering. New physics appearing at a mass scale Λ, much heavier than the experimentally accessible energies E, can have its effects described via a low-energy effective field theory. The anomalous $\gamma\gamma\gamma Z$ interaction could then be parametrized by dimension-8 operators such as

$$\mathcal{L}^{(1)}_{Z3\gamma} = \zeta\, F^{\mu\nu}F_{\mu\nu}F^{\rho\sigma}Z_{\rho\sigma} + \tilde{\zeta}\, F^{\mu\nu}\tilde{F}_{\mu\nu}F^{\rho\sigma}\tilde{Z}_{\rho\sigma}\,. \tag{3.74}$$

This is an effective description and we recover our model by making $\zeta = \tilde{\zeta} = -\frac{1}{8\beta^2}s_\theta c_\theta^3$.

Baldenegro *et al.* studied in great detail the γZ production with intact protons in the forward region at the LHC using proton tagging [100]. In this way, a sensitivity of $\zeta < 2 \times 10^{-13}\,\mathrm{GeV}^{-4}$ could be established for the anomalous quartic gauge coupling $\gamma\gamma\gamma Z$ at an integrated luminosity of $300\,\mathrm{fb}^{-1}$. This improves the result obtained through the $Z \to \gamma\gamma\gamma$ measurement by about three orders of magnitude. This improvement in the anomalous coupling sensitivity would, in turn, translate into an improvement on the sensitivity of $\sqrt{\beta}$, putting it at the order of a few hundred GeV.

Very recently, Inan and Kisselev studied very carefully the $\gamma\gamma \to \gamma Z$ scattering of photons produced by Compton backscattering at the CLIC and estimated the sensitivity to the anomalous quartic coupling $\gamma\gamma\gamma Z$ [101]. They used the following parametrization:

$$\mathcal{L}^{(2)}_{Z3\gamma} = g_1\, F^{\rho\mu}F^{\alpha\nu}\partial_\rho F_{\mu\nu}Z_\alpha + g_2\, F^{\rho\mu}F^{\nu}_{\mu}\partial_\rho F_{\alpha\nu}Z^\alpha. \tag{3.75}$$

We can relate these coefficients with the previous ones through $g_1 = 8(\tilde{\zeta} - \zeta)$ and $g_2 = 8\tilde{\zeta}$. The authors considered both polarized and unpolarized e^+e^- colisions at 1.5 and 3 TeV, obtaining exclusion limits on the aQGCs and comparing their results with the previous bounds obtained from γZ production at the LHC. The best bounds found by the authors for the couplings $g_{1,2}$ were approximately $4.4 \times 10^{-14}\,\mathrm{GeV}^{-4}$ and $5.1 \times 10^{-15}\,\mathrm{GeV}^{-4}$ for the e^+e^- energies 1.5 and 3 TeV, respectively. They conclude that the sensitivities on the anomalous couplings obtained at CLIC are roughly one to two orders of magnitude stronger than the limits that can be obtained at the LHC. Such an improvement would be enough to put the sensitivity on our non-linear parameter $\sqrt{\beta}$ at the TeV scale.

Let us now move on to the anomalous coupling $\gamma\gamma\gamma\gamma$. We can describe the non-linear effects on LbL scattering by means of the following effective Lagrangian:

$$\mathcal{L}^{(1)}_{4\gamma} = \zeta_1 F_{\mu\nu}F^{\mu\nu}F_{\rho\sigma}F^{\rho\sigma} + \zeta_2 F_{\mu\nu}F^{\nu\rho}F_{\rho\sigma}F^{\sigma\mu}\,. \tag{3.76}$$

This can be related to our description if we write it in a different, but equivalent basis

given by:

$$\mathcal{L}_{4\gamma}^{(2)} = \xi F_{\mu\nu}F^{\mu\nu}F_{\rho\sigma}F^{\rho\sigma} + \tilde{\xi} F_{\mu\nu}\tilde{F}^{\mu\nu}F_{\rho\sigma}\tilde{F}^{\rho\sigma}\,, \tag{3.77}$$

where the relation between the above parameters is given by $\xi = \zeta_1 + \frac{1}{2}\zeta_2$ and $\tilde{\xi} = \frac{1}{4}\zeta_2$. We can recover our model if we take the particular combination $\xi = \tilde{\xi} = \frac{c_\theta^4}{32}\frac{1}{\beta^2}$.

Fichet *et al.* analyzed the sensitivities to the anomalous coupling $\gamma\gamma\gamma\gamma$ at the LHC through diphoton production with intact outgoing protons [102, 103]. The reported limits at 14 TeV with an integrated luminosity of $L = 300\,\mathrm{fb}^{-1}$ on $|\zeta_1|$ and $|\zeta_2|$ were $1.5 \times 10^{-14}\,\mathrm{GeV}^{-4}$ and $3.0 \times 10^{-14}\,\mathrm{GeV}^{-4}$, respectively. For the High-Luminosity LHC (HL-LHC) the sensitivities obtained were a factor of two stronger. These results are strong and can put the sensitivity on our $\sqrt{\beta}$ at the TeV scale.

Very recently, Inan and Kisselev examined the anomalous couplings $\gamma\gamma\gamma\gamma$ in the polarized LbL scattering at CLIC [104]. Their results at 1.5 TeV were comparable with the bound obtained at HL-LHC stated above, but their results for 3 TeV were approximately one order of magnitude stronger, improving further the sensitivity on $\sqrt{\beta}$, but still keeping it at the TeV scale. A similar result could be found considering the best sensitivities on the anomalous couplings obtained through $\gamma\gamma \to ZZ$ in ref. [105] and also through $Z\gamma\gamma$ production in ref. [106], both considering e^+e^- collisions at 3 TeV at CLIC.

Finally, let us conclude this Chapter by reporting the latest experimental results on the anomalous couplings of interest here. A more general effective description including the nine independent dimension-8 operators respecting the $SU(2)_\mathrm{L} \times U(1)_\mathrm{Y}$ gauge symmetry as well as charge conjugation and parity invariance can be found in ref. [107]. This effective description includes in particular

$$\mathcal{L} \supset F_{T,8}\, B_{\mu\nu}B^{\mu\nu}B_{\rho\sigma}B^{\rho\sigma} + F_{T,9}\, B_{\mu\nu}B^{\nu\rho}B_{\rho\sigma}B^{\sigma\mu}\,. \tag{3.78}$$

To the best of our knowledge, the strongest experimental bounds on these anomalous couplings are given by the very recent CMS results reported in refs. [108, 109, 110, 111], considering different measurements in proton-proton collisions at $\sqrt{s} = 13\,\mathrm{TeV}$ performed at the LHC. In particular, the strongest bounds on the anomalous couplings $F_{T,8}$ and $F_{T,9}$ are reported in ref. [111] and give $|F_{T,8}| < 4.7 \times 10^{-13}\,\mathrm{GeV}^{-4}$ and $|F_{T,9}| < 9.1 \times 10^{-13}\,\mathrm{GeV}^{-4}$. These coefficients are translated into our model by taking $F_{T,8} + F_{T,9}/2 = 1/32\beta^2$ and $F_{T,9}/4 = 1/32\beta^2$. Therefore, these experimental results put the bound on $\sqrt{\beta}$ at the order of a few hundred GeV.

In the very recent Ref. [112], the authors search for exclusive two-photon production via photon exchange in proton-proton collisions, $pp \to p\gamma\gamma p$, with intact protons using the CMS and TOTEM detectors at a center-of-mass energy of 13 TeV at the LHC. They report the following bounds on the anomalous four-photon coupling parameters: $|\zeta_1| < 2.88 \times 10^{-13}\,\mathrm{GeV}^{-4}$ and $|\zeta_2| < 6.02 \times 10^{-13}\,\mathrm{GeV}^{-4}$. This would give us a limit on $\sqrt{\beta}$

around the same order of magnitude as the result reported above.

The most recent and strong contribution to the subject (to our knowledge) was recently given by Ellis *et al.* [113], constraining the non-linear scale of a BI extension of the SM to be $\gtrsim$ 5TeV considering $gg \to \gamma\gamma$ at the LHC. The authors estimate the sensitivities at possible future pp colliders with $\sqrt{s} = 100\,\text{TeV}$ to be around $\gtrsim 20\,\text{TeV}$.

Therefore, we conclude that the LHC results can give very strong constraints on aQGC. These can be translated as bounds on $\sqrt{\beta}$ typically at the order of a few hundred GeV up to the TeV scale. Nevertheless, future colliders are expected to be able to supersede these constraints, consequently improving the sensitivity on $\sqrt{\beta}$.

Chapter 4

Concluding remarks

The Electroweak Theory is extremely successful, but there still remains an important unanswered question of topological nature. In fact, even if it has never been observed, it can be shown that it admits EW monopole solutions, with classical infinite energy, rendering, therefore, impossible to predict its mass. We are presenting here a regularization for the EW monopole energy obtained by extending the hypercharge sector to a non-linear version based on Logarithmic and Exponential versions of Electrodynamics. Furthermore, we identified the constraints that a more general non-linear extension should obey to yield finite energy solutions. We have also worked out an estimate of the monopole mass in each non-linear scenario here contemplated; the results are compared with the result already known for the BI extension. We conclude that, in the cases we investigate, our monopole solutions are lighter than the known BI solutions, but, unfortunately, our masses remain still out of reach for the current colliders. We estimate the lower bound for the monopole energy in our approach and conclude that it is possible to suitably modify our solution to have an energy accessible at LHC. Finally, we investigated the simpler case of a non-linear Dirac monopole in pure Electromagnetism, estimating its mass in different non-linear scenarios and concluding that although this is a simplified scenario, these energies are achievable at LHC.

Motivated by these recent results in the physics of electroweak monopoles, we investigated the consequences of a non-linear extension in the weak hypercharge sector in high-energy processes. The first and most promising one, Z-decay, is a rare process occurring only at loop-level in the SM, but induced at tree-level by non-linear effects. We are confident that the experimental upper limit on the branching ratio will be significantly improved in the near future, thus enabling us to set more stringent bounds on $\sqrt{\beta}$, readily excluding the range $\sqrt{\beta} \lesssim m_Z$, cf. Fig. 3.1. We remark that, in a scenario where experiment reaches the level of the SM prediction, lower bounds ~ 300 GeV could be set. The second process analyzed was electron-positron annihilation into three photons, also a relatively rare process. It is well described by QED and the non-linear extension provides small corrections also at tree-level. The non-linear effects are much smaller than

the available precision and it was not possible to obtain viable bounds with the current experimental data, but we project that the necessary improvements may be within the reach of the next-generation lepton colliders. Finally, we have also analyzed selected scattering processes involving exclusively neutral gauge bosons. The unpolarized tree-level cross sections may reach a few hundred fb at $\sqrt{s} = 200$ GeV for $\sqrt{\beta} = 250$ GeV, cf. Fig. 3.2. These processes are good candidates to detect possible signatures from the non-linear extension in future experiments, given that they occur only at loop-level in the SM, but are induced at tree-level via Eq. (3.13). In this respect, we also reported recent results giving constraints on anomalous quartic gauge couplings obtained at the LHC considering neutral gauge-boson scatterings. We used them to estimate the corresponding limits on $\sqrt{\beta}$ and found that typically they give us bounds of a few hundred GeV. Furthermore, we analyzed the projections for these anomalous couplings in future lepton colliders and found that they improve the sensitivity on $\sqrt{\beta}$, putting it at the TeV scale.

To conclude this Part, we remark that a more general implementation of the non-linear extension of the electroweak sector is possible. Here we have considered the $U(1)_{\mathrm{Y}}$ sector, but an analogous modification may be performed in the $SU(2)_{\mathrm{L}}$ sector. In this case, a new electroweak monopole could be found. Moreover, the already analyzed neutral sector would receive small modifications, and interesting non-linear effects would also be induced in the charged sector of the SM. This topic will be the subject of a future work.

Part II

Abelian vortices in parity-invariant Maxwell-Chern-Simons models

Chapter 5

Introduction

Vortices are ubiquitous in nature, appearing from the rotating water in a sink to the winds surrounding a tornado. Such configurations can also be found throughout the physics literature, as illustrated in Refs. [114, 115, 116, 117, 118, 119, 120]. In field theory, vortices are defined as solitons and can appear whenever we have a continuous symmetry that is spontaneously broken and a vacuum manifold with a circular structure, as for example, in a (2+1)-dimensional abelian gauge theory in the Higgs phase [121].

In this sense, the first appearance of vortices in the literature was in the context of superconductivity, through the work of Abrikosov in 1957 [122]. In 1973, Nielsen and Olesen showed [123] that the Abelian-Higgs (AH) model in 2+1 dimensions (the relativistic generalization of the Ginzburg-Landau model) admits finite-energy vortex solutions with a quantized magnetic flux. An exact vortex solution was found by de Vega and Schaposnik in 1976 [124], considering the particular relation between the couplings for which scalar and vector bosons have the same mass. The Abrikosov-Nielsen-Olesen (ANO) vortex described above is electrically neutral and, in fact, it was shown later by Julia and Zee in 1975 [6] that charged vortices with finite-energy cannot exist in the AH model.

A very interesting and subtle class of 2+1 topologically massive gauge theories was introduced in 1982 by Deser, Jackiw, and Templeton [125, 126], called nowadays Chern-Simons (CS) theories, after the pioneering work [127] (see also Refs. [128, 129, 130, 131]). The CS term is exclusive of odd-dimensions, typically $\mathcal{P}$- and $\mathcal{T}$- odd, and topological in nature. In 2+1 dimensions, it gives a gauge-invariant mass to the gauge field, providing a mass gap that cures the infrared divergences of these theories, changing drastically their physical content and leading to a quantization of the ratio between the CS parameter and the gauge coupling. Over the years, CS theories have found applications all around physics, but the most famous breakthrough came with the work of Witten [132], about the relationship between CS theories and the Jones polynomial. For an introduction to CS physics, see Ref. [133]; for a review of vortices in this context, see Ref. [134].

It is well-known that a CS term has the property of flux attachment when coupled to matter fields, that is, it relates the electric charge with the magnetic flux. In 1986, it

was shown that finite-energy charged vortices solutions exist in Abelian [135] and non-abelian [136, 137, 138] Higgs models in the presence of a CS term (see also Ref. [139]); the existence of quantum charged vortices has been shown in Ref. [140]. Interestingly enough, charged vortices can play an important role in condensed matter, for example, in the fractional quantum Hall effect [141], high-T_c superconductors [142], and superfluids [143].

In the pure CS limit, when the Maxwell kinetic term is absent, peculiar charged vortices were shown to exist [144], with magnetic field vanishing at the origin, instead of taking a finite value as usual. An interesting work studying vortices in a Maxwell-Chern-Simons-Higgs model, interpolating between AH model and pure CS-Higgs case was done in Ref. [145]. Upon choosing a suitable potential, it was shown in Refs. [146, 147] that it is possible to obtain a Bogomol'nyi-type [148] energy lower bound with first order equations that describe self-dual topological charged vortices in the Higgs phase of the Chern-Simons-Higgs model. We remark that there are non-topological solitons with non-zero flux in the symmetric vacuum [149]. Since Supersymmetry and self-duality are intimately related [150, 151, 152, 153], a $\mathcal{N} = 2$ supersymmetric extension is possible [154] (see also [155, 156, 157]). In Ref. [158] the authors studied topological and non-topological vortices in self-dual models with both Maxwell and Chern-Simons terms; for more details on self-dual CS theories, one can see Ref. [159]. This kind of soliton solutions can also be found in non-relativistic theories (see, for instance, Refs. [160, 161, 162, 163]).

It is usually said that the presence of a CS term necessarily causes the violation of $\mathcal{P}$ and $\mathcal{T}$ symmetries. Although usually correct, this is not always true. In fact, it was already pointed out in [125, 126] and later shown by Hagen [164](see also Ref. [165]), that a gauge and parity-invariant CS theory can be constructed by essentially doubling the gauge degrees of freedom and adopting their respective CS terms with opposite signs. A different approach was proposed by Del Cima and Miranda [166] a few years ago in the context of graphene physics (see also Ref. [167]). The authors introduced a parity-preserving $U(1) \times U(1)$ massive quantum electrodynamics (QED) with two gauge fields having different behaviors under parity, and a CS term mixing them, a distinctive feature of the model. Its massless version was studied in Ref. [168], and it was shown that it exhibits quantum parity conservation at all orders in perturbation theory [169]. Recently, it was shown in Ref. [170], that the massive version is ultraviolet finite, that is, exhibits vanishing β-functions associated to the gauge coupling constants and CS parameter, and also vanishing anomalous dimensions. Furthermore, it was shown that the model is parity and gauge anomaly free at all orders in perturbation theory.

Vortices in this context have already been discussed in the literature. In Ref. [171], the authors studied vortices in a $U(1) \times U(1)$ CS model coupled with scalar matter exhibiting fractional and mutual statistics. Following this work, the low energy dynamics of vortices was investigated in [172] (see also [173]), hybrid anyons in [174], and vortices in a CS theory coupled with fermions in [175]. These works had as a background

experiments sugesting parity-invariance in high-T_c superconductors [176, 177, 178], and the subsequent theoretical models agreeing with them [179, 180, 181, 182]. Finally, this subject is also investigated in the mathematical physics literature [183, 184, 185], and interestingly enough, similar models with a mixed CS term find many applications in condensed matter [186, 187, 188, 189, 190, 191, 192, 193, 194, 195].

In the last few years, there have been several contributions to the literature of vortices, and here we briefly mention some of them. In Ref. [196], the authors reported a new topological vortex solution in a $U(1) \times U(1)$ Maxwell-Chern-Simons theory. Considering the situation in which one of the $U(1)$'s was spontaneously broken, they obtained a long-range force, protected at the quantum level by the Coleman-Hill theorem [197]. Another interesting development was achieved in Refs. [198, 199], where the authors used a systematic expansion in inverse powers of n to study giant vortices with large topological charge, observed experimentally in condensed matter systems [200, 201, 202]. In Ref. [203], the authors considered a $U(1) \times U(1)$, $\mathcal{N} = 2$ supersymmetric model in $2 + 1$ dimensions, investigating magnetic vortex formation and discussing applications of it. For some recent developments on vortex solutions within the gravitational context, see for instance Refs. [204, 205]. Other interesting recent works can be found in Refs. [206, 207, 208, 209, 210, 211]. Here, we propose a parity-invariant Maxwell-Chern-Simons $U(1) \times U(1)$ scalar QED in 2+1 dimensions, in analogy with the fermionic matter case studied in Ref. [166], and investigate the existence of topological vortices in the Higgs phase of this model. Therefore, it comes as one more step towards the description of physical phenomena where charged vortices or anyonic matter may play an important role while preserving $\mathcal{P}$ and $\mathcal{T}$.

Part II is organized in 4 Chapters, being the first one given by this Introduction. Chapter 6 is organized as follows: in Sec. 6.1, we present the model and build the theoretical setup; in Sec. 6.2 we discuss general properties of the topological configurations considered here; we present explicit vortex solutions in Sec. 6.3 and discuss its main features; finally, the analysis of limiting cases is done in Sec. 6.4. Chapter 7 is organized as follows: in Sec. 7.1 we build the main theoretical setup; in Sec. 7.2, we present the self-duality equations and discuss the boundary conditions; we exhibit and discuss explicit numerical solutions in Sec. 7.3. Finally, in Chapter 8, we state our concluding remarks for the second part of this thesis.

Chapter 6

Vortices in a parity-invariant scenario

In this Chapter, we introduce the parity-invariant Maxwell-Chern-Simons $U(1)\times U(1)$ model coupled with charged scalar matter in 2+1 dimensions. We describe the main features of this model, and show that it admits finite-energy topological vortices in its Higgs phase. We exhibit explicit numerical solutions, discuss their main properties, and analyze different interesting regimes that can be found in some special limits. Here we adopt $\epsilon^{012}=-1$ and $\epsilon^{ij}\equiv\epsilon^{0ij}$, with Latin indices referring to spatial components.[1]

6.1 Theoretical setup

Let us introduce the parity-invariant Maxwell-Chern-Simons $U(1)_A\times U(1)_a$ scalar QED in 2+1 dimensions with Lagrangian given by

$$\begin{aligned}\mathcal{L}=&-\frac{1}{4}F_{\mu\nu}F^{\mu\nu}-\frac{1}{4}f_{\mu\nu}f^{\mu\nu}+\mu\epsilon^{\mu\nu\rho}A_\mu\partial_\nu a_\rho\\&+|D_\mu\phi_+|^2+|D_\mu\phi_-|^2-V\left(|\phi_+|,|\phi_-|\right),\end{aligned}\tag{6.1}$$

where the covariant derivative with respect to the gauge group $U(1)_A\times U(1)_a$ acting on the complex scalar fields ϕ_+ and ϕ_- is given by

$$D_\mu\phi_\pm=\partial_\mu\phi_\pm+ieA_\mu\phi_\pm\pm iga_\mu\phi_\pm.\tag{6.2}$$

In the above expression, e and g are the gauge couplings associated with the gauge groups $U(1)_A$ and $U(1)_a$, respectively, and $\mu>0$ is the CS parameter. The field strength tensors

[1] This Chapter is based on arXiv: 2205.10427 [hep-th].

are given by

$$F_{\mu\nu} = \partial_\mu A_\nu - \partial_\nu A_\mu,$$
$$f_{\mu\nu} = \partial_\mu a_\nu - \partial_\nu a_\mu. \tag{6.3}$$

Notice that the scalar fields have the same charge under $U(1)_A$ but opposite charges under $U(1)_a$. The mass dimensions here are: $[e^2] = [g^2] = [\mu] = 1$ and $[A_\mu] = [a_\mu] = [\phi_\pm] = 1/2$. In this model, in analogy with the fermionic version studied in Ref. [166], the gauge field a_μ is a pseudo-vector under parity.

The Lagrangian presented here is by construction invariant under $U(1)_A \times U(1)_a$ gauge transformations:

$$\phi'_\pm(x) = e^{i(\rho(x) \pm \xi(x))}\phi_\pm(x),$$
$$A'_\mu(x) = A_\mu(x) - \frac{1}{e}\partial_\mu \rho(x),$$
$$a'_\mu(x) = a_\mu(x) - \frac{1}{g}\partial_\mu \xi(x). \tag{6.4}$$

To ensure parity-invariance, the scalar fields should behave somehow in the same way under parity as the fermionic matter in Ref. [166]. Thus, we will extend the parity concept to include a transformation in the space of fields that swaps the role of $\phi_\pm$:

$$A^P_\mu = \mathcal{P}_\mu^{\ \nu} A_\nu,$$
$$a^P_\mu = -\mathcal{P}_\mu^{\ \nu} a_\nu,$$
$$\phi^P_\pm = \eta\, \phi_\mp, \tag{6.5}$$

where we have $\mathcal{P}_\mu^{\ \nu} = diag(+ - +)$, and η is a complex phase. Here, every time we do a statement about parity, it must be understood that we are referring to this extended parity concept. Moreover, we would like to point out that the mixed CS term is a crucial ingredient if we want to have a topological gauge-invariant mass term without breaking parity. Using the above parity transformations, one can immediately see that our model is parity-invariant (assuming that a suitable potential V is chosen, of course).

The most general renormalizable potential compatible with the symmetries is

$$\begin{aligned} V = {} & m^2\left(|\phi_+|^2 + |\phi_-|^2\right) + \frac{M_1}{2}\left(|\phi_+|^4 + |\phi_-|^4\right) \\ & + M_2|\phi_+|^2|\phi_-|^2 + \frac{g_1}{3}\left(|\phi_+|^6 + |\phi_-|^6\right) \\ & + g_2\left(|\phi_+|^2|\phi_-|^4 + |\phi_-|^2|\phi_+|^4\right), \end{aligned} \tag{6.6}$$

where the parameters should be carefully chosen in order to ensure the presence of only stable vacua. It should be clear that, depending on the parameters, different vacua

structures might appear, which could in principle lead to the spontaneous breaking of one, both, or none of the $U(1)$ symmetries. Let us choose the simplest scalar potential that leads to a spontaneously broken but parity-symmetric vacuum. Thus, we will consider, with $\lambda > 0$:

$$V(\phi_+, \phi_-) = \frac{\lambda}{4}\left(|\phi_+|^2 - v^2\right)^2 + \frac{\lambda}{4}\left(|\phi_-|^2 - v^2\right)^2. \tag{6.7}$$

This is the simplest extension of the Abelian-Higgs potential for the case under study. Taking $v \neq 0$, it will clearly induce a non-trivial vacuum expectation value (VEV) for the scalar fields, putting the theory into the Higgs phase, where we have $\langle|\phi_\pm|\rangle = v$. This potential is not stable under quantum corrections, but this will not be an issue, since we are focusing on classical solutions.

An important remark must be made at this point. If one defines the fields $A^\pm_\mu = (A_\mu \pm a_\mu)/\sqrt{2}$, the pure gauge part of the Lagrangian would be rewritten as

$$\begin{aligned}\mathcal{L} \supset & -\frac{1}{4}F^+_{\mu\nu}F^{\mu\nu+} - \frac{1}{4}F^-_{\mu\nu}F^{\mu\nu-} \\ & + \frac{\mu}{2}\epsilon^{\mu\nu\rho}\left(A^+_\mu\partial_\nu A^+_\rho - A^-_\mu\partial_\nu A^-_\rho\right),\end{aligned} \tag{6.8}$$

realizing the parity-invariance of the model in a different, although equivalent, form, as studied in Ref. [164]. The other part of the Lagrangian in this setting is written as

$$\begin{aligned}\mathcal{L} \supset & \left|\left(\partial_\mu + iq_1A^+_\mu + iq_2A^-_\mu\right)\phi_+\right|^2 \\ & + \left|\left(\partial_\mu + iq_2A^+_\mu + iq_1A^-_\mu\right)\phi_-\right|^2 - V\left(|\phi_+|, |\phi_-|\right).\end{aligned} \tag{6.9}$$

In the above expression, one can see that ϕ_+ and ϕ_- have swapped effective charges, defined as $q_1 = (e+g)/\sqrt{2}$ and $q_2 = (e-g)/\sqrt{2}$. The parity transformation is realized by $A^\pm_\mu \to \mathcal{P}_\mu{}^\nu A^\mp_\nu$ and $\phi_\pm \to \eta\phi_\mp$. This setup explicitly exhibits the parity-invariance of the CS sector. It is possible to show that, the on-shell free fields A^+_μ and A^-_μ provide the vector representations of the three-dimensional Poincaré group with spins equal to +1 and -1 (for $\mu > 0$), respectively, as one can see in Ref. [212]. Following the same reasoning, we could as well construct the complex fields $\sigma = (\phi_+ + \phi_-)/\sqrt{2}$ and $\pi = i(\phi_+ - \phi_-)/\sqrt{2}$ that transform under parity as a scalar and a pseudo-scalar, respectively. In this work, although, we have chosen to work with the variables A_μ, a_μ and $\phi_\pm$ for convenience.

The equations of motion following from the Lagrangian are given by

$$\begin{aligned}\partial_\mu F^{\mu\nu} + \mu\epsilon^{\nu\alpha\beta}\partial_\alpha a_\beta &= e\left(J^\nu_+ + J^\nu_-\right), \\ \partial_\mu f^{\mu\nu} + \mu\epsilon^{\nu\alpha\beta}\partial_\alpha A_\beta &= g\left(J^\nu_+ - J^\nu_-\right), \\ D_\mu D^\mu\phi_\pm &= -\frac{dV}{d\phi^*_\pm},\end{aligned} \tag{6.10}$$

where the currents are $J^\nu_\pm = i\left[\phi^*_\pm D^\nu \phi_\pm - \phi_\pm D^\nu \phi^*_\pm\right]$.

Let us take a look at the peculiar Gauss laws that this model presents. Define the electric and magnetic fields associated with the gauge fields A_μ and a_μ by $E^i = F^{i0}$, $B = \epsilon^{ij}\partial_i A_j$ and $e^i = f^{i0}$, $b = \epsilon^{ij}\partial_i a_j$, respectively. From the gauge fields equations of motion, and using $\rho_\pm = J^0_\pm$:

$$\begin{aligned}\vec{\nabla}\cdot\vec{E} + \mu b &= e\left(\rho_+ + \rho_-\right),\\ \vec{\nabla}\cdot\vec{e} + \mu B &= g\left(\rho_+ - \rho_-\right).\end{aligned} \tag{6.11}$$

Defining the electric charge $Q = e\int d^2x\ (\rho_+ + \rho_-)$ and the g-electric charge $G = g\int d^2x\ (\rho_+ - \rho_-)$, and defining also the magnetic flux as $\Phi \equiv \int d^2x\, B$ and the g-magnetic flux as $\chi \equiv \int d^2x\, b$, we obtain upon integration:

$$Q = \mu\chi, \quad G = \mu\Phi. \tag{6.12}$$

That is, the electric charge associated with one gauge field is proportional to the magnetic flux associated with the other. It is well-known that there is a flux attachment caused by the CS term, but in our case this charge-flux relation happens between two different gauge fields. This mutual statistics behavior [165] is a distinctive feature of this class of models [171], but here we implement the flux attachment in a parity-invariant way.

The energy-momentum tensor here can be written as

$$\begin{aligned}T^{\mu\nu} &= \left(\eta^{\mu\nu}\frac{1}{4}F_{\alpha\beta}F^{\alpha\beta} - F^{\mu\beta}F^{\nu}{}_{\beta}\right)\\ &+ \left(\eta^{\mu\nu}\frac{1}{4}f_{\alpha\beta}f^{\alpha\beta} - f^{\mu\beta}f^{\nu}{}_{\beta}\right)\\ &+ D^\mu\phi^*_+ D^\nu\phi_+ + D^\mu\phi_+ D^\nu\phi^*_+ - \eta^{\mu\nu}|D_\alpha\phi_+|^2\\ &+ D^\mu\phi^*_- D^\nu\phi_- + D^\mu\phi_- D^\nu\phi^*_- - \eta^{\mu\nu}|D_\alpha\phi_-|^2\\ &+ \eta^{\mu\nu}V.\end{aligned} \tag{6.13}$$

The energy functional following from this expression is

$$\begin{aligned}E = \int d^2x \Big[&\frac{1}{2}\left(\vec{E}^2 + B^2\right) + \frac{1}{2}\left(\vec{e}^2 + b^2\right) + V\\ &+|D_0\phi_+|^2 + |D_0\phi_-|^2 + |D_i\phi_+|^2 + |D_i\phi_-|^2\Big].\end{aligned} \tag{6.14}$$

We are interested only in the static regime, *i.e.*, $\partial_0 \equiv 0$. In the sequence, we briefly address the perturbative spectrum of the model and its dispersion relations.

The vacuum configuration of the system is given by the absolute minimum of the energy functional, that can be achieved, for instance, considering $\phi_\pm = v$ and $A_\mu = a_\mu = 0$. In the unitary gauge we can write $\phi_\pm(x) = v + h_\pm(x)/\sqrt{2}$. The quadratic part of the

Lagrangian here is given by

$$\begin{aligned}\mathcal{L}^{\text{quad}} &= -\frac{1}{4}F_{\mu\nu}F^{\mu\nu} - \frac{1}{4}f_{\mu\nu}f^{\mu\nu} + \frac{1}{2}(\partial_\mu h_+)^2 + \frac{1}{2}(\partial_\mu h_-)^2 \\ &+ 2v^2\left(e^2A_\mu A_\mu + g^2 a_\mu a_\mu\right) - \frac{\lambda v^2}{2}(h_+^2 + h_-^2) \\ &+ \frac{\mu}{2}\epsilon^{\mu\nu\rho}A_\mu\partial_\nu a_\rho + \frac{\mu}{2}\epsilon^{\mu\nu\rho}a_\mu\partial_\nu A_\rho. \end{aligned} \tag{6.15}$$

From the above expression we can immediately see that we have two degenerate massive scalars with $m_S = \sqrt{\lambda v^2}$. For the gauge quadratic part we can write

$$\mathcal{L}^{\text{quad}}_{\text{gauge}} = \frac{1}{2}\begin{pmatrix} A_\mu & a_\mu \end{pmatrix} O^{\mu\nu} \begin{pmatrix} A_\nu \\ a_\nu \end{pmatrix}, \tag{6.16}$$

where we defined the gauge dynamical operator

$$O^{\mu\nu} = \begin{pmatrix} \Box\Theta^{\mu\nu} + 4e^2v^2\eta^{\mu\nu} & \mu\epsilon^{\mu\rho\nu}\partial_\rho \\ \mu\epsilon^{\mu\rho\nu}\partial_\rho & \Box\Theta^{\mu\nu} + 4g^2v^2\eta^{\mu\nu} \end{pmatrix}. \tag{6.17}$$

After some manipulations, from the inverse of Eq. (6.17), one can find the dispersion relations $p_\pm^2 = m_\pm^2$, where:

$$\begin{aligned} m_\pm^2 &= \frac{1}{2}[\mu^2 + 4v^2(e^2+g^2)] \\ &\pm \frac{1}{2}\sqrt{\left[\mu^2 + 4v^2(e^2+g^2)\right]^2 - (8v^2eg)^2}. \end{aligned} \tag{6.18}$$

It should be stressed that the above relation is necessarily real and non-negative, which ensures the absence of taquions in the model. We can see that the gauge fields will acquire mass contributions coming from the Higgs mechanism and also from the CS term. In particular, in the absence of a CS term ($\mu = 0$), we would have two massive vector bosons with $M_e = 2ev$ and $M_g = 2gv$. In the case without spontaneous symmetry breaking ($v = 0$), the Higgs mechanism does not take place and we find only a topological mass given by μ. In the absence of a Maxwell term, we obtain two copies of the dispersion relation $p^2 = 16e^2g^2v^4/\mu^2$, and we have degenerate gauge boson masses.

6.2 Topological configurations

In this section, we will see what are the asymptotic conditions that allow finite-energy static solutions and propose a vortex *ansatz* to investigate the possibility of a topologically non-trivial solution in this model.

6.2.1 Asymptotic conditions

In order to have finite energy, each non-negative term in Eq. (6.14) must asymptote to zero as $|\vec{x}| = r \to \infty$ sufficiently fast in order to compensate the asymptotic behavior of the measure and make the integral convergent. These asymptotic conditions can be seen as boundary conditions for the fields at the boundary of space, that we can see as an asymptotic sphere $S^1_\infty \equiv \partial\mathbb{R}^2$ (the circle at infinity). In particular, the scalar fields must asymptote to the vacuum manifold, *i.e.*, with a fixed norm on the space of fields, but with phase freedom given by an angle that parametrizes the sphere at infinity. Thus, in the asymptotic limit we can take $\phi_\pm \to ve^{i\omega_\pm(\theta)}$ where θ parametrizes the sphere S^1_∞, together with $A_i \to -\partial_i\left(\omega_+ + \omega_-\right)/2e$ and $a_i \to -\partial_i\left(\omega_+ - \omega_-\right)/2g$, to ensure that the covariant derivatives vanish at spatial infinity. To satisfy the remaining asymptotic conditions, we can take $A_0, a_0 \to 0$ as well as $\partial_i A_0, \partial_i a_0 \to 0$.

Furthermore, since we have ϕ_+ and ϕ_-, there are two phase degrees of freedom in the asymptotic limit. The asymptotic behavior of the fields defines a function from the boundary of space into the gauge group, giving us a map

$$\Phi_\infty : S^1_\infty \to S^1 \times S^1 \equiv U(1) \times U(1), \tag{6.19}$$

since topologically speaking $U(1)$ and S^1 are equivalents. Any such map can be classified by homotopy classes, and in particular, the maps from the circle S^1 to the torus $S^1 \times S^1$ can be classified using two integers determined by the fundamental homotopy group $\pi_1\left(S^1 \times S^1\right) \equiv \mathbb{Z} \times \mathbb{Z}$. Mappings of different homotopy classes cannot be deformed in each other by a continuous transformation, and therefore give rise to inequivalent configurations. This is the topological origin of the stability of vortex solutions. Therefore we conclude that the finite-energy condition implies an homotopy classification leading to a labeling of the configurations by two integers.

Let us define a (m,n)-vortex as a finite-energy static configuration obeying the boundary conditions stated above with the particular structure:

$$\begin{aligned} \phi_\pm &\to ve^{i(m\pm n)\theta}, \\ A_i &\to -\frac{m}{e}\partial_i\theta, \\ a_i &\to -\frac{n}{g}\partial_i\theta, \end{aligned} \tag{6.20}$$

where θ parametrizes the sphere at infinity as before, and we have $\vec{\nabla} \equiv \hat{r}\partial_r + \hat{\theta}\frac{1}{r}\partial_\theta$.

In principle, we demand only that $m \pm n \in \mathbb{Z}$, allowing m and n to take simultaneously half-integer values. In the light of the natural doubling of degrees of freedom necessary to ensure parity invariance, the possibility of half-integer numbers should not be worrisome.

From the equations of motion, we already know that there is a relation between charges

and magnetic fluxes. But, by definition,

$$\Phi = \int d^2x\, \epsilon^{ij} \partial_i A_j = \int_{S^1_\infty} dS\, \hat{r}_i\, \epsilon^{ij} A_j. \tag{6.21}$$

Upon using the asymptotic behavior of the gauge field and the relations $\hat{\theta}_i = \epsilon_{ij}\hat{r}_j$ and $\epsilon_{ij}\epsilon_{jk} = -\delta_{ik}$, we have,

$$\Phi = \int d\theta\, r\, \hat{r}_i\, \epsilon^{ij} \left(-\frac{m}{er}\epsilon_{jk}\hat{r}_k\right) = \frac{2\pi}{e} m. \tag{6.22}$$

Doing a totally equivalent reasoning, we can also find $\chi = \frac{2\pi}{g} n$. Thus:

$$\Phi = \frac{2\pi}{e} m, \quad \chi = \frac{2\pi}{g} n. \tag{6.23}$$

Therefore, we can conclude that besides the magnetic flux associated with one gauge field being proportional to the electric charge of the other, they are all topologically quantized, and can be written as

$$Q = \frac{2\pi}{g}\, \mu\, n, \quad G = \frac{2\pi}{e}\, \mu\, m. \tag{6.24}$$

6.2.2 The vortex *ansatz*

Let us search now for an explicit vortex solution. To accomplish this, we will first write an *ansatz* and then the differential equations that follow from the equations of motion. We propose the following radially symmetric (m,n)-vortex *ansatz*:

$$\begin{aligned}
\phi_\pm &= v\, F_\pm(r)\, e^{i(m\pm n)\theta}, \\
A_i &= \frac{1}{er}\, [A(r) - m]\, \hat{\theta}_i, \\
a_i &= \frac{1}{gr}\, [a(r) - n]\, \hat{\theta}_i, \\
A_0 &= \frac{1}{er}\, \alpha(r), \\
a_0 &= \frac{1}{gr}\, \beta(r).
\end{aligned} \tag{6.25}$$

To satisfy the asymptotic conditions, the functions above must satisfy the following boundary conditions:

$$F_\pm(\infty) = 1,\ A(\infty) = a(\infty) = 0. \tag{6.26}$$

We impose $F_\pm(0) = 0$, $A(0) = m$, $a(0) = n$, and also $\alpha(0) = \beta(0) = 0$ to avoid a singularity at the origin, except when $m = \pm n$, because in this case one of the scalar

profiles can take a non-zero value at the origin. Under a parity transformation in the vortex configuration, we have $(m,n) \to (-m,n)$, $r \to r, \theta \to -\theta - \pi$ and $F_\pm \to F_\mp, A \to -A, a \to a, \alpha \to \alpha, \beta \to -\beta$.

The energy density functional, considering this *ansatz*, can be written as

$$\begin{aligned}\epsilon =& \frac{1}{2e^2r^2}\left[\dot{A}^2 + \left(\dot{\alpha} - \frac{\alpha}{r}\right)^2\right] + \frac{1}{2g^2r^2}\left[\dot{a}^2 + \left(\dot{\beta} - \frac{\beta}{r}\right)^2\right] \\ &+ \frac{\lambda v^4}{4}\left[(F_+^2-1)^2 + (F_-^2-1)^2\right] \\ &+ \frac{v^2}{r^2}\left[F_+^2(\alpha+\beta)^2 + F_-^2(\alpha-\beta)^2\right] \\ &+ v^2\left[\dot{F}_+^2 + \frac{F_+^2}{r^2}(A+a)^2 + \dot{F}_-^2 + \frac{F_-^2}{r^2}(A-a)^2\right]. \end{aligned} \tag{6.27}$$

One can also compute the angular momentum of these finite-energy static vortex-like configurations, given by

$$J = \int d^2x\, \epsilon^{ij} r_i T_{0j}. \tag{6.28}$$

In general, we can write

$$\begin{aligned} T_{0j} =& \epsilon_{jk}\left(E^k B + e^j b\right) \\ &+ 2\mathbb{R}\mathrm{e}\left(D_0\phi_+^* D_j\phi_+ + D_0\phi_-^* D_j\phi_-\right). \end{aligned} \tag{6.29}$$

Therefore, the angular momentum can be written as a sum of a contribution J_g coming from the gauge fields and another, J_s from the scalar field sector. Defining $\phi_\pm = |\phi_\pm| e^{i\omega_\pm}$, we can write:

$$\mathbb{R}\mathrm{e}\left(D_0\phi_\pm^* D_j\phi_\pm\right) = (eA_0 \pm ga_0)\left(eA_j \pm ga_j + \partial_j\omega_\pm\right)|\phi_\pm|^2 \tag{6.30}$$

Using the rotationally symmetric *ansatz*, where $\omega_\pm = (m \pm n)\theta$, we can rewrite:

$$\mathbb{R}\mathrm{e}\left(D_0\phi_\pm^* D_j\phi_\pm\right) = \frac{|\phi_\pm|^2}{r}\left[eA_0 \pm ga_0\right]\left[A \pm a\right]\hat{\theta}_j. \tag{6.31}$$

But in the static limit we can write for the charge densities, $\rho_\pm = -2\left(eA_0 \pm ga_0\right)|\phi_\pm|^2$, and thus,

$$\begin{aligned} &2\mathbb{R}\mathrm{e}\left(D_0\phi_+^* D_j\phi_+ + D_0\phi_-^* D_j\phi_-\right) \\ &= -\frac{1}{r}\left[A\ (\rho_+ + \rho_-) + a\ (\rho_+ - \rho_-)\right]\hat{\theta}_j. \end{aligned} \tag{6.32}$$

Upon using the Gauss laws (7.7), we obtain for the scalar sector contribution:

$$J_s = \int d^2x \left[\frac{A}{e} \left(\nabla \cdot E + \mu b \right) + \frac{a}{g} \left(\nabla \cdot e + \mu B \right) \right]. \tag{6.33}$$

Now, integrating by parts and using the boundary conditions, this expression will give us a contribution that exactly cancels J_g, and another that is entirely given in terms of A and a:

$$\begin{aligned} J_s = & \int d^2x \left(B\, r_i E^i + b\, r_i e^i \right) \\ & - \frac{2\pi\mu}{eg} \left[A(\infty)a(\infty) - A(0)a(0) \right]. \end{aligned} \tag{6.34}$$

Thus, using the *ansatz*, boundary conditions and equations of motion, in the static limit we can obtain for the angular momentum of our (m,n)-vortices:

$$J = \frac{2\pi\mu}{eg}\, nm = \frac{QG}{2\pi\mu}. \tag{6.35}$$

We conclude that the angular momentum of these configurations is quantized, proportional to the product of charges, and fractional, with an anyonic nature. A similar result exhibiting these features was already obtained before, as one can see for instance Ref. [171].

Inserting this *ansatz* in the equations of motion, we obtain differential equations that must be solved in order to find an explicit solution. From the equations of motion, we obtain:

$$\ddot{\alpha} - \frac{\dot{\alpha}}{r} + \frac{\alpha}{r^2} + \mu \frac{e}{g} \dot{a} = \frac{M_e^2}{2} \left[\alpha\, \Delta F_+^2 + \beta\, \Delta F_-^2 \right], \tag{6.36}$$

$$\ddot{\beta} - \frac{\dot{\beta}}{r} + \frac{\beta}{r^2} + \mu \frac{g}{e} \dot{A} = \frac{M_g^2}{2} \left[\beta\, \Delta F_+^2 + \alpha\, \Delta F_-^2 \right]. \tag{6.37}$$

and,

$$\ddot{A} - \frac{\dot{A}}{r} + \mu \frac{e}{g} \left(\dot{\beta} - \frac{\beta}{r} \right) = \frac{M_e^2}{2} \left[A\, \Delta F_+^2 + a\, \Delta F_-^2 \right], \tag{6.38}$$

$$\ddot{a} - \frac{\dot{a}}{r} + \mu \frac{g}{e} \left(\dot{\alpha} - \frac{\alpha}{r} \right) = \frac{M_g^2}{2} \left[a\, \Delta F_+^2 + A\, \Delta F_-^2 \right], \tag{6.39}$$

where we defined $\Delta F_\pm^2 = F_+^2 \pm F_-^2$. The first two equations correspond to the $\nu = 0$ components, and the last two to the $\nu = i$ components. From the scalar sector:

$$\ddot{F}_\pm + \frac{\dot{F}_\pm}{r} + \frac{F_\pm}{r^2} \left[(\alpha \pm \beta)^2 - (A \pm a)^2 \right] = \frac{m_S^2}{2} \left(F_\pm^2 - 1 \right) F_\pm. \tag{6.40}$$

These are the differential equations that we need to solve considering the boundary

conditions given in Eq. (6.26) and the initial conditions stated in sequence. We were not able to find an analytical solution for these equations, and therefore, in the next section we will present for numerical solutions considering some particular cases that represent different possible scenarios. In passing, we comment that, to recover the AH model differential equations (and therefore the ANO vortex solution), we need only to take $F_- = a = \alpha = \beta = 0$.

In the above differential equations, one can note the appearance of a few mass scales, given by $m_S = \sqrt{\lambda v^2}$, $M_e = 2ev$, $M_g = 2gv$, and finally, μ. We can introduce the dimensionless coefficients $K_1 = \mu/m_S$, $K_2 = M_e/M_g = e/g$, and $K_3 = M_e/m_S$, writing the equations above using the dimensionless distance $x = m_S\, r$ (the derivatives from now on are with respect to x), in such a way that the differential equations can be written:

$$
\begin{aligned}
&\ddot{F}_+ + \frac{\dot{F}_+}{x} + \frac{F_+}{x^2}\left[(\alpha+\beta)^2 - (A+a)^2\right] = \frac{1}{2}\left(F_+^2 - 1\right)F_+,\\
&\ddot{F}_- + \frac{\dot{F}_-}{x} + \frac{F_-}{x^2}\left[(\alpha-\beta)^2 - (A-a)^2\right] = \frac{1}{2}\left(F_-^2 - 1\right)F_-,\\
&\ddot{A} - \frac{\dot{A}}{x} + K_1K_2\left(\dot{\beta} - \frac{\beta}{x}\right) = \frac{K_3^2}{2}\left[A\,\Delta F_+^2 + a\,\Delta F_-^2\right],\\
&\ddot{a} - \frac{\dot{a}}{x} + \frac{K_1}{K_2}\left(\dot{\alpha} - \frac{\alpha}{x}\right) = \frac{K_3^2}{2K_2^2}\left[a\,\Delta F_+^2 + A\,\Delta F_-^2\right],\\
&\ddot{\alpha} - \frac{\dot{\alpha}}{x} + \frac{\alpha}{x^2} + K_1K_2\dot{a} = \frac{K_3^2}{2}\left[\alpha\,\Delta F_+^2 + \beta\,\Delta F_-^2\right],\\
&\ddot{\beta} - \frac{\dot{\beta}}{x} + \frac{\beta}{x^2} + \frac{K_1}{K_2}\dot{A} = \frac{K_3^2}{2K_2^2}\left[\beta\,\Delta F_+^2 + \alpha\,\Delta F_-^2\right].
\end{aligned}
\tag{6.41}
$$

Before diving headfirst in the numerical solutions for these differential equations, we can briefly analyze the asymptotic behavior of the vortex configurations. In fact, considering the asymptotic behaviors for the profiles $F_\pm \to 1$ and $A, a, \alpha, \beta \to 0$, we can write $F_\pm = 1 - \tilde{F}_\pm$, $A = 0 + \tilde{A}$, $a = 0 + \tilde{a}$, $\alpha = 0 + \tilde{\alpha}$ and $\beta = 0 + \tilde{\beta}$, where all the quantities with tilde are very small for large x. In this regime, we will consider only first order terms in the quantities with tilde, neglecting higher orders.

In this approximation, the first two equations in Eq. (6.41) become $\ddot{\tilde{F}} + \dot{\tilde{F}}/x - \tilde{F} = 0$, where we already used the expansion described above and neglected higher order terms. Notice that this is a modified Bessel equation, therefore we can write for the asymptotic behavior of the scalar profiles, $F(r) \approx 1 - C\mathcal{K}_0(m_S\, r)$, and conclude that the scalar fields will approach their asymptotic value exponentially with a characteristic decay length given by the scalar mass. In the same way, we can consider the third and last equations in Eq. (6.41). Using the same approximation discussed above, we obtain the following equations: $\ddot{\tilde{A}} - \frac{\dot{\tilde{A}}}{x} + K_1K_2\left(\dot{\tilde{\beta}} - \frac{\tilde{\beta}}{x}\right) = K_3^2\tilde{A}$ and $\ddot{\tilde{\beta}} - \frac{\dot{\tilde{\beta}}}{x} + \frac{\tilde{\beta}}{x^2} + \frac{K_1}{K_2}\dot{\tilde{A}} = \frac{K_3^2}{K_2^2}\tilde{\beta}$. These differential equations lead to the following asymptotic behavior in terms of the modified Bessel

functions of the second kind:

$$A(r) \approx C_{\pm}\, r\, \mathcal{K}_1(m_{\pm} r),$$
$$\beta(r) \approx D_{\pm}\, \mathcal{K}_0(m_{\pm}\, r). \tag{6.42}$$

Therefore, the gauge profiles approach their asymptotic value exponentially, with a decay length given by the gauge field masses $m_{\pm}$, given in Eq. (6.18). The question of whether both m_+ and m_- are equally valid is a subtle one (see Refs. [144, 213, 214]), and should be investigated elsewhere. The same analysis can be done with the remaining equations and naturally gives us similar results.

6.3 Explicit vortex solutions

In this section we will exhibit explicit numerical solutions for the differential equations presented in the last section. The general strategy adopted here is as follows. We propose to expand the profile functions $F_+, F_-, A, a, \alpha, \beta$ in powers of x around the origin, for example, $A(x) = \sum_k A_k x^k$. Plugging these expansions in the above differential equations and using the initial conditions, we can obtain constraints in the expansion coefficients. With these expansions near the origin at hand, we can proceed to search the numerical solutions that will also satisfy the boundary conditions at infinity using a shooting method. It is important to note that, since we have $A(0) = m$, $a(0) = n$, we need first of all to specify which (m, n)-vortex we are trying to find.

In general lines, for the equations and initial conditions considered here, there are six coefficients to be adjusted; the others vanish or can be found in terms of these six and of the mass quotients K_i. Roughly speaking, near the origin we obtained the following structure of expansions:

$$\begin{aligned}
F_+(x) &= f_+\, x^{|n+m|} + ..., \\
F_-(x) &= f_-\, x^{|n-m|} + ..., \\
A(x) &= m + A_2 x^2 + A_+ x^{2|n+m|+2} + A_- x^{2|n-m|+2} + ..., \\
a(x) &= n + a_2 x^2 + a_+ x^{2|n+m|+2} + a_- x^{2|n-m|+2} + ..., \\
\alpha(x) &= \alpha_1 x + \alpha_+ x^{2|n+m|+1} + \alpha_- x^{2|n-m|+1} + ..., \\
\beta(x) &= \beta_1 x + \beta_+ x^{2|n+m|+1} + \beta_- x^{2|n-m|+1} + ...,
\end{aligned} \tag{6.43}$$

where $f_+, f_-, A_2, a_2, \alpha_1, \beta_1$ are free parameters that are determined for each set of parameters (m, n, K_1, K_2, K_3), in order to satisfy the asymptotic conditions at infinity.

In the following, we consider some examples representing distinctive classes of vortices. For each case, we show explicit numerical solutions and analyze some aspects of them,

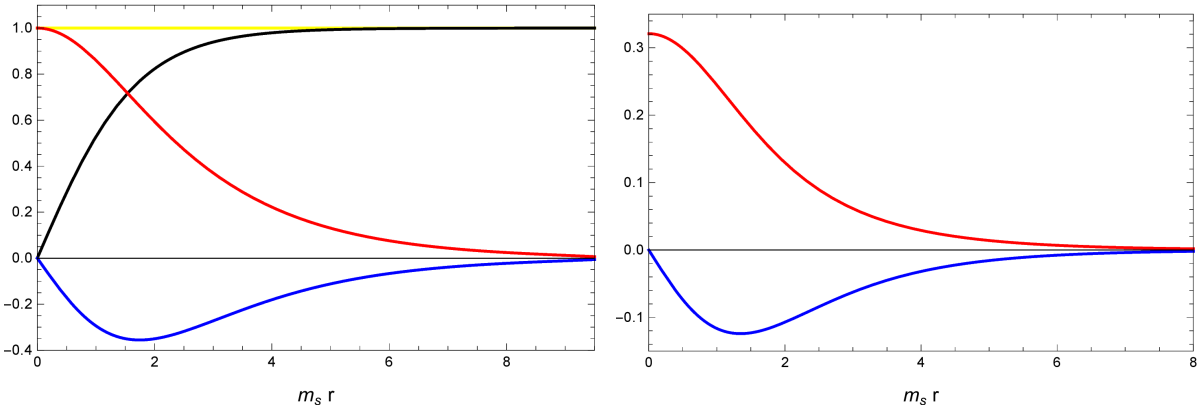

Figure 6.1: Left panel: Vortex solution for $m = 0, n = 1$. The scalar profile F is shown in black, and the gauge profiles a and α in red and blue, respectively, as functions of $x = m_S\, r$. The other profiles are identically zero. The relevant parameters here are: $F_1 = 0.58939309$, $a_2 = -0.16046967$, $\alpha_1 = -0.36281397$. Right Panel: The g-magnetic (in red) and electric (in blue) fields as functions of $x = m_S\, r$ for the $m = 0, n = 1$ solution, in units of g/m_S^2 and e/m_S^2, respectively.

stating the relevant parameters for the solution. In Sec. 6.3.1, we will analyze the situation where one of the integers is zero, using the case $(m = 0, n = 1)$ as an example; In Sec. 6.3.2, we investigate the situation where m and n are equal and non-zero, adopting the case $(m = n = 1)$ as illustration, and briefly commenting on $(m = n = 1/2)$; In Sec. 6.3.3, we study the case where m and n are non-zero and different, using the case $(m = 2, n = 1)$ as an example, and commenting on the case $(m = 1/2, n = 3/2)$; Finally, in Sec. 6.3.4, we analyze solutions obtained with different coefficients K_i.

6.3.1 m=0, n=1

Let us focus first on the solutions with $m = 0$ and $n = 1$, since this is the simplest possible scenario. In this case, we obtain $\Phi = 0$, implying $G = 0$ and $J = 0$, but $\chi = 2\pi/g$, giving $Q = 2\pi\mu/g$. Thus, we would be dealing with configurations without magnetic flux, g-electric charge and angular momentum, but with non-trivial g-magnetic flux and electric charge.

Following the procedure described in the beginning of this section, we found a numerical solution for the full set of differential equations that has the property of giving equal profiles $F_+ = F_-$ and identically zero solutions for $A = \beta = 0$. This means that, for this simple $(m = 0, n = 1)$ case, we found *a posteriori* that only half of the differential equations are non-trivial, and therefore in the numerical analysis we only considered these ones to simplify the analysis. The non-trivial profiles for the vortex solution are exhibited in Fig. 6.1, together with its g-magnetic and electric fields.

Notice that the g-magnetic field is finite, non-vanishing, and acquires its maximum value at the origin. The electric field is zero at the origin, maximum at a finite distance

and vanishes asymptotically. This is exactly the situation reported in Ref. [135], where the authors considered an AH model in the presence of a CS term, and obtained a charged vortex solution. This is not a coincidence, because, although physically different, mathematically speaking we are in a similar situation, since we have exactly the same differential equations to be solved. But it should be stressed that, besides the parity-invariance of the model and different field content (for instance, we have two gauge fields instead of only one), our vortex solution has zero angular momentum, instead of a non-zero and fractional value as reported in Ref. [135]. The charge and g-current densities display a similar behavior, vanishing at the origin, attaining their maximum value at a finite distance and decaying asymptotically to zero. We remark that an equivalent situation occurs when we consider the case $m = 1, n = 0$.

We were not able to find numerical solutions for $m = 0$ or $n = 0$ with $F_+ \neq F_-$ and $A \neq 0, \beta \neq 0$. It seems that, at least in this simple scenario with vanishing m or n, there is a natural trivialization of a sector. One might wonder if this trivialization is somehow a consequence of taking the K_i parameters all equal to 1, since they represent quotients between mass scales appearing in our physical system, but it does not seems to be so. In fact, in Sec. 6.3.4, we will consider a few numerical solutions for different values of K_i, and in all cases we obtained similar scalar and gauge profiles, exhibiting the trivialization property reported above.

It is interesting to see, for completeness, the solutions for $n = 1, 2, 3$ while keeping $m = 0$, to illustrate the different profiles that can appear in this setup. The scalar profiles are shown in Fig. 6.2, and we can note the typical power-law behavior near the origin as we change n. We also plot the gauge profiles a and α for $n = 1, 2, 3$. Comparing them, we see that in the cases with $n \neq 1$, the g-magnetic field does not attain its maximum value at the origin, but at a finite distance. The electric field, on the other hand, keeps its qualitative behavior, only changing where it attains its maximum value, cf. Fig. 6.3.

6.3.2 m=n=1

Now, let us search for solutions with $m = n = 1$. In this case, looking to Eq. (6.24) we immediately see that $Q = \frac{2\pi\mu}{g}$ and $G = \frac{2\pi\mu}{e}$. This vortex has a non-trivial angular momentum given by $J = \frac{2\pi\mu}{eg}$, differently from the previous solution. We report this vortex in Fig. 6.4, together with its electric and magnetic fields.

Notice that we obtained *a posteriori* a simplified solution where $A = a$, $\alpha = \beta$, and $F_- = 1$. For the scalar profiles, it is important to remember that the exponential part of the scalar fields $\phi_\pm$ involves $m \pm n$. Therefore, the fact that F_- gives us a constant and F_+ displays a typical 2-vortex behavior is an indication that the true winding numbers are given by $m + n$ and $m - n$, instead of m and n separately.

One can wonder again whether the trivial behavior of the gauge profiles is due to

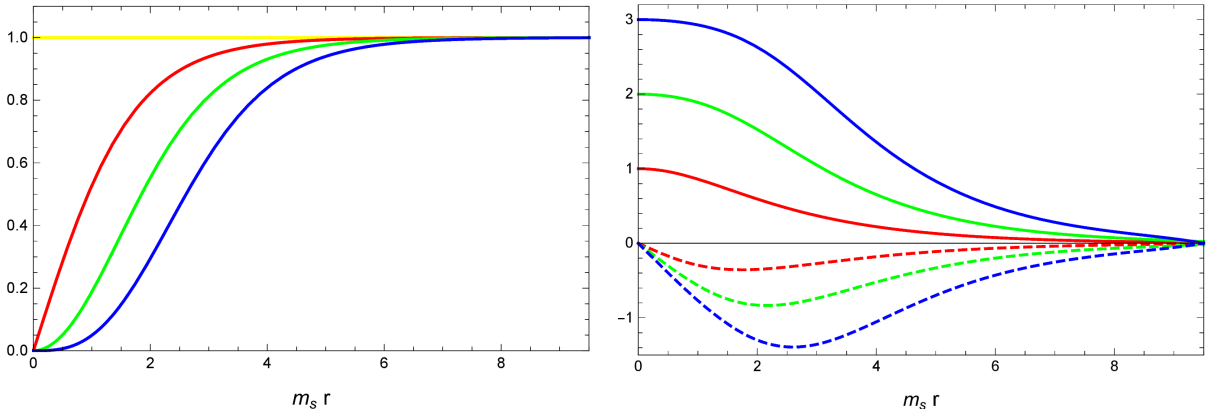

Figure 6.2: Left Panel: The scalar profiles F as a function of $x = m_S\, r$ for the solutions with m=0 and n = 1 (red), 2 (green), 3 (blue). Right panel: The gauge profiles a and α as functions of $x = m_S\, r$ for the solutions with m=0 and n = 1 (red), 2 (green), 3 (blue). The solid lines correspond to the profile a and the dashed lines to the profile α.

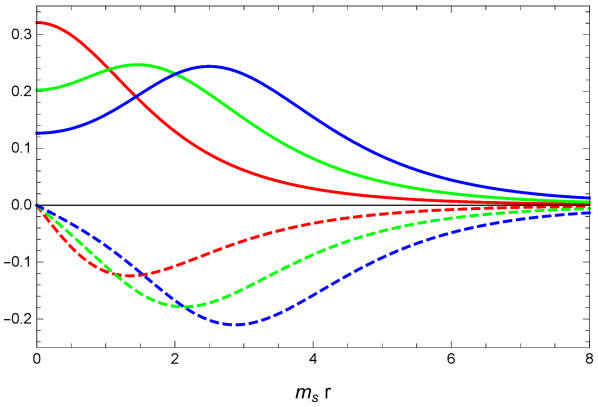

Figure 6.3: The g-magnetic and electric fields as functions of $x = m_S\, r$ for the solution with m=0 and n = 1 (red), 2 (green), 3 (blue). The solid lines correspond to the g-magnetic field b in units of g/m_S^2 and the dashed lines correspond to the electric field E_r in units of e/m_S^2.

the choice of coefficients. Unlike the previous case, the answer is affirmative, at least with respect to the variation of K_2 governing the relationship between different gauge couplings. In fact, starting from the degenerate case and varying K_2, the solutions for profiles A and a as well as α and β are not degenerate anymore; however, the scalar profiles do not present any appreciable qualitative change. Varying K_1 and K_3, we will find a behavior similar to the ones described in the last case, as depicted in Sec. 6.3.4.

The case $m = n = 1/2$ does not present any appreciable qualitative change in comparison with the solution presented here, except by the scalar profile near the origin, that displays a typical 1-vortex behavior, and by its lowest value of energy and angular momentum ($J = \pi\mu/2eg$). The energy hierarchy of our solutions will be shortly discussed in the next subsection.

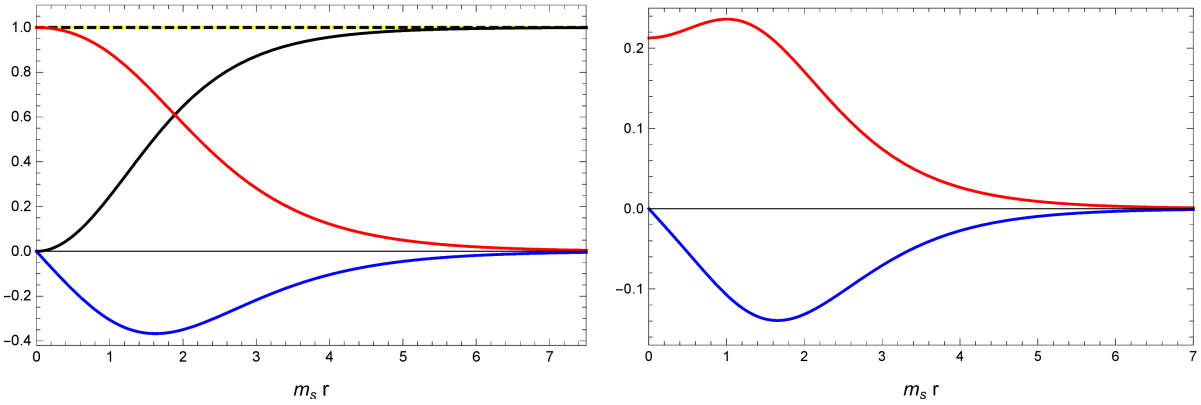

Figure 6.4: Left panel: Vortex solution for $m = n = 1$. The scalar profile F_+ is shown in solid black, F_- in dashed black, and the gauge profiles a and α in red and blue respectively, as functions of $x = m_S\, r$. Notice that here we have $A = a$ and $\alpha = \beta$. The relevant parameters here are $F_{+2} = 0.28684863$, $F_{-0} = 1$, $A_2 = a_2 = -0.10644717$, $\alpha_1 = \beta_1 = -0.36047370$. Right panel: The magnetic (in red) and electric (in blue) fields as functions of $x = m_S\, r$ for the $m = n = 1$ solution, in units of e/m_S^2. Notice that here we have $B = b$ and $E_r = e_r$.

6.3.3 m=2, n=1

Finally, we will consider the case $m = 2$ and $n = 1$. Here, we readily obtain $Q = \frac{2\pi\mu}{g}$ and $G = \frac{4\pi\mu}{e}$. Notice that we also have a non-vanishing angular momentum given by $J = \frac{4\pi\mu}{eg}$. In this case, we expect to see a totally novel result, since there are no simplifications in consequence of the choice of m and n.

The numerical solution obtained in this case is given in Fig. 6.5, together with its electric and magnetic fields (as well as the g-electric and g-magnetic). As one can see, this time there is no degeneracy in the profiles, being all of them non-trivial. In the scalar profiles, notice that F_- displays a behavior near the origin characteristic of a 1-vortex, and F_+ of a 3-vortex. For the first time, we observe an oscillating behavior in the electric and g-magnetic fields, and in particular, we see that there is a finite distance where they vanish. We remark that the gauge fields here are not necessarily related with electromagnetic phenomena, possibly being used to describe some effective degree of freedom in a condensed matter system, for instance, therefore one should be careful before drawing any conclusion.

The case $m = 1/2, n = 3/2$ does not present any appreciable qualitative change in comparison with the solution presented here, except by the scalar profiles near the origin, since F_+ and F_- display a behavior typical of 2-vortex and 1-vortex solutions, respectively.

At this point, armed with all these vortex solutions, we can discuss their energy densities and highlight the mass hierarchy between them. Let us first call attention to the fact that we have been successful in finding finite-energy configurations, as one can immediately see in Fig. 6.6. From these energy densities, defining $M_{(m,n)}$ as the mass

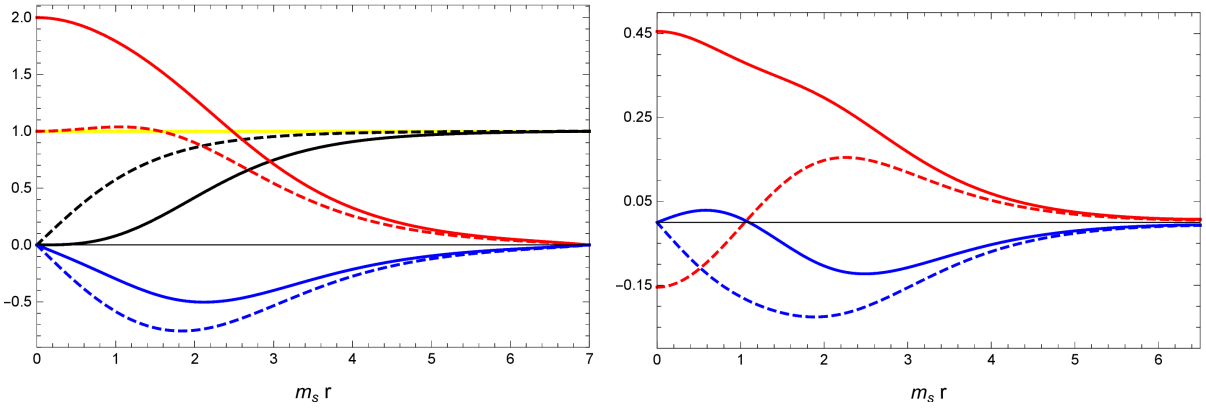

Figure 6.5: Left panel: Vortex solution for $m = 2, n = 1$. The scalar profile F_+ is shown in solid black, F_- in dashed black; the gauge profile A is shown in solid red, a in dashed red; the profile α is shown in solid blue, β in dashed blue; all of them are given as functions of $x = m_S\, r$. The relevant parameters here are $F_{+3} = 0.07723697$, $F_{-1} = 0.66377069$, $a_2 = 0.07718614$, $A_2 = -0.22754617$, $\alpha_1 = -0.27824800$, $\beta_1 = -0.68551826$. Right panel: The magnetic (solid red) and electric (solid blue) fields in units of e/m_S^2; the g-magnetic (dashed red) and g-electric (dashed blue) fields in units of g/m_S^2. All of them as functions of $x = m_S\, r$ for the $m = 2, n = 1$ solution.

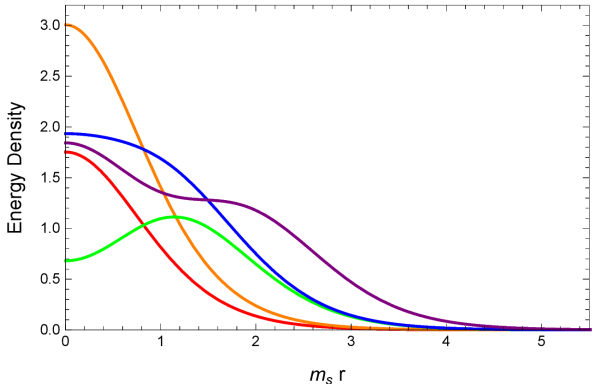

Figure 6.6: The energy density for the (m,n)-vortex solutions in units of $1/v^2\, m_S^2$. In red, (1/2,1/2); in orange, (0,1); in green, (1,1); in blue, (1/2,3/2); in purple, (2,1).

associated with the (m,n)-vortex, we obtained the following mass hierarchy in units of v^2: $M_{(1/2,1/2)} \approx 1.31 < M_{(0,1)} \approx 2.27 < M_{(1,1)} \approx 2.92 < M_{(1/2,3/2)} \approx 3.87 < M_{(2,1)} \approx 5.70$. Interestingly enough, one can observe that $M_{(1/2,1/2)} + M_{(-1/2,1/2)} = 2M_{(1/2,1/2)} > M_{(0,1)}$. Remember that in the $(\pm 1/2, 1/2)$-vortex, $F_\pm$ is 1-vortex scalar profile, while $F_\mp$ lies in the vacuum, whereas in the $(0, 1)$-vortex both of them are typical 1-vortex scalar profiles. This suggests that there might be an attraction between these vortices. However, to truly understand the interactions between these vortices and conclusively assert this, a more thorough analysis should be done elsewhere, along the lines presented in Ref. [215].

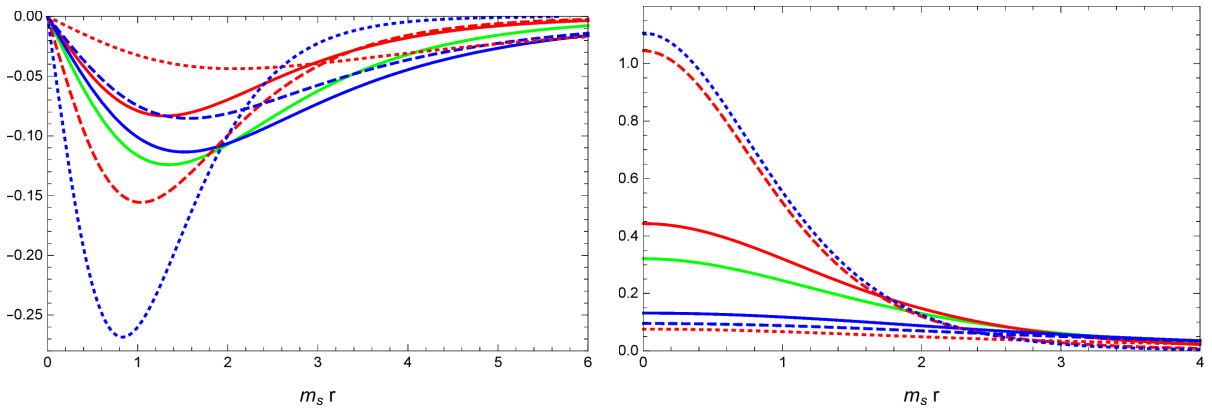

Figure 6.7: Left panel: The electric fields associated with $m = 0, n = 1$ solution in units of e/m_S^2 for different values of (K_1, K_2, K_3). In solid green, $(1, 1, 1)$; in solid red, $(1/2, 1, 1)$; in solid blue, $(2, 1, 1)$; in dashed red, $(1, 1/2, 1)$; in dashed blue, $(1, 2, 1)$; in dotted red, $(1, 1, 1/2)$; in dotted blue, $(1, 1, 2)$. Right panel: The g-magnetic fields associated with $m = 0, n = 1$ solution in units of g/m_S^2 for different values of (K_1, K_2, K_3). In solid green, $(1, 1, 1)$; in solid red, $(1/2, 1, 1)$; in solid blue, $(2, 1, 1)$; in dashed red, $(1, 1/2, 1)$; in dashed blue, $(1, 2, 1)$; in dotted red, $(1, 1, 1/2)$; in dotted blue, $(1, 1, 2)$.

6.3.4 Vortex solutions for different K_i's

In this section, we investigate the existence of vortex solutions and their main properties upon varying the coefficients K_i. In the following, we will use as a reference the case $K_1 = K_2 = K_3 = 1$, already studied in the last sections, and change each K_i by a factor of two keeping the others fixed, to find different vortex solutions and compare their main features. It is important to keep in mind that each set of parameters K_i characterizes a different physical system, and upon varying a K_i coefficient, we need to adjust the parameters in order to obtain a vortex solution.

Focusing first in the case $m = 0, n = 1$, the variation of K_i led to qualitatively similar scalar and gauge profiles, and the trivialization property already highlighted before. As one can see from Fig. 6.7, the electric field qualitative behavior is the same for all the values considered: zero at the origin, attaining a finite non-zero maximum value at some distance and decaying to zero at large distances. Notice that by varying K_1, there are only small changes in the profile. By lowering K_2, we can observe a more pronounced decay and an improvement in its maximum value. On the other hand, by increasing K_3 we observe a sensible increase at the absolute value of the maximum electric field value, accompanied by a more pronounced decay and a small shift in the position where this maximum occur. For the g-magnetic field, the qualitative behavior is also the same as we vary K_i: attains a finite non-zero maximum value at the origin and decays monotonically as we increase the distance going to zero in the asymptotic limit. By increasing K_1, we see that the maximum value of the g-magnetic field diminishes, and this is compatible with the behavior observed in Ref. [145]. Lowering K_2 or increasing K_3, we observe a strong

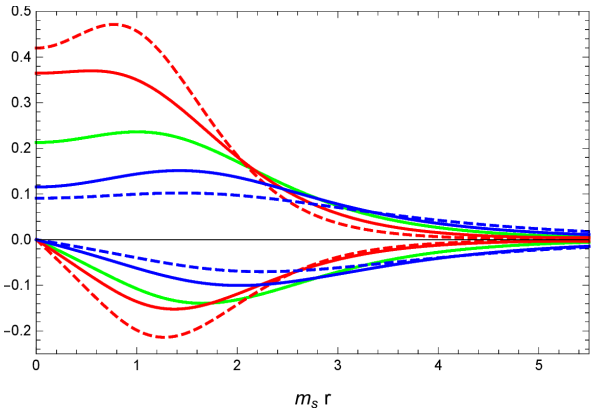

Figure 6.8: The magnetic (B), g-magnetic (b), electric (E_r) and g-electric (e_r) fields associated with the $m = n = 1$ solutions, for different values of K_2. The solid lines refer to B and E_r; the dashed lines refer to b and e_r. B and b are shown in the upper part; E_r and e_r are shown in the lower part. In green, $K_2 = 1$; in red, $K_2 = 1/2$; in blue, $K_2 = 2$.

change in the maximum value of the g-magnetic field as well as a more pronounced decay as we go far from the origin. Lowering K_1, increasing K_2, or lowering K_3, as before, has the opposite effect, cf. Fig. 6.7.

Proceeding to the $m = n = 1$ solution, as already highlighted in the main text, the degeneracy that we have found is due to the equality of the couplings when $K_2 = 1$. When we depart from this simpler case, we find vortex solutions with $A \neq a$ and $\alpha \neq \beta$, naturally leading to different magnetic and g-magnetic (as well as electric and g-electric) fields, as one can see in Fig. 6.8. Upon varying K_1 and K_3, we observed the same behavior as described in the previous case.

Finally, we remark that in the case $m = 2, n = 1$ the variation of the coefficients K_i did not lead to any substantial difference from the cases already discussed here.

For completeness, it would be interesting to analyze what happens in some limiting cases of this model, for instance, when the CS terms or the Maxwell terms are absent. This analysis is done in the next section.

6.4 Vortices in limiting cases

In this section, we study two particular limits of our model. First, we will briefly address the simpler case in which we do not have a CS term, that is, $\mu = 0$. From a practical point of view, this can be achieved by setting $K_1 = 0$, and the conclusions in this part will come straightforwardly. Notice that this scenario bears resemblance to the usual ANO vortex, since this is nothing but a scalar QED with two gauge fields and two scalars with different charges.

Second, we will analyze our model in the absence of Maxwell terms, with the gauge kinetic part given solely by the CS term. This allows us to solve the Gauss laws and write

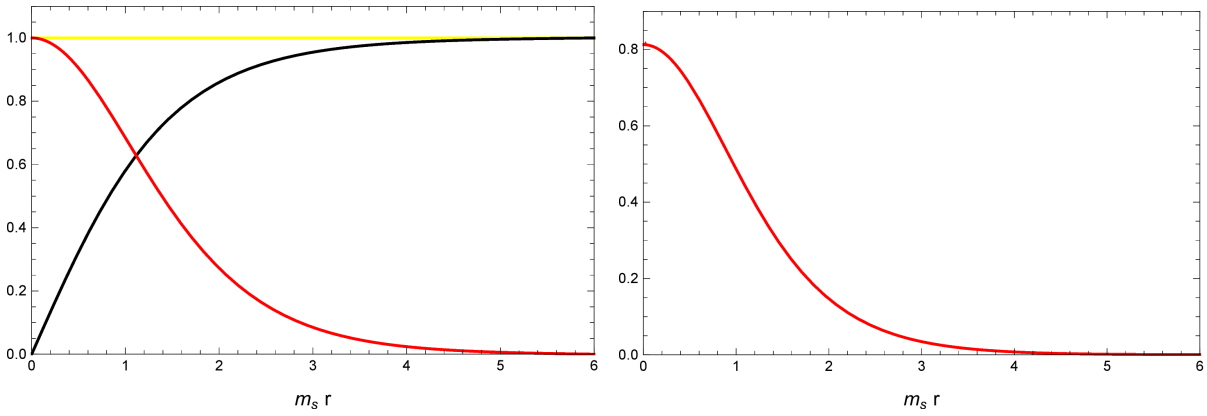

Figure 6.9: Left panel: Vortex solution for $m = 0, n = 1$ in the pure Maxwell limit. The scalar profile F is shown in black and the gauge profile a in red, respectively, as functions of $x = m_S\, r$. The other profiles are identically zero. Right panel: The g-magnetic field in the pure Maxwell limit, in units of g/m_S^2, as a function of $x = m_S\, r$. The magnetic field as well as the electric and g-electric fields are zero here.

the time components of the gauge fields as functions of other quantities. This scenario, where the CS term dominates and the Maxwell terms can be neglected, could be seen as the low-energy regime of our model.

We remark that the results obtained in this section could be inferred by looking at the behavior of magnetic and electric fields when we changed the coefficient K_1 while keeping the others coefficients fixed, since this increases (or decreases) the importance of CS parameter with respect to the other scales of the system. Although it can give us a hint of what would happen in the limits considered here, it is important to remark that the passage from the model considered to the pure CS limit is a subtle one, as one can see for instance in Ref. [145], which justifies a separate investigation of the latter.

Now, we briefly state the results for $K_1 = \mu/m_S = 0$. We will consider the case $m = 0$ and $n = 1$ with $K_2 = K_3 = 1$ for definiteness, but we would have similar results in the other examples. The vortex solution *per se* does not exhibit any appreciable change in the profiles F and a as one can see in Fig. 6.9. But now we have $\alpha = 0$, and this fact is the most striking difference that appears in this regime. Since we do not have the CS Gauss law constraint anymore, the electric field vanishes and we conclude that the vortex is neutral, as expected. The g-magnetic field in this regime is stronger in magnitude, but exhibit the usual profile, attaining a maximum at the origin and decaying as we increase x, as one can also see in Fig. 6.9. This is in accordance with the already known results (see for example Ref. [145]).

Proceeding to the more interesting scenario in which we can neglect the Maxwell terms,

the Gauss laws constraints become much simpler,

$$\begin{aligned} \mu b &= e\left(\rho_+ + \rho_-\right), \\ \mu B &= g\left(\rho_+ - \rho_-\right). \end{aligned} \tag{6.44}$$

Without Maxwell terms, we are able to obtain A_0 and a_0 directly from the other fields. In fact, we can find:

$$\begin{aligned} eA_0 &= \Lambda\left[eB\left(|\phi_+|^2 - |\phi_-|^2\right) - gb\left(|\phi_+|^2 + |\phi_-|^2\right)\right] \\ ga_0 &= \Lambda\left[gb\left(|\phi_+|^2 - |\phi_-|^2\right) - eB\left(|\phi_+|^2 + |\phi_-|^2\right)\right], \end{aligned} \tag{6.45}$$

where we defined $\Lambda \equiv \mu/8eg|\phi_+|^2|\phi_-|^2$ for convenience. Plugging the *ansatz*, and writing in dimensionless variables using $x = m_S\, r$ and the coefficients K_i as before, we obtain the following expressions for α and β:

$$\begin{aligned} \alpha &= \frac{K_1 K_2}{2K_3^2}\frac{1}{F_+^2 F_-^2}\left[\dot{a}\left(F_+^2 + F_-^2\right) - \dot{A}\left(F_+^2 - F_-^2\right)\right], \\ \beta &= \frac{K_1 K_2}{2K_3^2}\frac{1}{F_+^2 F_-^2}\left[\dot{A}\left(F_+^2 + F_-^2\right) - \dot{a}\left(F_+^2 - F_-^2\right)\right]. \end{aligned} \tag{6.46}$$

Now, we need only to plug these analytic expressions for α and β in the differential equations (6.41), ignoring the contributions coming from the Maxwell terms, and solve them for given m and n. Notice that we need only to care about the first four equations, since the last two are already satisfied when we write α and β as above.

Although this is a legitimate path to be followed, we simply solved the full set of differential equations in the absence of Maxwell contributions, without using explicitly the CS constraint, stated here only for completeness. In the following, we will exhibit the solution profiles and also the electric and magnetic (as well as g-electric and g-magnetic) fields associated with them. For all of them, we considered $K_1 = K_2 = K_3 = 1$ for simplicity.

The solution for the equations of motion in the pure CS regime for the case $m = 0, n = 1$ is given in Fig. 6.10 together with the electric and g-magnetic fields. Notice that they are zero at the origin, attains their maximum value at a finite distance and decays asymptotically, exactly as reported in Ref. [147], for example. The $m = n = 1$ case gives very similar results, see Fig. 6.11. Remember that we are considering here the particular case in which $K_2 = 1$ and therefore we have degenerate solutions, as we already discussed before. The case $m = 2, n = 1$ presents a more complicated behavior, but it is reminiscent of the solution presented in the main text. In fact, the solutions are shown in Fig. 6.12 together with its electric and magnetic (as well as g-electric and g-magnetic) fields. We still have non-trivial solutions for all profiles and an oscillating behavior for the fields.

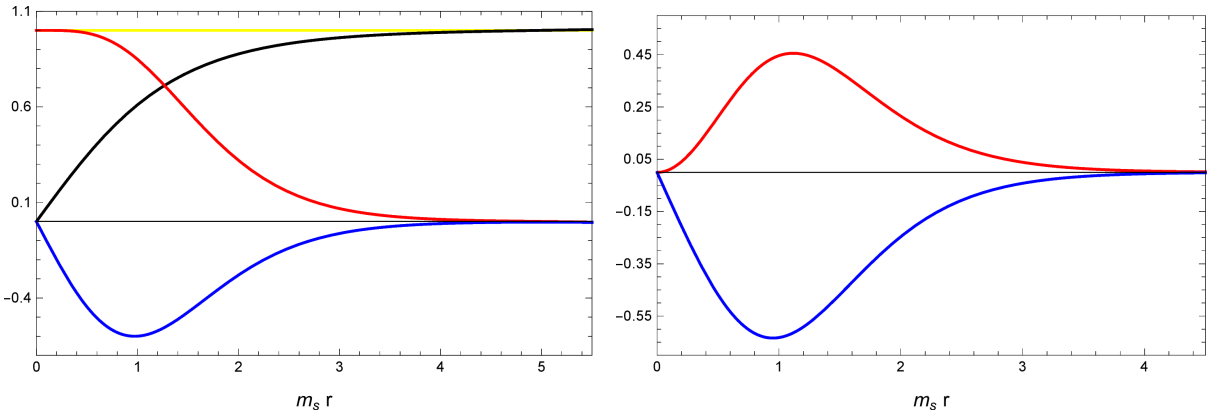

Figure 6.10: Left panel: Vortex solution for $m = 0, n = 1$ in the pure CS limit. The scalar profile F is shown in black; the gauge profiles a and α are shown in red and blue, respectively, as functions of $x = m_S\, r$. The other profiles are identically zero. Right panel: The g-magnetic (in red) and electric (in blue) fields as functions of $x = m_S\, r$ for the $m = 0, n = 1$ solution in the pure CS limit, in units of g/m_S^2 and e/m_S^2, respectively.

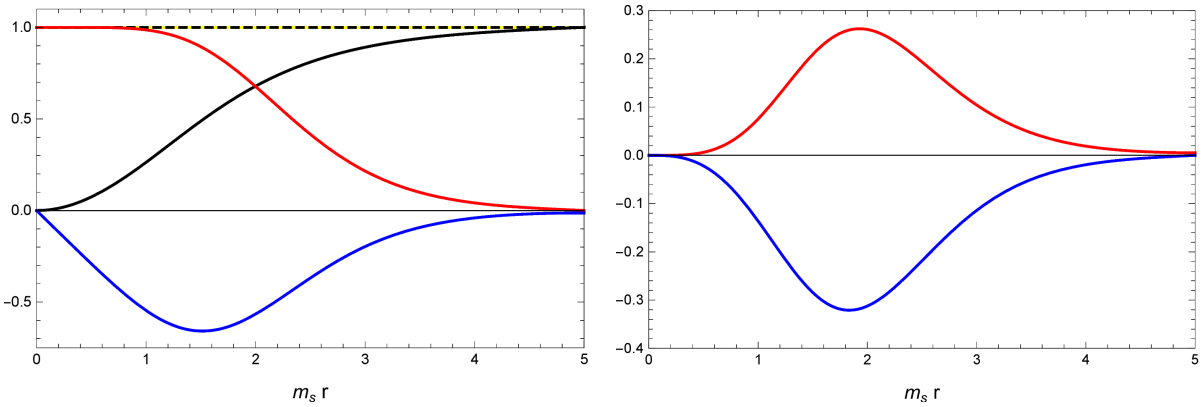

Figure 6.11: Left panel: Vortex solution for $m = n = 1$ in the pure CS limit. The scalar profile F_+ is shown in solid black and F_- in dashed black; the gauge profiles A and α are shown in red and blue, respectively, as functions of $x = m_S\, r$. Notice that here we have $A = a$ and $\alpha = \beta$. Right panel: The magnetic (in red) and electric (in blue) fields as functions of $x = m_S\, r$ for the $m = n = 1$ solution in the pure CS limit, in units of e/m_S^2. Notice that here we have $B = b$ and $E_r = e_r$.

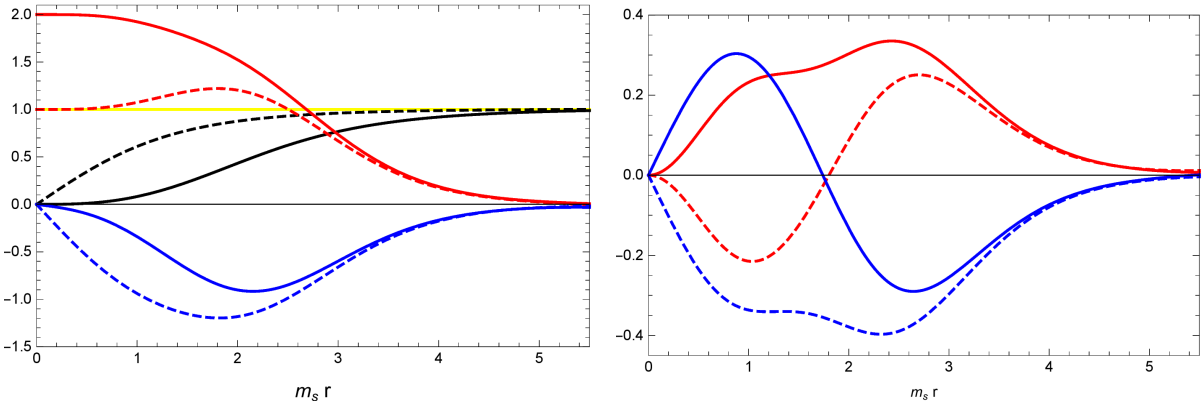

Figure 6.12: Left panel: Vortex solution for $m = 2, n = 1$ in the pure CS limit. The scalar profile F_+ is shown in solid black, F_- in dashed black; the gauge profile A is shown in solid red, a in dashed red; the profile α is shown in solid blue, β in dashed blue; all of them are given as functions of $x = m_S\, r$. Right panel: The magnetic (solid red) and electric (solid blue) fields in units of e/m_S^2; the g-magnetic (dashed red) and g-electric (dashed blue) fields in units of g/m_S^2. All of them as functions of $x = m_S\, r$ for the $m = 2, n = 1$ solution in the pure CS limit.

Chapter 7

A self-dual regime

In this Chapter, we present a self-dual version of the parity-invariant Maxwell-CS model studied in Chapter 6. We show that by choosing a suitable potential, the model admits a Bogomol'nyi-type bound for the energy, whose saturation leads to first order self-duality equations. We perform a detailed analysis of this system, examining its main properties. We present explicit numerical solutions corresponding to finite-energy topological vortices and non-topological solitons, discussing their main features.[1]

7.1 Theoretical setup

Let us consider the parity-invariant $U(1)_A \times U(1)_a$ Maxwell-CS model coupled with scalar matter, in the presence of additional fields N and M:

$$\begin{aligned}\mathcal{L} = &-\frac{1}{4}F_{\mu\nu}F^{\mu\nu} - \frac{1}{4}f_{\mu\nu}f^{\mu\nu} + \mu\epsilon^{\mu\nu\rho}A_\mu\partial_\nu a_\rho \\ &+ |D_\mu\phi_+|^2 + |D_\mu\phi_-|^2 + \frac{1}{2}\left(\partial_\mu N\right)^2 + \frac{1}{2}\left(\partial_\mu M\right)^2 \\ &- V\left(|\phi_+|, |\phi_-|, N, M\right), \end{aligned} \tag{7.1}$$

where we define $D_\mu\phi_\pm = \partial_\mu\phi_\pm + ieA_\mu\phi_\pm \pm iga_\mu\phi_\pm$. Here we have $F_{\mu\nu} = \partial_\mu A_\nu - \partial_\nu A_\mu$ and $f_{\mu\nu} = \partial_\mu a_\nu - \partial_\nu a_\mu$, the gauge couplings associated with $U(1)_A$ and $U(1)_a$ are e and g, respectively, and $\mu > 0$ is the CS parameter.

This model has $U(1)_A \times U(1)_a$ gauge symmetry by construction, with the following

[1]This Chapter is based on Phys. Lett. B **833**, 137326 (2022).

transformations:

$$\begin{cases} \phi'_{\pm} &= e^{i\rho(x)}\phi_{\pm}, \\ A'_{\mu} &= A_{\mu} - \frac{1}{e}\partial_{\mu}\rho(x)\ , \\ a'_{\mu} &= a_{\mu}\ ; \end{cases} \qquad \begin{cases} \phi'_{\pm} &= e^{\pm i\xi(x)}\phi_{\pm}, \\ A'_{\mu} &= A_{\mu}\ , \\ a'_{\mu} &= a_{\mu} - \frac{1}{g}\partial_{\mu}\xi(x)\ . \end{cases} \tag{7.2}$$

Parity invariance is achieved here by extending the usual parity concept to include a transformation that swaps the role of ϕ_+ and ϕ_- in the space of fields:

$$\begin{aligned} A^P_{\mu} &= \mathcal{P}_{\mu}^{\ \nu}\, A_{\nu}, \quad & a^P_{\mu} &= -\mathcal{P}_{\mu}^{\ \nu}\, a_{\nu}, \\ \phi^P_{+} &= \eta\, \phi_{-}, & \phi^P_{-} &= \eta\, \phi_{+}, \\ N^P &= N, & M^P &= -M. \end{aligned} \tag{7.3}$$

where $\mathcal{P}_{\mu}^{\ \nu} = diag(+\,-\,+)$, and η is a complex phase. This model is also time-reversal invariant, but we will not discuss it here, since we will be mainly interested in static configurations. Here one could also define $A^{\pm}_{\mu} = \left(A_{\mu} \pm a_{\mu}\right)/\sqrt{2}$, with parity acting as $A^{\pm}_{\mu} \to \mathcal{P}^{\nu}_{\mu} A^{\mp}_{\nu}$, as already emphasized before.

To the purpose of investigating the existence of self-dual solitons, let us propose the following potential:

$$\begin{aligned} V = {} & (eN + gM)^2|\phi_+|^2 + (eN - gM)^2|\phi_-|^2 \\ & + \frac{1}{2}\left[e\left(|\phi_+|^2 - |\phi_-|^2\right) - \mu M\right]^2 \\ & + \frac{1}{2}\left[g\left(|\phi_+|^2 + |\phi_-|^2 - 2v^2\right) - \mu N\right]^2. \end{aligned} \tag{7.4}$$

This potential is consistent with all the symmetries of the model, and despite not being the most general possibility, it arises naturally from the requirement of a Bogomol'nyi bound for the energy. Setting $|\phi_+| = |\phi_-|$, $M = 0$, $e = g$, and appropriately rescaling the remaining parameters, it exactly reproduces the potential proposed in [158], which is known to contain both pure Maxwell and pure CS self-dual vortices as limiting cases. Instead, if $N = M = 0$ and $e = g$, we can recover the potential used in Chapter 6.

The equations of motion for this model are given by

$$\begin{aligned} \partial_{\mu}F^{\mu\nu} + \mu\epsilon^{\nu\alpha\beta}\partial_{\alpha}a_{\beta} &= e\left(J^{\nu}_{+} + J^{\nu}_{-}\right), \\ \partial_{\mu}f^{\mu\nu} + \mu\epsilon^{\nu\alpha\beta}\partial_{\alpha}A_{\beta} &= g\left(J^{\nu}_{+} - J^{\nu}_{-}\right), \\ D_{\mu}D^{\mu}\phi_{\pm} &= -\frac{dV}{d\phi^*_{\pm}}, \end{aligned} \tag{7.5}$$

supplemented by the equations for N and M

$$\begin{aligned}(\Box+\mu^2)N =& -2e\left[(eN+gM)|\phi_+|^2+(eN-gM)|\phi_-|^2\right]\\ &+\mu\left[g(|\phi_+|^2+|\phi_-|^2-2v^2)\right]\\ (\Box+\mu^2)M =& -2g\left[(eN+gM)|\phi_+|^2-(eN-gM)|\phi_-|^2\right]\\ &+\mu\left[e(|\phi_+|^2-|\phi_-|^2)\right].\end{aligned} \tag{7.6}$$

The currents above are $J^\nu_\pm = i\left[\phi^*_\pm D^\nu\phi_\pm - \phi_\pm D^\nu\phi^*_\pm\right]$. We can define the electric and g-eletric fields as $E^i = F^{i0}$, $e^i = f^{i0}$ as well as the magnetic and g-magnetic fields as $B = \epsilon^{ij}\partial_i A_j$, $b = \epsilon^{ij}\partial_i a_j$. From the zeroth component of the gauge fields equations, we can obtain

$$\begin{aligned}\vec{\nabla}\cdot\vec{E}+\mu b &= e\left(\rho_+ + \rho_-\right),\\ \vec{\nabla}\cdot\vec{e}+\mu B &= g\left(\rho_+ - \rho_-\right),\end{aligned} \tag{7.7}$$

where $\rho_\pm = J^0_\pm$. The electric and g-electric charges are given by $Q = e\int d^2x\ (\rho_+ + \rho_-)$, $G = g\int d^2x\ (\rho_+ - \rho_-)$, and the magnetic and g-magnetic fluxes by $\Phi \equiv \int d^2x\, B$, $\chi \equiv \int d^2x\, b$, respectively. Upon integration, we obtain:

$$Q = \mu\chi, \quad G = \mu\Phi, \tag{7.8}$$

relating the charge associated with one gauge field with the magnetic flux associated with the other. This mutual statistics behavior [165] is a characteristic feature of models with a mixed CS term [171], here implementing the flux attachment in a parity-invariant way.

The energy functional for this model is of the form:

$$\begin{aligned}E =& \int d^2x\left[\frac{1}{2}\left(\vec{E}^2+B^2\right)+\frac{1}{2}\left(\vec{e}^2+b^2\right)+V\right.\\ &+|D_0\phi_+|^2+|D_0\phi_-|^2+|D_i\phi_+|^2+|D_i\phi_-|^2\\ &\left.+\frac{1}{2}\Big((\partial_0 M)^2+(\partial_0 N)^2+(\partial_i M)^2+(\partial_i N)^2\Big)\right]\end{aligned} \tag{7.9}$$

The minimum energy configuration can be achieved, for instance, with $A_\mu = a_\mu = 0$ and constant scalar fields, provided that they minimize the potential. Inspection of Eq. (7.4)

indicates that $V = 0$ if, and only if:

$$\begin{aligned}
&(eN + gM)^2|\phi_+|^2 = 0,\\
&(eN - gM)^2|\phi_-|^2 = 0,\\
&e\left(|\phi_+|^2 - |\phi_-|^2\right) - \mu M = 0,\\
&g\left(|\phi_+|^2 + |\phi_-|^2 - 2v^2\right) - \mu N = 0.
\end{aligned} \tag{7.10}$$

Out of which only four possibilities arise:

$$\begin{aligned}
&\bullet\ (0,0) : |\phi_+|^2 = |\phi_-|^2 = 0;\ M = 0;\ N = -\frac{2gv^2}{\mu},\\
&\bullet\ (1,1) : |\phi_+|^2 = |\phi_-|^2 = v^2;\ M = N = 0,\\
&\bullet\ (0,1) : |\phi_+|^2 = 0;\ |\phi_-|^2 = v^2;\ M = -\frac{ev^2}{\mu};\ N = -\frac{gv^2}{\mu},\\
&\bullet\ (1,0) : |\phi_+|^2 = v^2;\ |\phi_-|^2 = 0;\ M = \frac{ev^2}{\mu};\ N = -\frac{gv^2}{\mu}.
\end{aligned} \tag{7.11}$$

The first vacuum corresponds to the symmetric, the second, to the asymmetric, and the last two, to the partially symmetric phases of the gauge symmetry, respectively. Notice that the first two vacua are invariant under parity, while the last two are not, transforming into each other. All these vacua are degenerate, therefore, there can also be domain walls solutions connecting them, but this case will not be considered here. We will focus on the parity-invariant vacua, investigating the existence of topological vortices and non-topological solitons.

Let us briefly discuss the perturbative spectrum by considering the quadratic part of the fluctuations around each vacuum. We can see that in the $(0,0)$-vacuum we do not have spontaneous symmetry breaking since the only field acquiring a non-trivial vacuum expectation value (VEV) is neutral, and that in the $(1,1)$-vacuum, both $U(1)$'s are spontaneously broken. The quadratic part of the Lagrangian in this case is

$$\begin{aligned}
\mathcal{L}^{\text{quad}}_{(0,0)} = &-\frac{1}{4}F_{\mu\nu}F^{\mu\nu} - \frac{1}{4}f_{\mu\nu}f^{\mu\nu} + \mu\epsilon^{\mu\rho\nu}A_\mu\partial_\rho a_\nu\\
&+ |\partial_\mu\phi_+|^2 + |\partial_\mu\phi_-|^2 + \frac{1}{2}\left(\partial_\mu M\right)^2 + \frac{1}{2}\left(\partial_\mu\tilde{N}\right)^2\\
&-\left(\frac{2egv^2}{\mu}\right)^2\left(|\phi_+|^2+|\phi_-|^2\right) - \frac{\mu^2}{2}\left(M^2+\tilde{N}^2\right)
\end{aligned} \tag{7.12}$$

Thus, on the $(0,0)$-vacuum, one can find two massive complex scalar fields with masses $m_{\phi_+} = m_{\phi_-} = 2egv^2/\mu$, a real scalar and a real pseudoscalar with masses $m_N = m_M = \mu$, and two massive gauge bosons with masses equal to μ. We remark that this gauge boson mass have a topological origin, since there is no Higgs mechanism taking place here, and also that it is equal to the real scalar and pseudoscalar masses.

In the $(1,1)$-vacuum, both charged scalar fields acquire a non-trivial VEV, putting the theory totally into the Higgs phase, where both $U(1)$'s are spontaneously broken. Here we expect that there will be a contribution to the mass coming from the Higgs mechanism and another contribution of a topological nature coming from the CS term. In the unitary gauge we can write $\phi_{\pm}(x) = v + h_{\pm}(x)/\sqrt{2}$, and therefore, the quadratic part of the Lagrangian reads:

$$\begin{aligned}\mathcal{L}^{\text{quad}}_{(1,1)} &= -\frac{1}{4}F_{\mu\nu}F^{\mu\nu} - \frac{1}{4}f_{\mu\nu}f^{\mu\nu} + \mu\epsilon^{\mu\nu\rho}A_{\mu}\partial_{\nu}a_{\rho} \\ &+ 2v^2\left(e^2A_{\mu}A^{\mu} + g^2a_{\mu}a^{\mu}\right) \\ &+ \frac{1}{2}\Big[(\partial_{\mu}h_{+})^2 + (\partial_{\mu}h_{-})^2 + (\partial_{\mu}M)^2 + (\partial_{\mu}N)^2\Big] \\ &- \frac{1}{2}\Big[2v^2(e^2+g^2)(h_{+}^2+h_{-}^2) + 4v^2(g^2-e^2)h_{+}h_{-} \\ &- 2\sqrt{2}ve\mu(h_{+}-h_{-})M - 2\sqrt{2}vg\mu(h_{+}+h_{-})N \\ &+ (\mu^2+4v^2g^2)M^2 + (\mu^2+4v^2e^2)N^2\Big]. \end{aligned} \tag{7.13}$$

Thus, in the $(1,1)$-vacuum, one can find the same dispersion relation for the scalar and gauge sectors, of the form $p^2 = m_{\pm}^2$, with

$$m_{\pm}^2 = \frac{1}{2}\left(\mu^2 + M_e^2 + M_g^2 \pm \sqrt{(\mu^2+M_e^2+M_g^2)^2 - 4M_e^2M_g^2}\right), \tag{7.14}$$

where each one has multiplicity 2 and the mass parameters are defined as $M_e^2 = 4e^2v^2$ and $M_g^2 = 4g^2v^2$. Therefore, we have 4 massive gauge and 4 massive scalar degrees of freedom with mass squared $m_{\pm}^2$ distributed equally. Here we observe pairs of propagating modes for a given mass, which is a common characteristic of self-dual models [158]. The mass degeneracy for different spins even suggests a supersymmetric nature for the model.

7.2 Self-duality equations

The self-dual potential (7.4) makes it possible to rewrite the energy functional (7.9) in a very suggestive form. Upon using the equations of motion and some integrations by

parts, we can write (here we are using $D_\pm \equiv D_1 \pm iD_2$):

$$\begin{aligned} E=&\int d^2x \left[\frac{1}{2}\left(\vec{E}\pm\vec{\nabla}N\right)^2+\frac{1}{2}\left(\vec{e}\pm\vec{\nabla}M\right)^2\right. \\ &+|D_\pm\phi_+|^2+|D_\mp\phi_-|^2+\frac{1}{2}(\partial_0 M)^2+\frac{1}{2}(\partial_0 N)^2 \\ &+\frac{1}{2}\left\{B\pm\left[e\left(|\phi_+|^2-|\phi_-|^2\right)-\mu M\right]\right\}^2 \\ &+\frac{1}{2}\left\{b\pm\left[g\left(|\phi_+|^2+|\phi_-|^2-2v^2\right)-\mu N\right]\right\}^2 \\ &+|D_0\phi_+\mp i(eN+gM)\phi_+|^2 \\ &+|D_0\phi_-\mp i(eN-gM)\phi_-|^2 \\ &\left.\pm 2gv^2 b\right], \end{aligned} \tag{7.15}$$

Therefore, since we have a sum of non-negative terms, we are naturally lead to a Bogomol'nyi-type bound [148] to the energy functional, given by $E \geq 2gv^2|\chi|$ (for $\chi > 0$ we choose the upper sign, and for $\chi < 0$ we choose the lower sign). Our main interest here is to investigate the finite-energy static field configurations that saturate these bounds, satisfying first order self-duality equations determined by Eq. (7.15). Since we consider only the static regime, in particular, $\partial_0 M = \partial_0 N = 0$. The field configurations saturating the Bogomol'nyi bound have minimum energy given by $E = 2gv^2|\chi|$, and must satisfy the first order self-duality equations:

$$D_\pm\phi_+ = 0, \quad D_\mp\phi_- = 0 \tag{7.16a}$$

$$D_0\phi_+ \mp i(eN+gM)\phi_+ = 0, \tag{7.16b}$$

$$D_0\phi_- \mp i(eN-gM)\phi_- = 0, \tag{7.16c}$$

$$\vec{E}\pm\vec{\nabla}N = 0, \quad \vec{e}\pm\vec{\nabla}M = 0 \tag{7.16d}$$

$$B\pm\left[e\left(|\phi_+|^2-|\phi_-|^2\right)-\mu M\right] = 0, \tag{7.16e}$$

$$b\pm\left[g\left(|\phi_+|^2+|\phi_-|^2-2v^2\right)-\mu N\right] = 0. \tag{7.16f}$$

To satisfy Eqs. (7.16b), (7.16c), (7.16d), it is sufficient to take

$$A_0 = \pm N, \quad a_0 = \pm M. \tag{7.17}$$

The Eq. (7.16a) can be rewritten as:

$$\begin{aligned} D_i\phi_+ &= \pm i\epsilon_{ij}D_j\phi_+, \\ D_i\phi_- &= \mp i\epsilon_{ij}D_j\phi_-. \end{aligned} \tag{7.18}$$

Using the parametrization $\phi_\pm = |\phi_\pm| e^{i\omega_\pm}$ for the scalar fields, we can obtain from Eq. (7.16a) the following structure for the gauge fields spatial components:

$$\begin{aligned} eA_i &= \pm\frac{1}{2}\epsilon_{ij}\partial_j \ln\frac{|\phi_+|}{v} \mp \frac{1}{2}\epsilon_{ij}\partial_j \ln\frac{|\phi_-|}{v} - \frac{1}{2}\partial_i(\omega_+ + \omega_-) \\ ga_i &= \pm\frac{1}{2}\epsilon_{ij}\partial_j \ln\frac{|\phi_+|}{v} \pm \frac{1}{2}\epsilon_{ij}\partial_j \ln\frac{|\phi_-|}{v} - \frac{1}{2}\partial_i(\omega_+ - \omega_-) \end{aligned} \tag{7.19}$$

Notice that, upon determining all the scalar fields, thanks to the self-dual structure, we are able to obtain all the information present in the gauge fields. Now, acting with $\epsilon^{ki}\partial_i$, we can obtain the magnetic and g-magnetic fields.

$$\begin{aligned} eB &= \mp\frac{1}{2}\nabla^2 \ln\frac{|\phi_+|}{v} \pm \frac{1}{2}\nabla^2 \ln\frac{|\phi_-|}{v} \\ gb &= \mp\frac{1}{2}\nabla^2 \ln\frac{|\phi_+|}{v} \mp \frac{1}{2}\nabla^2 \ln\frac{|\phi_-|}{v}. \end{aligned} \tag{7.20}$$

Substituting this result into the self-dual equations (7.16e) and (7.16f), after some manipulations we can find

$$\begin{aligned} \nabla^2 \ln\frac{|\phi_+|}{v} &= \Big[(e^2+g^2)|\phi_+|^2 - (e^2-g^2)|\phi_-|^2 \\ &\qquad -\mu\left(eM + gN + \frac{2v^2g^2}{\mu}\right)\Big] \\ \nabla^2 \ln\frac{|\phi_-|}{v} &= \Big[(e^2+g^2)|\phi_-|^2 - (e^2-g^2)|\phi_+|^2 \\ &\qquad -\mu\left(-eM + gN + \frac{2v^2g^2}{\mu}\right)\Big]. \end{aligned} \tag{7.21}$$

Finally, from the remaining equations, we can obtain:

$$\begin{aligned} \left(\nabla^2 - \mu^2\right)N &= 2e\left[(eN+gM)|\phi_+|^2 + (eN-gM)|\phi_-|^2\right] \\ &\quad -\mu\left[g\left(|\phi_+|^2 + |\phi_-|^2 - 2v^2\right)\right] \\ \left(\nabla^2 - \mu^2\right)M &= 2g\left[(eN+gM)|\phi_+|^2 - (eN-gM)|\phi_-|^2\right] \\ &\quad -\mu\left[e\left(|\phi_+|^2 - |\phi_-|^2\right)\right]. \end{aligned} \tag{7.22}$$

This is exactly the static limit of the equations of motion for N and M, cf. Eq. (7.6). The equations (7.21) and (7.22), are the ones that must be solved in order to find the static self-dual solutions.

In order to achieve finite energy, as we saw in the last Chapter, each term in Eq. (7.9) must go asymptotically to zero in the limit $|\vec{x}| = r \to \infty$. This asymptotic behavior can be interpreted as boundary conditions at $S^1_\infty \equiv \partial\mathbb{R}^2$. In particular, the complex scalar fields $\phi_\pm$ must go asymptotically to the vacuum manifold, with a fixed norm, but still keeping a phase freedom. This will define a map $\Phi_\infty : S^1_\infty \to S^1 \times S^1 \equiv U(1) \times U(1)$.

These can be classified by two integers determined by the fundamental homotopy group $\pi_1\left(S^1\times S^1\right)\equiv\mathbb{Z}\times\mathbb{Z}$. Therefore, the requirement of finite-energy implies an homotopy classification leading to a labeling of our configurations by two integers. This reasoning apply strictly when asymptoting to the $(1,1)$-vacuum, but can be adapted for other cases.

In the previous Chapter, we showed that the parity-invariant Maxwell-Chern-Simons $U(1)\times U(1)$ model admits finite-energy topological vortices characterized by two integers. As already emphasized there, we only demanded that $m\pm n\in\mathbb{Z}$, allowing m and n to take half-integer values simultaneously. These configurations have quantized magnetic fluxes and charges, that are related by some peculiar Gauss laws. Interestingly enough, their angular momentum is quantized, proportional to the product of charges, and fractional. Here we follow a different route, using the Bogomol'nyi equations to search for self-dual solutions. Notice that such configurations must have finite energy, since they saturate the Bogomol'nyi lower bound, $E=2gv^2|\chi|$.

It is important to notice that there are 4 different degenerate vacua to which our scalar fields can asymptote, and each of them would imply different asymptotic conditions. In the following, we will consider mainly the situation in which the fields go asymptotically to the $(1,1)$-vacuum, to investigate the existence of topological vortices and also the possibility of non-topological vortices when we asymptote to the $(0,0)$-vacuum. It should be noted that, although not analyzed here for the sake of scope, the parity-breaking vacua $(1,0)$ and $(0,1)$ must also be investigated elsewhere, together with its solitons.

Let us consider here the following radially symmetric *ansatz* for the scalar fields:

$$\begin{aligned}\phi_{\pm}(r,\theta)&=v\,F_{\pm}(r)\,e^{i(m\pm n)\theta},\\ N(r,\theta)&=v\,\hat{N}\left(r\right),\\ M(r,\theta)&=v\,\hat{M}\left(r\right),\end{aligned}\tag{7.23}$$

where $m\pm n\in\mathbb{Z}$, and the profiles $F_{\pm}$, $\hat{N}$, and $\hat{M}$ are dimensionless. Plugging the *ansatz* above in Eqs. (7.19), we can obtain the gauge structure (here $\hat{\theta}_i=\epsilon_{ij}x^j/r$):

$$\begin{aligned}A_i(r,\theta)&=\frac{1}{er}\left[A(r)-m\right]\hat{\theta}_i,\\ a_i(r,\theta)&=\frac{1}{gr}\left[a(r)-n\right]\hat{\theta}_i,\end{aligned}\tag{7.24}$$

where we defined the gauge profiles as:

$$\begin{aligned}A(r)&=\pm\frac{1}{2}\left(\frac{rF_{+}'}{F_{+}}-\frac{rF_{-}'}{F_{-}}\right)\\ a(r)&=\pm\frac{1}{2}\left(\frac{rF_{+}'}{F_{+}}+\frac{rF_{-}'}{F_{-}}\right),\end{aligned}\tag{7.25}$$

or, equivalently:

$$F'_{+} = \pm \frac{F_{+}\,(A+a)}{r},$$
$$F'_{-} = \mp \frac{F_{-}\,(A-a)}{r}. \tag{7.26}$$

It should be stressed that, although the gauge field structure above (7.24) is the same used in Chapter 6, here it does not appear as an independent *ansatz* for the gauge fields, but it has its structure totally determined by the scalar fields *ansatz*, and as a consequence of the self-dual equations obtained by saturating the Bogomol'nyi bound.

Let us first discuss the profiles behavior at the origin. Looking to the gauge structure (7.24), in order to avoid a singularity at the origin, we must have $A(0) = m$ and $a(0) = n$. Using Eq.(7.26) we see that they need to satisfy

$$(n+m)\,F_{+}(0) = 0,$$
$$(n-m)\,F_{-}(0) = 0. \tag{7.27}$$

These considerations imply the following behavior:

$$\begin{cases} F_{+}(r) \approx r^{\pm(n+m)} \\ F_{-}(r) \approx r^{\pm(n-m)} \end{cases} \quad \text{as } r \to 0. \tag{7.28}$$

Therefore, to ensure that the fields have a regular behavior at the origin, we must have $\pm n > |m|$. Notice that if we take $n = 0$, we cannot ensure a regular behavior at the origin for both fields simultaneously, unless we also set $m = 0$, in which case $F_{+}(0)$ and $F_{-}(0)$ remain undetermined. Finally, if we consider $n = -m \neq 0$, then $F_{+}(0)$ is undetermined while $F_{-}(0) = 0$; if we consider $n = m \neq 0$, then $F_{-}(0)$ is undetermined while $F_{+}(0) = 0$. It should be noted that the behavior of $\hat{N}$ and $\hat{M}$ near the origin will follow from their equations of motion, once the behavior of F_{+} and F_{-} for small r are determined.

Now, we proceed to the discussion of the asymptotic conditions. The energy contribution coming from the potential implies that for any finite-energy configurations, we must have $F_{+}(\infty)$ and $F_{-}(\infty)$ equal to 0 or 1. Furthermore, the covariant derivatives contribution to the energy functional include the following terms:

$$E \supset 2\pi v^2 \int dr \left[\frac{F_{+}^2\,(A+a)^2}{r} + \frac{F_{-}^2\,(A-a)^2}{r} \right] \tag{7.29}$$

Therefore, from the finite-energy condition, we find the following asymptotic conditions:

$$[A(\infty) + a(\infty)]\,F_{+}(\infty) = 0,$$
$$[A(\infty) - a(\infty)]\,F_{-}(\infty) = 0. \tag{7.30}$$

First of all, let us consider the case in which the scalar profiles asymptote to the $(1,1)$-vacuum, that is, when $F_+(\infty) = F_-(\infty) = 1$. In this case, we are dealing with topological vortices, and we must have $A(\infty) = a(\infty) = 0$. These configurations have quantized magnetic fluxes ($\Phi = \frac{2\pi}{e}\, m$ and $\chi = \frac{2\pi}{g}\, n$), charges ($Q = \frac{2\pi}{g}\mu n$ and $G = \frac{2\pi}{e}\mu m$) and energy ($E = 2gv^2|\chi| = 4\pi v^2|n|$).

Furthermore, we consider the case in which we asymptote to the $(0,0)$-vacuum, that is, when we have $F_+(\infty) = F_-(\infty) = 0$. In this case, we can generically assume that we have $F_+(r) \approx 1/r^{\pm(\alpha+\beta)}$ and $F_-(r) \approx 1/r^{\pm(\alpha-\beta)}$ in the limit $r \to \infty$, with $\pm\alpha > \beta$. We are now dealing with non-topological vortices, and we have $A(\infty) \equiv -\beta$ and $a(\infty) \equiv -\alpha$. These configurations do not have quantized magnetic fluxes, that now are given by $\Phi = \frac{2\pi}{e}(m+\beta)$ and $\chi = \frac{2\pi}{g}(n+\alpha)$, being α and β real numbers. Nonetheless, they are also self-dual configurations that still saturate the energy bound, that can be written as $E = 4\pi v^2|n+\alpha|$. We remark that the case $\alpha = 0$ only makes sense if we also take $\beta = 0$, recovering therefore the previous situation of topological vortices.

Last but not least, we comment that there is another asymptotic behavior that could be considered. One could also analyze finite-energy configurations that asymptote to a parity-breaking vacuum by considering $F_+(\infty) = 0$, $F_-(\infty) = 1$ or $F_+(\infty) = 1$, $F_-(\infty) = 0$, which amounts to choosing $\beta = \alpha$ or $\beta = -\alpha$, respectively. These will not be investigated here, because we are only concerned with the parity-preserving scenario.

The angular momentum of these configurations is given by

$$J = \int d^2x\, \epsilon^{ij} r_i T_{0j}. \tag{7.31}$$

In Chapter 6, one can find the following expression for the angular momentum of the finite-energy, static, rotationally symmetric vortices:

$$J = \frac{2\pi\mu}{eg}\left[A(0)a(0) - A(\infty)a(\infty)\right]. \tag{7.32}$$

It should be noted that the model considered here does not lead to any change in the above angular momentum expression. Here we have $A(0) = m, a(0) = n$ and also $A(\infty) \equiv -\beta, a(\infty) \equiv -\alpha$. Thus, we can rewrite this expression in the following way:

$$J = \frac{2\pi\mu}{eg}\left(n\, m - \alpha\, \beta\right) = \frac{QG}{2\pi\mu} - \frac{Q}{e}\beta - \frac{G}{g}\alpha. \tag{7.33}$$

This is in agreement with the result found in Ref.[171].

(n,m)	$(\frac{1}{2},\frac{1}{2})$		$(1,0)$		$(\frac{3}{2},\frac{1}{2})$		$(0,0)$
	NT	T	NT	T	NT	T	NT
$E(1/4\pi v^2)$	5.38	0.50	5.76	1.00	8.53	1.50	3.25
$J(eg/2\pi\mu)$	-4.78	0.25	0.81	0.00	0.75	0.75	0.75
$\Phi(e/2\pi)$	1.53	0.50	-0.17	0.00	0.50	0.50	-0.23
$\chi(g/2\pi)$	5.38	0.50	5.76	1.00	8.53	1.50	3.25

Table 7.1: Physical properties of topological vortices (T) and non-topological solitons (NT) for different values of n and m.

7.3 Explicit solutions and discussion

In this section, we exhibit explicit numerical solutions for the self-duality equations. First of all, we rewrite the differential equations using dimensionless quantities given by $x = gv\,r$, $\gamma = \mu/gv$ and $\kappa = e/g$. After the dust has settled, the differential equations are:

$$\begin{aligned}
\nabla_x^2 \ln F_+^2 &= (1+\kappa^2)F_+^2 + (1-\kappa^2)F_-^2 - \gamma\kappa\hat{M} - \gamma\kappa\hat{N} - 2, \\
\nabla_x^2 \ln F_-^2 &= (1+\kappa^2)F_-^2 + (1-\kappa^2)F_+^2 + \gamma\kappa\hat{M} - \gamma\kappa\hat{N} - 2, \\
\nabla_x^2 \hat{N} &= -\gamma\left(F_+^2 + F_-^2 - 2\right) + 2\kappa^2\hat{N}\left(F_+^2 + F_-^2\right) \\
&\quad + 2\kappa\hat{M}\left(F_+^2 - F_-^2\right) + \gamma^2\hat{N}, \\
\nabla_x^2 \hat{M} &= -\gamma\kappa\left(F_+^2 - F_-^2\right) + 2\hat{M}\left(F_+^2 + F_-^2\right) \\
&\quad + 2\kappa\hat{N}\left(F_+^2 - F_-^2\right) + \gamma^2\hat{M},
\end{aligned} \tag{7.34}$$

The general strategy adopted here is the same one used in Chapter 6: we expand the profile functions $F_+, F_-, \hat{N}, \hat{M}$ in powers of x around the origin, using the generic notation $A(x) = \sum_k A_k x^k$. Applying these expansions in the differential equations and using the initial conditions, we can find constraints in the expansion coefficients. With these expressions at hand, we can search for numerical solutions that also satisfy the asymptotic boundary conditions using a shooting method. In general lines, for the differential equations and initial conditions considered here, there are 4 coefficients to be adjusted; the others vanish or can be determined in terms of these 4.

In the following, we consider some examples with the lowest possible values for n and m that represent each possible class of solutions. It is important to remember that $\pm n \geq |m|$ and that $E \propto |n + \alpha|$. The topological vortices (asymptoting to the $(1,1)$-vacuum) and non-topological solitons (asymptoting to the $(0,0)$-vacuum), with its physical fields (*i.e.*, electric, magnetic, g-electric and g-magnetic), for the cases $(n,m) = (\frac{1}{2},\frac{1}{2}), (1,0), (\frac{3}{2},\frac{1}{2})$ and $(0,0)$ are shown in Figs. 7.1, 7.2, 7.3, 7.4, 7.5, 7.6, 7.7, respectively. Their relevant physical properties are shown in Table 7.1. The charges are not shown there, but can

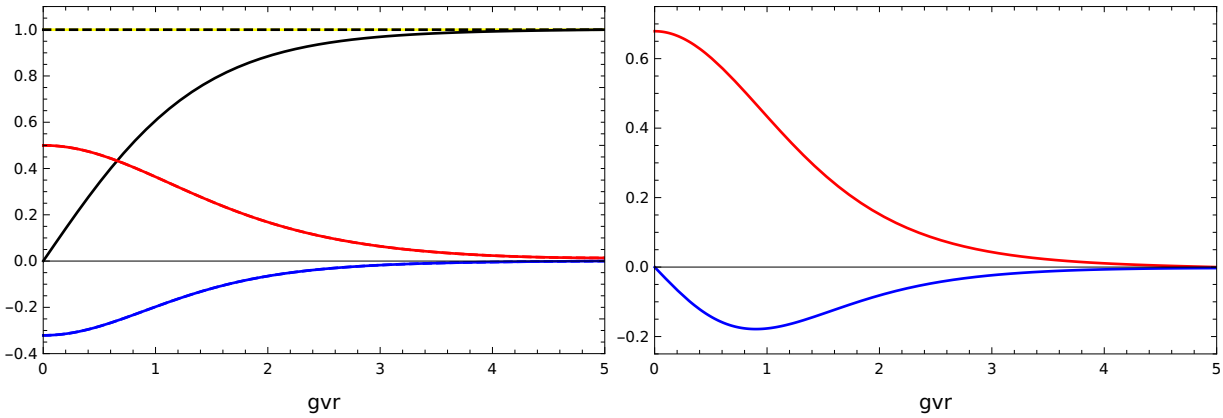

Figure 7.1: Topological vortex solution for $n = m = 1/2$ and its physical fields in units of gv^2 as functions of $x = gv\,r$. *Upper figure*: F_+ and F_- are shown in solid and dashed black, $N = M$ in blue, and $A = a$ in red, respectively. *Lower figure*: In red, the magnetic field; in blue, the electric field. Notice that in this case we have $B = b$ and $E_r = e_r$.

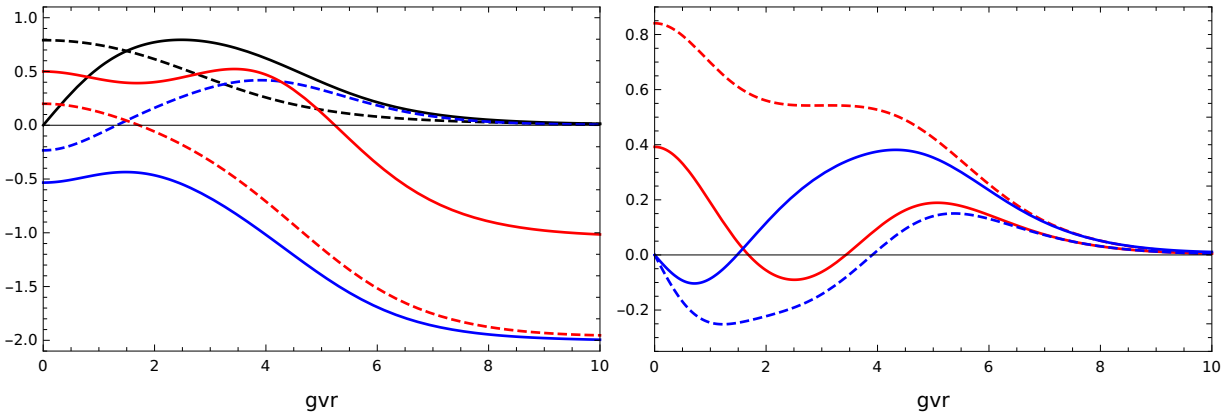

Figure 7.2: Non-topological soliton for $n = 1/2, m = 1/2$ and its physical fields in units of gv^2, as functions of $x = gv\,r$. *Upper figure*: F_+ and F_- are shown in solid and dashed black, N and M in solid and dashed blue, A and $0.4a$ in solid and dashed red, respectively (a was rescaled to facilitate the visualization). Here we have $\beta \simeq 1.03$ and $\alpha \simeq 4.88$. *Lower figure*: The magnetic (solid red), g-magnetic (dashed red), electric (solid blue) and g-electric (dashed blue) fields.

immediately be found remembering that $Q = \mu\chi$ and $G = \mu\Phi$. Here we adopt $\gamma = \kappa = 1$ for simplicity, but in the end of this section we comment about the relevant changes in the solutions when we vary these coefficients.

The topological vortices have quantized physical properties while non-topological solitons do not, and the later have energy bigger than the former. The angular momentum for topological vortices is quantized, proportional to the product of the charges and fractional, exhibiting an anyonic nature. Therefore, having one of the charges equal to zero is sufficient to have $J = 0$, what does not happen for the non-topological solitons. For $n = m = 0$, the only solution asymptoting to the $(1, 1)$-vacuum is the trivial one.

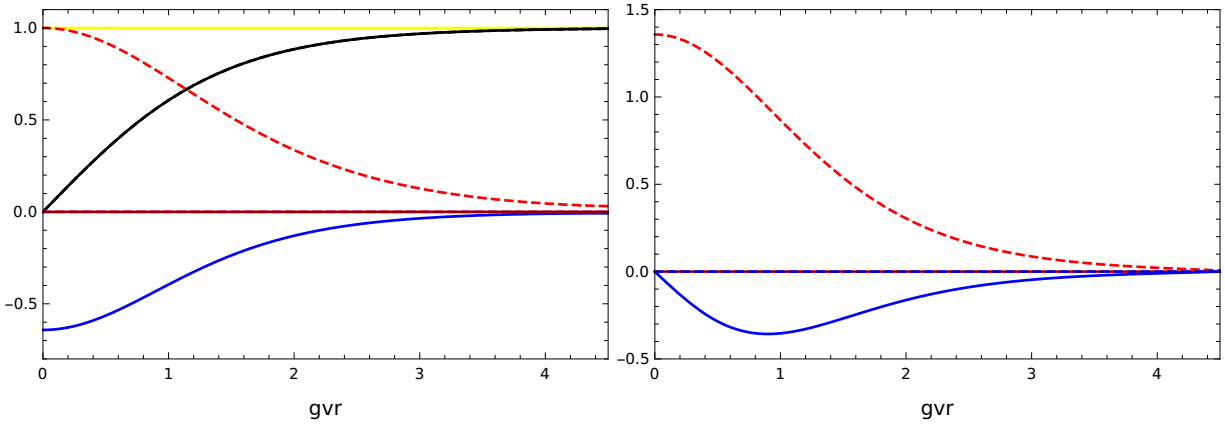

Figure 7.3: Topological vortex for $n = 1, m = 0$ and its physical fields in units of gv^2, as functions of $x = gv\,r$. *Upper figure*: $F_+ = F_-$ are shown in black, N and M in solid and dashed blue, A and a in solid and dashed red, respectively. Here we have $A = M = 0$. *Lower figure*: In red, the g-magnetic field; in blue, the electric field. Here have $B = e_r = 0$.

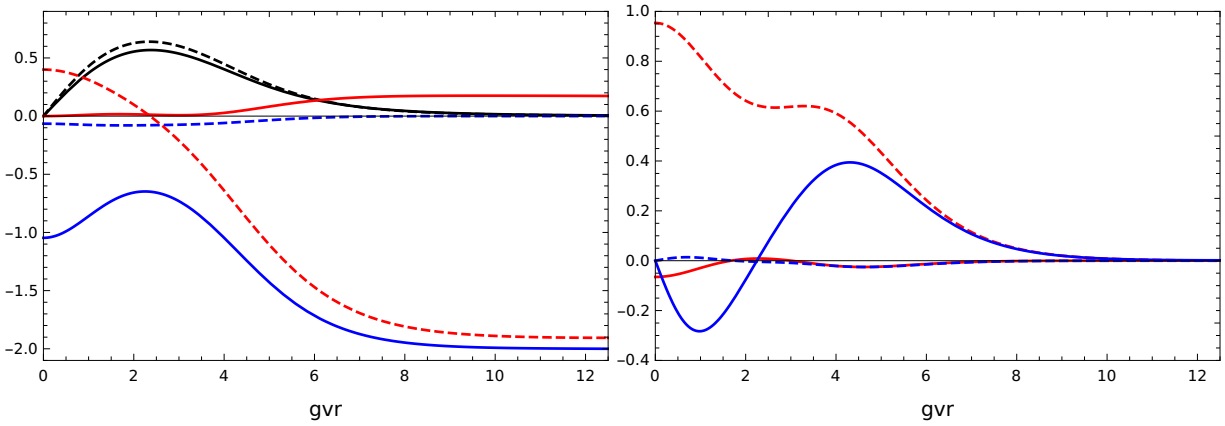

Figure 7.4: Non-topological soliton for $n = 1, m = 0$ and its physical fields in units of gv^2, as functions of $x = gv\,r$. *Upper figure*: F_+ and F_- are shown in solid and dashed black, N and M in solid and dashed blue, A and $0.4a$ in solid and dashed red, respectively (a was rescaled to facilitate the visualization). Here we have $\beta \simeq -0.17$ and $\alpha \simeq 4.76$. *Lower figure*: The magnetic (solid red), g-magnetic (dashed red), electric (solid blue), and g-electric (dashed blue) fields.

The multiplicity of zeros of the scalar field is related to the winding number of the vortex. Therefore, the power-law behavior of F_+ and F_- in Eq. (7.28) clearly indicates that the true winding numbers are given by $n + m$ and $n - m$, instead of m and n separately, as is clearly illustrated in the explicit solutions that we found.

The most distinctive signature of a symmetry in a system is the presence of a degeneracy in the spectrum, hence it is reasonable to expect that the parity invariance of our model should reproduce this effect. To this end, we state how the vortex solutions change under parity transformations: $(n, m) \to (n, -m)$, $r \to r, \theta \to -\theta - \pi, F_\pm \to F_\mp, M \to -M, N \to N, \beta \to -\beta, \alpha \to \alpha$, being all the others directly inferred from the self-duality

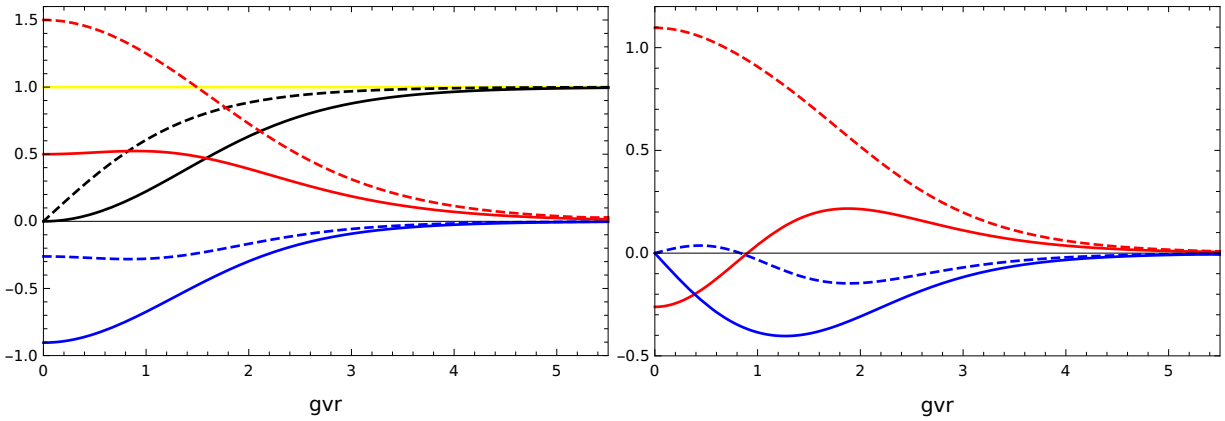

Figure 7.5: Topological vortex for $n = 3/2, m = 1/2$ and its physical fields in units of gv^2, as functions of $x = gv\,r$. *Upper figure*: F_+ and F_- are shown in solid and dashed black, N and M in solid and dashed blue, A and a in solid and dashed red, respectively. *Lower figure*: The magnetic (solid red), g-magnetic (dashed red), electric (solid blue), and g-electric (dashed blue) fields.

equations.

Considering the self-dual topological vortices, that is, that satisfy $E \propto |n|$, it is immediate to conclude that a given solution and its parity-transformed version have the same energy. But the complete independence of the energy from m suggests a much greater degeneracy. In fact, from the condition of regularity of the solutions as $r \to 0$, we observed that $\pm n \geq |m|$, which in turn implies that, for $n > 0$ ($n < 0$) there are $2n + 1$ ($2|n| + 1$) solutions of the same energy. Since the energy does not depend on the sign of n, we obtain a $2(2|n| + 1)$-fold degeneracy. It is reasonable to speculate whether this comes from a larger symmetry group. In the light of previous comments, a good candidate would be supersymmetry or, given the structure of the degeneracy, an internal $SU(2)$. This investigation should be pursued elsewhere. The above discussion does not apply to the non-topological solitons.

In the last Chapter, we studied the energies of different vortices, obtaining the following result: $M_{(1/2,1/2)} + M_{(1/2,-1/2)} = 2M_{(1/2,1/2)} > M_{(1,0)}$, where $M_{(n,m)}$ is the mass associated with the (n, m)- topological vortex. The left-hand side of the inequality represents the static energy of well-separated F_+ and F_- vortices of winding 1, while the right-hand side is their energy when superimposed at the origin. Therefore, the inequality suggested a possible attraction between these vortices. Now, in the self-dual model studied here, on the other hand, $2M_{(1/2,1/2)} = M_{(1,0)}$, indicating that these vortices do not interact with each other, allowing, for example, the existence of static multi-vortex configurations, as it is usually the case for self-dual models.

In this section we considered $\gamma = \kappa = 1$ for simplicity, but the existence of solitons here is not conditioned to this assumption, and we were able to find solutions for different values of these coefficients. Interestingly enough, keeping κ fixed and increasing γ, we see

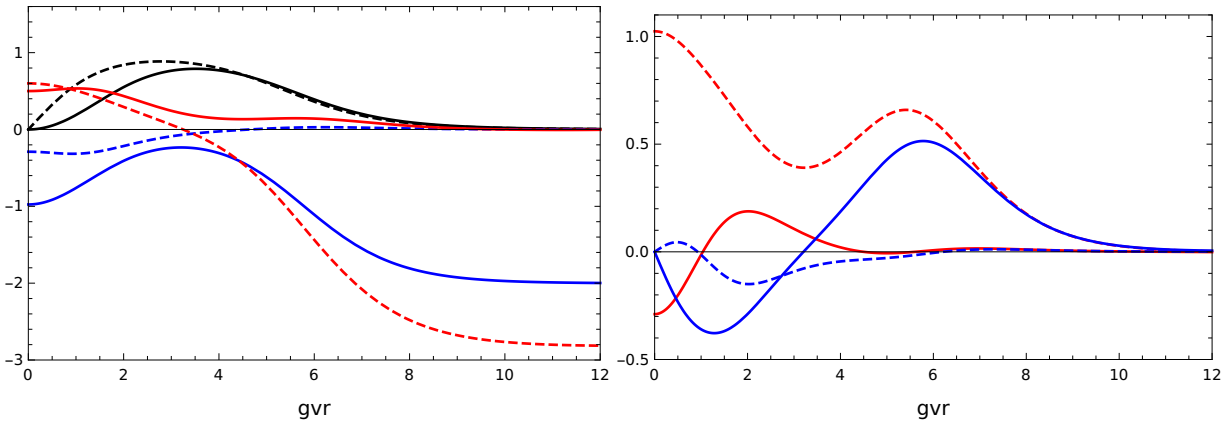

Figure 7.6: Non-topological soliton for $n = 3/2, m = 1/2$ and its physical fields in units of gv^2, as functions of $x = gv\,r$. *Upper figure*: F_+ and F_- are shown in solid and dashed black; N and M in solid and dashed blue; A and $0.4a$ in solid and dashed red, respectively (a was rescaled to facilitate the visualization). Here we have $\beta \simeq 0.00$ and $\alpha \simeq 7.03$. *Lower figure*: The magnetic (solid red), g-magnetic (dashed red), electric (solid blue) and g-electric (dashed blue) fields

that the magnetic field at the origin decreases; decreasing γ, the magnetic field increases, cf. Fig. 7.8. Since $\gamma \propto \mu$, this suggests that it would reach a maximum value in the pure Maxwell limit and go to zero in the pure CS limit, as it happens in the usual Maxwell-CS case [145]. It is well-known that in the absence of a CS term, the vortices are electrically neutral, therefore having zero electric field. In fact, we observed that in decreasing γ, the maximum value of the electric field diminished, in accordance with what is expected. Furthermore, keeping γ fixed and considering $\kappa \neq 1$, we can see that for $n = m = 1/2$, the electric and magnetic fields will not be degenerate anymore, cf. Fig. 7.8. In the other examples considered, taking $\kappa \neq 1$ does not lead to significant qualitative changes.

Finally, we also found solitons asymptoting to the parity-breaking $(1, 0)$- and $(0, 1)$-vacua. Given the rich vacuum structure of this theory, in principle, one could also find domain walls connecting any pair of degenerate vacua. These were not discussed here for reasons of scope, since we focused on the parity-invariant cases.

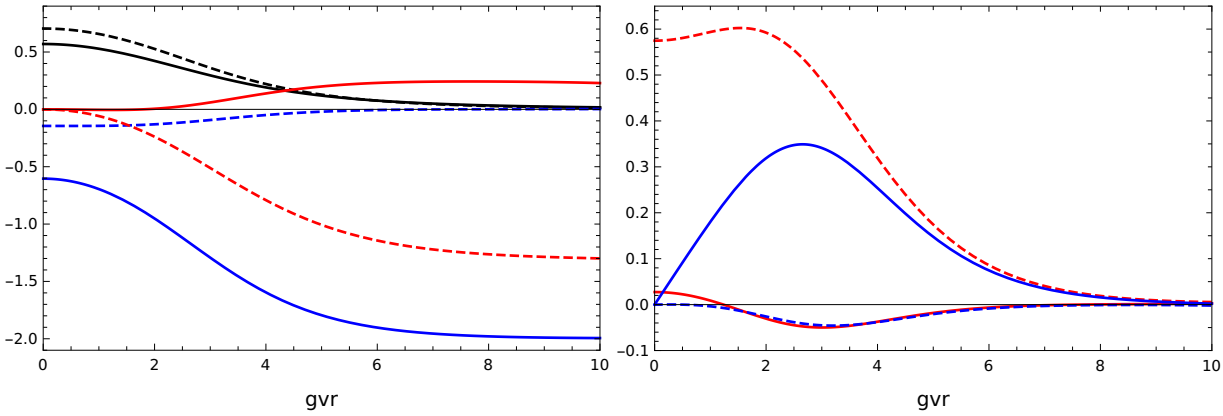

Figure 7.7: Non-topological soliton for $n = m = 0$ and its physical fields in units of gv^2, as functions of $x = gv\,r$. *Upper figure*: F_+ and F_- are shown in solid and dashed black; N and M in solid and dashed blue; A and $0.4a$ in solid and dashed red, respectively (a was rescaled to facilitate the visualization). Here we have $\beta \simeq -0.23$ e $\alpha \simeq 3.25$. *Lower figure*: The magnetic (solid red), g-magnetic (dashed red), electric (solid blue) and g-electric (dashed blue) fields.

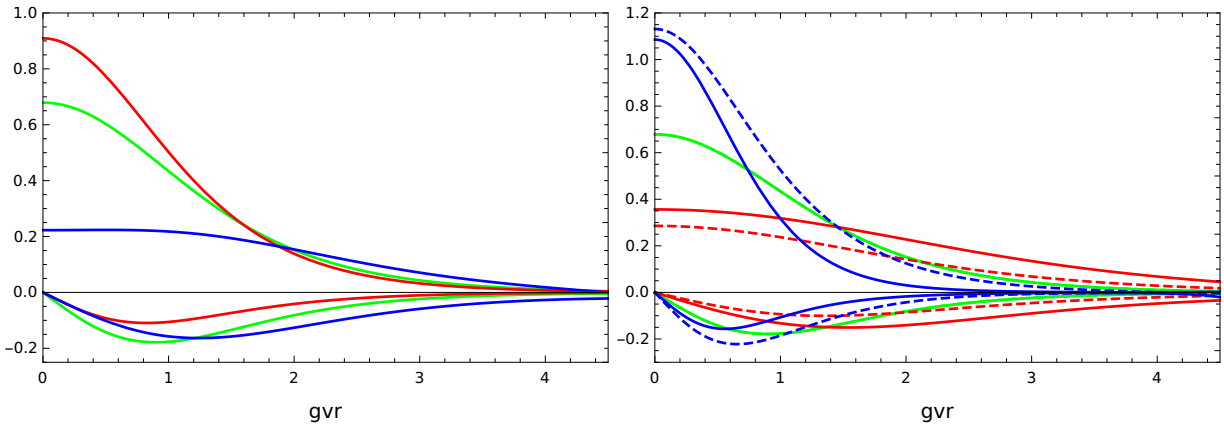

Figure 7.8: Physical fields associated with the $n = m = 1/2$ topological vortex. *Upper figure*: The electric (lower half-plane) and magnetic (upper half-plane) fields for $\kappa = 1$ and $\gamma = 1$ (green), 0.5 (red), 2 (blue). *Lower figure*: The magnetic, g-magnetic, electric and g-electric fields, for $\gamma = 1$ and $\kappa = 1$ (green), 0.5 (red), 2 (blue). The solid lines refer to B and E_r; the dashed lines to b and e_r. B and b are shown in the upper half-plane; E_r and e_r in the lower half-plane.

Chapter 8

Concluding remarks

We proposed a parity-invariant Maxwell-Chern-Simons $U(1) \times U(1)$ model coupled with charged scalars in 2+1 dimensions, and investigated the existence of topological vortices in this scenario. We described the main features of the model and discussed general properties of topological configurations that could be present in it. Using an appropriate *ansatz* and the equations of motion, we obtained the relevant differential equations and solved them numerically. We explicitly analyzed three examples that are representatives of the possible solutions and showed explicit vortex configurations for each case, describing their main properties such as the electric and magnetic fields related with each particular solution. We therefore conclude that there are vortex solutions in this novel class of parity-invariant Maxwell-CS models. Furthermore, we investigated a self-dual version of the parity-invariant Maxwell-CS $U(1) \times U(1)$ model coupled with scalar matter. We obtained a Bogomol'nyi bound for the energy, whose saturation led us to first-order self-duality equations. We exhibited explicit numerical solutions corresponding to topological vortices and non-topological solitons, and discussed their main properties.

There are many directions to be explored, for example, it would be interesting to analyze the quantization of the CS parameter, as well as studying this model in a more general manifold. A thorough investigation concerning the interaction between these vortices, answering the question whether they attract or repel, would also be enlightening. The role of monopole operators in this model should be understood, and the possibility of a theory dual to the one presented here could lead to interesting developments. Furthermore, the product structure of the angular momentum and the presence of two gauge potentials lead us to speculate about a relation between these charged vortices and Dirac monopoles, in the spirit of Refs. [216, 217, 218]. Therefore, it is important to consider the quantum aspects of this model, to study the dynamics of these vortices, and to investigate the existence of dualities in this context. Interestingly enough, similar models can find many applications in condensed matter [186, 187, 188, 189, 190, 191, 192, 193, 194, 195, 166, 168], and it would be exciting to find a physical system accurately described by our model, allowing it to be experimentally realized.

It is also important to investigate the physics of the parity and time-reversal breaking $(1,0)$- and $(0,1)$-vacua, and in particular, to study solitons asymptoting to them, as well as the existence of domain walls connecting the degenerate phases of this model. The role of parity and time-reversal in superconductors is a topic that has been attracting much interest recently [219, 220, 221], and perhaps our model could find some use on it.

To conclude this Part, we remark that a natural development of this project is to investigate the supersymmetric extension of our model, since self-duality and supersymmetry are intimately related [150, 154, 155, 157]. In fact, the model considered in the last Chapter can be shown to be the bosonic part of a $\mathcal{N} = 2$ supersymmetric model, with an entirely new fermionic part to be explored. Moreover, supersymmetry can find applications in graphene [222, 223, 224] and can dynamically emerge in condensed matter systems [225, 226, 227, 228]. Therefore, this could lead to physically interesting results.

Bibliography

[1] P.A.M. Dirac, *Quantised singularities in the electromagnetic field*, Proc. R. Soc. Lond. A **133**, 60 (1931).

[2] T. T. Wu and C. N. Yang, *Concept of nonintegrable phase factors and global formulation of gauge fields*, Phys. Rev. D **12**, 3845 (1975).

[3] G. 't Hooft, *Magnetic Monopoles in Unified Gauge Theories*, Nucl. Phys. B **79**, 276 (1974).

[4] A.M. Polyakov, *Particle Spectrum in Quantum Field Theory*, JETP Lett. **20**, 194 (1974).

[5] H. Georgi and S. L. Glashow, *Unity of All Elementary-Particle Forces*, Phys. Rev. Lett. **32**, 438 (1974).

[6] B.Julia and A. Zee, *Poles with both magnetic and electric charges in non-Abelian gauge theory*, Phys. Rev. D **11**, 2227 (1975).

[7] J. S. Schwinger, *A magnetic model of matter*, Science **165**, 757 (1969).

[8] E. Bogomolny, *Stability of Classical Solutions*, Sov. J. Nucl. Phys. **24**, 449 (1976).

[9] M. K. Prasad and C. M. Sommerfield, *Exact Classical Solution for the 't Hooft Monopole and the Julia-Zee Dyon*, Phys. Rev. Lett. **35**, 760 (1975).

[10] C. Dokos and T. Tomaras, *Monopoles and dyons in the SU(5) model*, Phys. Rev. D **21**, 2940 (1980).

[11] C. Montonen and D. I. Olive, *Magnetic Monopoles as Gauge Particles?*, Phys. Lett. B **72**, 117 (1977).

[12] E. Witten and D. I. Olive, *Supersymmetry Algebras That Include Topological Charges*, Phys. Lett. B **78**, 97 (1978).

[13] S.L. Glashow, *Partial Symmetries of Weak Interactions*, Nucl.Phys. **22**, 579 (1961).

[14] S. Weinberg, *A Model of Leptons*, Phys.Rev.Lett. **19**, 1264 (1967).

[15] A. Salam, *Weak and Electromagnetic Interactions*, Conf.Proc.C 680519, 367 (1968).

[16] ATLAS Collaboration, *Observation of a new particle in the search for the Standard Model Higgs boson with the ATLAS detector at the LHC*, Phys. Lett. B **716**, 1 (2012).

[17] Y.M. Cho and D. Maison, *Monopoles in Weinberg-Salam Model*, Phys. Lett. B **391**, 360 (1997).

[18] Y. Yang, *Dually charged particle-like solutions in the Weinberg-Salam theory*, Proc. R. Soc. Lond. A **454**, 155 (1998).

[19] Y. M. Cho, K. Kim, and J. H. Yoon, *Finite energy electroweak dyon*, Eur. Phys. J. C **75**, 67 (2015).

[20] J. Ellis, N. E.Mavromatos, and T. You, *The Price of an Electroweak Monopole*, Phys. Lett. B **756**, 29 (2016).

[21] F. Blaschke and P. Beneš, *BPS Cho–Maison monopole*, Prog. Theor. Exp. Phys. **2018**, 073B03 (2018).

[22] P. Zhang, L. Zou, and Y. M. Cho, *Regularization of electroweak monopole by charge screening and BPS energy bound*, Eur. Phys. J. C **80**, 280 (2020).

[23] S. Arunasalam and A. Kobakhidze, *Electroweak monopoles and the electroweak phase transition*, Eur. Phys. J. C **77**, 444 (2017).

[24] M. Born and L. Infeld, *Foundations of the New Field Theory*, Nature **132**, 1004 (1933).

[25] J. Ellis, N. E. Mavromatos, and T. You, *Light-by-Light Scattering Constraint on Born-Infeld Theory*, Phys. Rev. Lett. **118**, 261802 (2017).

[26] N. E. Mavromatos and S. Sarkar, *Finite-Energy Dressed String-Inspired Dirac-Like Monopoles*, Universe, **5**, 8 (2019).

[27] N. E. Mavromatos and S. Sarkar, *Regularized Kalb-Ramond magnetic monopole with finite energy*, Phys. Rev. D **97**, 125010 (2018).

[28] J. Alexandre and N. E. Mavromatos, *Weak-U(1) × strong-U(1) effective gauge field theories and electron-monopole scattering*, Phys. Rev. D **100**, 096005 (2019).

[29] B. Acharya *et al.*, (MoEDAL Collaboration), *Magnetic Monopole Search with the Full MoEDAL Trapping Detector in 13 TeV pp Collisions Interpreted in Photon-Fusion and Drell-Yan Production*, Phys. Rev. Lett. **123**, 021802 (2019).

[30] B. Acharya *et al.* (MoEDAL Collaboration), *The physics programme of the MoEDAL experiment at the LHC*, Int. J. Mod. Phys. A **29**, 1430050 (2014).

[31] O. Halpern, *Scattering processes produced by electrons in negative-energy states*, Phys. Rev. **44**, 855 (1933).

[32] W. Heisenberg, *Bemerkungen zur Diracschen Theorie des Positrons*, Z. Phys. **90**, 209 (1934).

[33] W. Heisenberg and H. Euler, *Consequences of Dirac's theory of positrons*, Zeit. Phys. **98**, 714 (1936).

[34] S. I. Kruglov, *Born–Infeld-type electrodynamics and magnetic black holes*, Annals of Physics **383**, 550 (2017).

[35] S. I. Kruglov, *Dyonic black holes with nonlinear logarithmic electrodynamics*, Gravitation and Cosmology **25**, 190 (2019).

[36] N. Breton and L. A. López, *Quasinormal modes of nonlinear electromagnetic black holes from unstable null geodesics*, Phys. Rev. D **94**, 104008 (2016).

[37] G. Panotopoulos, *Building (1+1) holographic superconductors in the presence of nonlinear electrodynamics*, Chin.J.Phys. **69**, 295 (2021).

[38] D. Momemi, M. Raza, and R. Myrzakulov, *More on Superconductors via Gauge/Gravity Duality with Nonlinear Maxwell Field*, J. Grav. **2013**, 782512 (2013).

[39] S. Gangopadhyay, *Holographic superconductors in Born–Infeld electrodynamics and external magnetic field*, Mod. Phys. Lett. A **29**, 1450088 (2014).

[40] N. Bretón, *Nonlinear electrodynamics and cosmology*, J. Phys.: Conf. Ser. **229**, 012006 (2010).

[41] P. V. Moniz, *Quintessence and Born-Infeld cosmology*, Phys. Rev. D **66**, 103501 (2002).

[42] R. García-Salcedo and N. Bretón, *Born–Infeld cosmologies*, Int. J. Mod. Phys. A **15**, 4341 (2000).

[43] P. Gaete and J.A. Helayël-Neto, *Finite field-energy and interparticle potential in logarithmic electrodynamics*, Eur. Phys. J. C **74**, 2816 (2014).

[44] P. Gaete and J. A. Helayël-Neto, *Remarks on nonlinear electrodynamics*, Eur. Phys. J. C **74**, 3182 (2014).

[45] P. Gaete and J. A. Helayël-Neto, *A note on nonlinear electrodynamics*, EPL **119**, 51001 (2017).

[46] I. Bandos, K. Lechner, D. Sorokin, and P. K. Townsend, *Nonlinear duality-invariant conformal extension of Maxwell's equations*, Phys. Rev. D **102**, 121703(R) (2020).

[47] I. Gullu and S. H. Mazharimousavi, *Double-logarithmic nonlinear electrodynamics*, Phys. Scr. **96**, 045217 (2021).

[48] M. J. Neves. J. B. de Oliveira, L. P. R. Ospedal, and J. A. Helayël-Neto, *Dispersion Relations in Non-Linear Electrodynamics and the Kinematics of the Compton Effect in a Magnetic Background*, Phys. Rev. D **104**, 015006 (2021).

[49] ATLAS Collaboration, *Evidence for light-by-light scattering in heavy-ion collisions with the ATLAS detector at the LHC*, Nature Physics **13**, 852 (2017).

[50] CMS Collaboration, *Evidence for light-by-light scattering and searches for axion-like particles in ultraperipheral PbPb collisions at* $\sqrt{s_{NN}} = 5.02\ TeV.$, Phys. Lett. B **797**, 134826 (2019).

[51] ATLAS Collaboration, *Observation of Light-by-Light Scattering in Ultraperipheral Pb + Pb Collisions with the ATLAS Detector*, Phys. Rev. Lett. **123**, 052001 (2019).

[52] P. Niau Akmansoy and L. G. Medeiros, *Constraining Born–Infeld-like nonlinear electrodynamics using hydrogen's ionization energy*, Eur. Phys. J. C **78**, 143 (2018).

[53] M. Fouché, R. Battesti, and C. Rizzo, *Limits on nonlinear electrodynamics*, Phys. Rev. D **93**, 093020 (2016).

[54] J. Ellis and S. Ge, *Constraining Gluonic Quartic Gauge Coupling Operators with*, Phys. Rev. Lett. **121**, 041801 (2018).

[55] N. E. Mavromatos and V. Mitsou, Int. J. Mod. Phys. A **35**, 2030012 (2020).

[56] Y. Cho, *Physical implications of electroweak monopole*, Phil. Trans. Roy. Soc. Lond. A **377**, 20190038 (2019).

[57] E. S. Fradkin and A. A. Tseytlin, *Non-linear electrodynamics from quantized strings*, Phys. Lett. B **163**, 123 (1985).

[58] C. G. Callan and J. M. Maldacena, *Brane dynamics from the Born-Infeld action* , Nucl. Phys. B **513**, 19 (1998).

[59] M. Baillargeon and F. Boudjema, *Contribution of the bosonic loops to the three photon decay of the Z*, Phys. Lett. B **272**, 158 (1991).

[60] X. Pham, *Non-Abelian effects in nonlinear quantum electrodynamics and in Z0 decay into three photons*, Phys. Lett. B **272**, 373 (1991).

[61] E. W. N. Glover, A. G. Morgan, *Z boson decay into photons*, Z. Phys. C **60**, 175 (1993).

[62] P.A. Zyla *et al.*, *Particle Data Group*, Prog. Theor. Exp. Phys. **2020**, 083C01 (2020) and 2021 update.

[63] ATLAS Collaboration, *Search for new phenomena in events with at least three photons collected in pp collisions at* $\sqrt{s}$ *= 8 TeV with the ATLAS detector*, Eur. Phys. J. C **76**, 210 (2016).

[64] L3 Collaboration, *Search for anomalous* $Z \to \gamma\gamma\gamma$ *events at LEP*, Phys. Lett. B **345**, 609 (1995).

[65] S. Villa, *Gauge boson couplings at LEP*, Nucl. Phys. B **142**, 391 (2005).

[66] M. A. Perez, G. Tavares-Velasco, and J. J. Toscano, *New physics effects in rare Z decays*, Int. J. Mod. Phys. A **19**, 159 (2004).

[67] M. Stohr and J. Horejsi, *Effective lagrangians for the Z boson decay into photons*, Phys. Rev. D **49**, 3775 (1994).

[68] M. J. Neves, L.P.R. Ospedal, J.A. Helayël-Neto, and Patricio Gaete, *Considerations on anomalous photon and Z-boson self-couplings from the Born-Infeld weak hypercharge action*, Eur. Phys. J. C **82**, 327 (2022).

[69] K. Buesser, *The International Linear Collider*, arXiv:physics.acc-ph/1306.3126.

[70] D.M. Asner *et al.*, *ILC Higgs White Paper*, arXiv:hep-ph/1310.0763v4.

[71] K. Fujii *et al.*, *ILC study questions for snowmass 2021*, arXiv:hep-ph/2007.03650v3.

[72] K. Fujii *et al.*, *Tests of the Standard Model at the International Linear Collider*, arXiv:hep-ex/1908.11299.

[73] A. Blondel and P. Janot, *FCC-ee overview: new opportunities create new challenges*, arXiv:hep-ex/2106.13885.

[74] P. Azzurri *et al.*, *A special Higgs challenge: Measuring the mass and production cross section with ultimate precision at FCC-ee*, arXiv:hep-ex/2106.15438.

[75] W. de Boer, *Precision experiments at LEP*, Adv. Ser. Direct. High Energy Phys. **23**, 107 (2015).

[76] T. Lesiak *Future e^+e^- colliders at the energy frontier*, EPJ Web Conf. **206**, 08001 (2019).

[77] CEPC-SPPC Study Group, *Electroweak physics at CEPC*, PoS ICHEP **2016**, 692 (2016).

[78] Aicheler, M. *et al.* (eds.), *The Compact Linear Collider (CLIC) - Project Implementation Plan*, CERN, 2018, arXiv:physics.acc-ph/1903.08655.

[79] L3 Collaboration, *A test of electrodynamics in the reaction $e^+e^- \to \gamma\gamma(\gamma)$*, Phys. Lett. B **288**, 404 (1992).

[80] L3 Collaboration, *Study of multiphoton final states and tests of QED in e^+e^- collisions at $\sqrt{s}$ up to 209 GeV*, Phys. Lett. B **531**, 28 (2002).

[81] F.A. Berends, R. Kleiss, *Distributions for electron-positron annihilation Into two and three photons*, Nucl. Phys. B **186**, 22 (1981).

[82] A.F. Zarnecki, *On the physics potential of ILC and CLIC*, arXiv:hep-ph/2004.14628.

[83] S. Yellin, *$\gamma\gamma$ physics with virtual bremstrahlung*, Int. J. Mod. Phys. A **11**, 1645 (1996).

[84] Kwang-Je Kim, *Gamma gamma collider based on Compton back scattering*, Nucl. Instrum. Meth. A **393**, 530 (1997).

[85] C. Friberg, *$\gamma\gamma$ physics at linear colliders*, arXiv:hep-ph/9911444.

[86] B. Badelek *et al.*, *TESLA Technical Design Report, Part VI, Chapter 1: The Photon Collider at TESLA*, Int. J. Mod. Phys. A **19**, 5097 (2004).

[87] R. Appleby and P. Bambade, *Photon production at the interaction point of the ILC*, arXiv:physics.acc-ph/0803.3519.

[88] H. Burkhardt, *Multi-TeV CLIC photon collider option*, Nucl. Instrum. Meth. A **472**, 67 (2001).

[89] I.F. Ginzburg and G.L. Kotkin, *High energy Photon Collider*, arXiv:hep-ph/1910.13961.

[90] V. I. Telnov, *Principles of photon colliders*, Nucl. Instrum. Meth. A **355**, 3 (1995).

[91] A. Denner, S. Dittmaier, and R. Schuster, *Radiative corrections to $\gamma\gamma \to W^+W^-$ in the electroweak Standard Model*, Nucl. Phys. B **452**, 80 (1995).

[92] E. Yehudai, *Probing W gamma couplings using $\gamma\,\gamma \to W^+\,W^-$*, Phys. Rev. D **44**, 3434 (1991).

[93] F.-X. Dong and X.-J. Zhou, $\gamma\gamma \to \gamma Z$ *scattering and its related processes*, Mod. Phys. Lett. A **15**, 2387 (2000).

[94] D.A. Dicus and C. Kao, *Production of Z boson pairs at photon linear colliders*, Phys. Rev. D **49**, 1265 (1994).

[95] G.V. Jikia, *Z boson pair production in high energy photon-photon collisions and the Higgs signal*, Phys. Lett. B **298**, 224 (1993).

[96] R. Karplus and M. Neuman, *The Scattering of Light by Light*, Phys. Rev. **83**, 776 (1951).

[97] L. Meitner and H. Köters (and M. Delbruck), *Ueber die streuung kurzwelliger γ-strahlen*, Z. Phys. **84**, 137 (1933).

[98] B. De Tollis, *The scattering of photons by photons*, Nuovo Cim. **35**, 1182 (1965).

[99] D. d'Enterria and G. G. Silveira, *Observing Light-by-Light Scattering at the Large Hadron Collider*, Phys. Rev. Lett. **111**, 080405 (2013); Erratum Phys. Rev. Lett. **116**, 129901 (2016).

[100] C. Baldenegro, S. Fichet, G. von Gersdor, and C. Royon, *Probing the anomalous $\gamma\gamma\gamma Z$ coupling at the LHC with proton tagging*, J. High Energ. Phys. **2017**, 142 (2017).

[101] S.C. Inan and A.V. Kisselev, *Probing anomalous $\gamma\gamma\gamma Z$ couplings through γZ production in $\gamma\gamma$ collisions at the CLIC*, J. High Energ. Phys. **2021**, 121 (2021).

[102] S. Fichet *et al.*, *Probing new physics in diphoton production with proton tagging at the Large Hadron Collider*, Phys. Rev. D **89**, 114004 (2014).

[103] S. Fichet *et al.*, *Light-by-light scattering with intact protons at the LHC: from standard model to new physics*, J. High Energ. Phys. **2015**, 165 (2015).

[104] S.C. Inan and A.V. Kisselev, *Probing anomalous quartic $\gamma\gamma\gamma\gamma$ couplings in light-by-light collisions at the CLIC*, Eur. Phys. J. C, **81**, 664 (2021).

[105] M. Köksal, V. Ari, and A. Senol, *Search for Anomalous Quartic $ZZ\gamma\gamma$ Couplings in Photon-Photon Collisions*, Adv. High Energy Phys. **2016**, 8672391 (2016).

[106] E. Gurkanli *et al.*, *Study of the projected sensitivity on the anomalous quartic gauge couplings via $Z\gamma\gamma$ production at the CLIC*, arXiv:hep-ph/2112.03948.

[107] O.J.P.Eboli, M.C. Gonzalez-Garcia, and J.K. Mizukoshi, *$pp \to jje^{\pm}\mu^{\pm}\nu\nu$ and $jje^{\pm}\mu^{\mp}\nu\nu$ at $\mathcal{O}(\alpha_{em}^6)$ and $\mathcal{O}(\alpha_{em}^4\alpha_s^2)$ for the study of the quartic electroweak gauge boson vertexat CERN LHC*, Phys. Rev. D **74**, 073005 (2006).

[108] CMS collaboration, *Measurement of the cross section for electroweak production of a Z boson, a photon and two jets in proton-proton collisions at* $\sqrt{s} = 13\ TeV$ *and constraints on anomalous quartic couplings*, J. High Energ. Phys. **2020**, 76 (2020).

[109] CMS Collaboration, *Evidence for electroweak production of four charged leptons and two jets in proton-proton collisions at* $\sqrt{s} = 13\ TeV$, Phys. Lett. B **812**, 135992 (2021).

[110] CMS Collaboration, *Measurements of the* $pp \to W^{\pm}\gamma\gamma$ *and* $pp \to Z\gamma\gamma$ *cross sections at* $\sqrt{s} = 13\ TeV$ *and limits on anomalous quartic gauge couplings*, J. High Energ. Phys. **2021**, 174 (2021).

[111] CMS Collaboration, *Measurement of the electroweak production of* $Z\gamma$ *and two jets in proton-proton collisions at* $\sqrt{s} = 13\ TeV$ *and constraints on anomalous quartic gauge couplings*, Phys. Rev. D **104**, 072001 (2021).

[112] The CMS and TOTEM Collaborations, *First search for exclusive diphoton production at high mass with tagged protons in proton-proton collisions at* $\sqrt{s} = 13\ TeV$, Phys. Rev. Lett. **129**, 011801 (2022).

[113] J. Ellis, S. Ge, and K. Ma, *Hadron Collider Probes of the Quartic Couplings of Gluons to the Photon and Z Bosons*, J. High Energ. Phys. **2022**, 123 (2022).

[114] A. Tonomura *et al.*, *Motion of vortices in superconductors*, Nature **397**, 308 (1999).

[115] G. Bewley, D. Lathrop, and K. Sreenivasan, *Visualization of quantized vortices*, Nature **441**, 588 (2006).

[116] C. Weiler *el al.*, *Spontaneous vortices in the formation of Bose–Einstein condensates*, Nature **455**, 948 (2008).

[117] S. Autti *et al.*, *Observation of Half-Quantum Vortices in Topological Superfluid* He^3, Phys. Rev. Lett. **117**, 255301 (2016).

[118] G. Gauthier *et al.*, *Giant vortex clusters in a two-dimensional quantum fluid*, Science **364**, 1264 (2019).

[119] V. Gladilin and M. Wouters, *Vortices in Nonequilibrium Photon Condensates*, Phys. Rev. Lett. **125**, 215301 (2020).

[120] E. Babaev, *Vortices with fractional flux in two-gap superconductors and in extended Faddeev model*, Phys. Rev. Lett. **89**, 067001 (2002).

[121] M. Shifman, *Advanced topics in quantum field theory: A lecture course*, Cambridge University Press (2012).

[122] A. A. Abrikosov, *On the Magnetic properties of superconductors of the second group*, Sov. Phys. JETP **5**, 1174 (1957).

[123] H. B. Nielsen and P. Olesen, *Vortex-line models for dual strings*, Nucl. Phys. B **61** 45 (1973).

[124] H. J. de Vega and F. A. Schaposnik, *Classical vortex solution of the Abelian Higgs model*, Phys. Rev. D **14**, 110 (1976).

[125] S. Deser, R. Jackiw, and S. Templeton, *Three-Dimensional Massive Gauge Theories*, Phys. Rev. Lett. **48**, 975 (1982).

[126] S. Deser, R. Jackiw, and S. Templeton, *Topologically Massive Gauge Theories*, Ann. Phys. **140**, 372 (1982); Ann. Phys. **281**, 409 (2000).

[127] S.-S. Chern and J. Simons, *Characteristic Forms and Geometric Invariants*, Ann. Math. **99**, 48 (1974).

[128] J. F. Schonfeld, *A mass term for three-dimensional gauge fields*, Nucl. Phys. B **185**, 157 (1981).

[129] R. Jackiw and S. Templeton, *How super-renormalizable interactions cure their infrared divergences*, Phys. Rev. D **23**, 2291 (1981).

[130] C. R. Hagen, *A New Gauge Theory without an Elementary Photon*, Ann. Phys. **157**, 342 (1984).

[131] C. R. Hagen, *What is the most general Abelian gauge theory in two spatial dimensions?*, Phys. Rev. Lett. **58**, 1074 (1987); Erratum Phys. Rev. Lett. **58**, 2003 (1987).

[132] E. Witten, *Quantum field theory and the Jones polynomial*, Comm. Math. Phys. **121**, 351 (1989).

[133] G. V. Dunne, *Aspects of Chern-Simons theory*, arXiv:9902115.

[134] P. Horváthy and P. Zhang, *Vortices in (Abelian) Chern-Simons gauge theory*, Phys. Rept. **481**, 83 (2009).

[135] S. K. Paul and A. Khare, *Charged Vortices in Abelian Higgs Model with Chern-Simons Term*, Phys. Lett. B **174**, 420 (1986).

[136] H. J. de Vega and F. A. Schaposnik, *Electrically Charged Vortices in Non-Abelian Gauge Theories with Chern-Simons Term*, Phys. Rev. Lett. **56**, 2564 (1986).

[137] H. J. de Vega and F. A. Schaposnik, *Vortices and electrically charged vortices in non-Abelian gauge theories*, Phys. Rev. D **34**, 3206 (1986).

[138] C. N. Kumar and A. Khare , *Charged vortex of finite energy in nonabelian gauge theories with Chern-Simons term*, Phys. Lett. B **178**, 395 (1986).

[139] R. D. Pisarski and S. Rao, *Topologically massive chromodynamics in the perturbative regime*, Phys. Rev. D **32**, 2081 (1985).

[140] J. Fröhlich and P.A. Marchetti, *Quantum field theories of vortices and anyons*, Commun. Math. Phys. **121**, 177 (1989).

[141] R. B. Laughlin, *Quantized motion of three two-dimensional electrons in a strong magnetic field*, Phys. Rev. B **27**, 3383 (1983).

[142] Y. H. Chen, F. Wilczek, E. Witten, and B. I. Halperin, *On anyon superconductivity*, Int. J. Mod. Phys. B **3**, 1001 (1989).

[143] G. E. Volovik and V. M. Yakovenko, *Fractional charge, spin and statistics of solitons in superfluid He^3 film*, J. Phys.: Condens. Matter **1**, 5263 (1989).

[144] D. P. Jatkar and A. Khare, *Peculiar charged vortices in Higgs models with pure Chern-Simons term*, Phys. Lett B **236**, 283 (1990).

[145] D. Boyanovsky, *Vortices in Landau-Ginzburg theories of anyonic superconductivity*, Nucl. Phys. B **350**, 906 (1991).

[146] J. Hong, Y. Kim, and P. Y. Pac, *Multivortex solutions of the Abelian Chern-Simons-Higgs theory*, Phys. Rev. Lett. **64**, 2230 (1990).

[147] R. Jackiw and E. Weinberg, *Self-dual Chern-Simons vortices*, Phys. Rev. Lett. **64**, 2234 (1990).

[148] E. B. Bogomolny, *Stability of Classical Solutions* , Sov. J. Nucl. Phys. **24**, 449 (1976).

[149] R. Jackiw, K. Lee and E. Weinberg, *Self-dual Chern-Simons solitons*, Phys. Rev. D **42**, 3488 (1990).

[150] E. Witten and D. Olive, *Supersymmetry algebras that include topological charges*, Phys. Lett. B **78**, 97 (1978).

[151] P. Di Vecchia and S. Ferrara, *Classical solutions in two-dimensional supersymmetric field theories*, Nucl. Phys. B **130**, 93 (1977).

[152] Z. Hlousek and D. Spector, *Why topological charges imply extended supersymmetry*, Nucl. Phys. B **370**, 143 (1992).

[153] Z. Hlousek and D. Spector, *Bogomol'nyi explained*, Nucl. Phys. B **397**, 173 (1993).

[154] C. Lee, K. Lee, and E. Weinberg, *Supersymmetry and self-dual Chern-Simons systems*, Phys. Lett. B **243**, 105 (1990).

[155] C. Lee, K. Lee, and H. Min, *Supersymmetric Chern-Simons vortex systems and fermion zero modes*, Phys. Rev. D **45**, 4588 (1992).

[156] J. Edelstein, C. Núnez, and F. Schaposnik, *Supersymmetry and Bogomol'nyi equations in the Abelian Higgs model*, Phys. Lett. B **329**, 39 (1994).

[157] H. R. Christiansen, M. S. Cunha, J. A. Helayël-Neto, L. R. U. Manssur, and A. L. M. A. Nogueira, *Selfdual vortices in a Maxwell-Chern-Simons model with nonminimal coupling*, Int. J. Mod. Phys. A **14**, 1721 (1999).

[158] C. Lee, K. Lee, and H. Min, *Self-dual Maxwell Chern-Simons solitons*, Phys. Lett. B **252**, 79 (1990).

[159] G. V. Dunne, *Selfdual Chern-Simons theories*, Lect. Notes Phys. M **36**, 1 (1995).

[160] R. Jackiw and S-Y. Pi, *Soliton Solutions to the Gauged Nonlinear Schrödinger Equation on the Plane*, Phys. Rev. Lett. **64**, 2969 (1990).

[161] R. Jackiw and S-Y. Pi, *Classical and quantal nonrelativistic Chern-Simons theory*, Phys. Rev. D **42**, 3500 (1990), (E) **48**, 3929 (1993).

[162] N. Manton, *First Order Vortex Dynamics*, Ann. Phys. **256**, 114 (1997).

[163] M. Hassaïne, P. Horváthy, and J. Yera, *Non-relativistic Maxwell-Chern-Simons Vortices*, Ann. Phys. **263**, 276 (1998).

[164] C. R. Hagen, *Parity conservation in Chern-Simons theories and the anyon interpretation*, Phys. Rev. Lett. **68**, 3821 (1992).

[165] F. Wilczek, *Disassembling Anyons*, Phys. Rev. Lett. **69**, 132 (1992).

[166] O. M. Del Cima and E. S. Miranda, *Electron-polaron–electron-polaron bound states in mass-gap graphene-like planar quantum electrodynamics: s-wave bipolarons*, Eur. Phys. J. B **91**, 212 (2018).

[167] E. V. Gorbar and S. V. Mashkevich, *Statistical screening in a P-, T-invariant model*, Z. Phys. C - Particles and Fields **65**, 705 (1995).

[168] W. B. De Lima, O. M. Del Cima, and E. S. Miranda, *On the electron–polaron–electron–polaron scattering and Landau levels in pristine graphene-like quantum electrodynamics*, Eur. Phys. J. B **93**, 187 (2020).

[169] O. M. Del Cima, D. H. T. Franco, L. S. Lima, and E. S. Miranda, *Quantum Parity Conservation in Planar Quantum Electrodynamics*, Int. J. Theor. Phys. **60**, 3063 (2021).

[170] W. B. De Lima, O. M. Del Cima, and E. S. Miranda, *On the ultraviolet finiteness of parity-preserving $U(1) \times U(1)$ massive QED_3*, Ann. Phys. **430**, 168504 (2021).

[171] C. Kim, C. Lee, P. Ko, B.-H. Lee, and H. Min, *Schrodinger fields on the plane with $[U(1)]^N$ Chern-Simons interactions and generalized selfdual solitons*, Phys. Rev. D **48**, 1821 (1993).

[172] J. Diziarmaga, *Low-energy dynamics of $[U(1)]^N$ Chern-Simons solitons*, Phys. Rev. D **49**, 5469 (1994).

[173] J. Shin, S. Hyun, and J. Yee, *Mutual fractional statistics of relativistic Chern-Simons solitons*, Phys. Rev. D **52**, 2591 (1995).

[174] J. Diziarmaga, *Only hybrid anyons can exist in broken symmetry phase of nonrelativistic $[U(1)]^2$ Chern-Simons theory*, Phys. Rev. D **50**, R2376(R) (1994).

[175] J. Shin and J. Yee, *Vortex solutions of parity invariant Chern-Simons gauge theory coupled to fermions*, Phys. Rev. D **50**, 4223 (1994).

[176] R. F. Keifl *et al.*, *Search for anomalous internal magnetic fields in high-T_c superconductors as evidence for broken time-reversal symmetry*, Phys. Rev. Lett. **64**, 2082 (1990).

[177] S. Spielman *et al.*, *Test for nonreciprocal circular birefringence in $YBa_2Cu_3O_7$ thin films as evidence for broken time-reversal symmetry*, Phys. Rev. Lett. **65**, 123 (1990).

[178] K. Lyons *et al.*, *Search for circular dichroism in high-T_c superconductors*, Phys. Rev. Lett. **64**, 2949 (1990).

[179] G. W. Semenoff and N. Weiss, *3D field theory model of a parity invariant anyonic superconductor*, Phys. Lett. B **250**, 117 (1990).

[180] N. Dorey and N. E. Mavromatos, *Superconductivity in 2+1 dimensions without parity or time-reversal violation*, Phys. Lett. B **250**, 107 (1990).

[181] A. Kovner and B. Rosenstein, *Kosterlitz-Thouless mechanism of two-dimensional superconductivity*, Phys. Rev. B **42**, 4748 (1990).

[182] N. Dorey and N. E. Mavromatos, *QED3 and two-dimensional superconductivity without parity violation*, Nucl. Phys. B **386**, 614 (1992).

[183] C.-S. Lin and J. Prajapat, *Vortex Condensates for Relativistic Abelian Chern-Simons Model with Two Higgs Scalar Fields and Two Gauge Fields on a Torus*, Commun. Math. Phys. **288**, 311 (2009).

[184] H.-Y. Huang, Y. Lee, and C.-S. Lin, *Uniqueness of topological multi-vortex solutions for a skew-symmetric Chern-Simons system*, J. Math. Phys. **56**, 041501 (2015).

[185] B. Guo and F. Li, *Doubly periodic vortices for a Chern–Simons model*, J. Math. Anal. Appl. **458**, 889 (2018).

[186] S.-P. Kou, X.-L. Qi, and Z.-Y. Weng, *Mutual Chern-Simons effective theory of doped antiferromagnets*, Phys. Rev. B **71**, 235102 (2005).

[187] S.-P. Kou, M. Levin, and X.-G. Wen, *Mutual Chern-Simons theory for Z_2 topological order*, Phys. Rev. B **78**, 155134 (2008).

[188] S.-P. Kou, X.-L. Qi, and Z.-Y. Weng, *Spin Hall effect in a doped Mott insulator*, Phys. Rev. B **72**, 165114 (2005).

[189] S.-P. Kou, J. Yu, and X.-G. Wen, *Mutual Chern-Simons Landau-Ginzburg theory for continuous quantum phase transition of Z_2 topological order*, Phys. Rev. B **80**, 125101 (2009).

[190] X.-L. Qi and Z.-Y. Weng, *Mutual Chern-Simons gauge theory of spontaneous vortex phase*, Phys. Rev. B **76**, 104502 (2007).

[191] P. Ye, L. Zhang, and Z.-Y. Weng, *Superconductivity in mutual Chern-Simons gauge theory*, Phys. Rev. B **85**, 205142 (2012).

[192] M. C. Diamantini, P. Sodano, and C. A. Trugenberger, *Self-duality and oblique confinement in planar gauge theories*, Nucl. Phys. B **448**, 505 (1995).

[193] M. C. Diamantini, P. Sodano, and C. A. Trugenberger, *Gauge theories of Josephson junction arrays*, Nucl. Phys. B **474**, 641 (1996).

[194] M. C. Diamantini, P. Sodano, and C. A. Trugenberger, *Superconductors with topological order*, Eur. Phys. J. B **53**, 19 (2006).

[195] S. Sakhi, *Tricritical behavior in the Chern-Simons-Ginzburg-Landau theory of self-dual Josephson junction arrays*, Phys. Rev. D **97**, 096015 (2018).

[196] M. M. Anber, Y. Burnier, E. Sabancilar, and M. Shaposhnikov, *Confined vortices in topologically massive $U(1) \times U(1)$ theory*, Phys. Rev. D **92**, 065013 (2015).

[197] S. R. Coleman and B. R. Hill, *No more corrections to the topological mass term in QED_3*, Phys. Lett. B **159**, 184 (1985).

[198] A.A. Penin and Q. Weller, *What Becomes of Giant Vortices in the Abelian Higgs Model*, Phys. Rev. Lett. **125** 251601 (2020).

[199] A. A. Penin and Q. Weller, *A theory of giant vortices*, J. High Energ. Phys. **2021**, 56 (2021).

[200] P. L. Marston and W. M. Fairbank, *Evidence of a Large Superfluid Vortex in He^4*, Phys. Rev. Lett. **39**, 1208 (1977).

[201] P. Engels *et al.*, *Observation of Long-Lived Vortex Aggregates in Rapidly Rotating Bose-Einstein Condensates*, Phys. Rev. Lett. **90**, 170405 (2003).

[202] T. Cren *et al.*, *Vortex Fusion and Giant Vortex States in Confined Superconducting Condensates*, Phys. Rev. Lett. **107**, 097202 (2011).

[203] Cristine N. Ferreira, J. A. Helayël-Neto, Álvaro L. M. A. Nogueira, and A. A. V. Paredes, *Vortex Formation in a $U(1) \times U(1)' - \mathcal{N} = 2 - D = 3$ Supersymmetric Gauge Model*, PoS **ICMP2013**, 011 (2013).

[204] A. Edery, *Non-singular vortices with positive mass in 2+1-dimensional Einstein gravity with AdS_3 and Minkowski background*, J. High Energ. Phys. **2021**, 166 (2021).

[205] J. Albert, *The Abrikosov vortex in curved space*, J. High Energ. Phys. **2021**, 12 (2021).

[206] P. Arias, A. Arza, F. A. Schaposnik, D. Vargas-Arancibia, and M. Venegas, *Vortex solutions in the presence of Dark Portals*, Int. J. Mod. Phys. A **37**, 2250087 (2022).

[207] A. Rapoport and F. A. Schaposnik, *A d=3 dimensional model with two U(1) gauge fields coupled via matter fields and BF interaction*, Phys. Lett. B **806**, 135472 (2020).

[208] G. S. Lozano and F. A. Schaposnik, *Vortices in fracton type gauge theories*, Phys. Lett. B **811**, 135978 (2020).

[209] D. Bazeia, M. A. Liao, and M. A. Marques, *Generalized Maxwell-Higgs vortices in models with enhanced symmetry*, Eur. Phys. J. C **82**, 316 (2022).

[210] I. Andrade, D. Bazeia, M.A. Marques, and R. Menezes, *Long range vortex configurations in generalized models with the Maxwell or Chern-Simons dynamics*, Phys. Rev. D **102**, 025017 (2020).

[211] D. Bazeia, M. A. Liao, M. A. Marques, and R. Menezes, *Multilayered vortices*, Phys. Rev. Research **1**, 033053 (2019).

[212] B. Binegar, *Relativistic field theories in three dimensions*, J. Math. Phys. **23**, 1511 (1982).

[213] V. I. Inozemtsev, *On Charged Vortices in the (2 + 1)-Dimensional Abelian Higgs Model*, EPL **5**, 113 (1988).

[214] G. Lozano, M. V. Manias, and F. A. Schaposnik, *Charged-vortex solution to spontaneously broken gauge theories with Chern-Simons term*, Phys. Rev. D **38**, 601 (1988).

[215] L. Jacobs, A. Khare, C. N. Kumar, and S. K. Paul, *The interaction of Chern-Simons vortices*, Int. J. Mod. Phys. A **6**, 3441 (1991).

[216] N. Cabibbo and E. Ferrari, *Quantum electrodynamics with Dirac monopoles*, Nuovo Cim. **23**, 1147 (1962).

[217] C. R. Hagen, *Noncovariance of the Dirac Monopole*, Phys. Rev. **140**, B804 (1965).

[218] A. Salam, *Magnetic monopole and two photon theories of C violation*, Phys. Lett. **23**, 683 (1966).

[219] S. Kanasugi and Y. Yanase, *Anapole superconductivity from $\mathcal{PT}$-symmetric mixed-parity interband pairing*, Commun Phys **5**, 39 (2022).

[220] S. K. Ghosh *et al.*, *Time-reversal symmetry breaking superconductivity in three-dimensional Dirac semimetallic silicides*, Phys. Rev. Research **4**, L012031 (2022).

[221] S. K. Ghosh *et al.*, *Recent progress on superconductors with time-reversal symmetry breaking*, J. Phys.: Condens. Matter **33**, 033001 (2021).

[222] E. M. C. Abreu *et al.*, *A supersymmetric model for graphene*, J. High Energ. Phys. **2011**, 1 (2011).

[223] M. Ezawa, *Supersymmetric structure of quantum Hall effects in graphene*, Phys. Lett. A **372**, 924 (2008).

[224] C. A. Dartora and G. G. Cabrera, *Wess–Zumino supersymmetric phase and superconductivity in graphene*, Phys. Lett. A **377**, 907 (2013).

[225] S.-S. Lee, *Emergence of supersymmetry at a critical point of a lattice model*, Phys. Rev. B **76**, 075103 (2007).

[226] T. Grover, D. N. Sheng, and A. Vishwanath, *Emergent Space-Time Supersymmetry at the Boundary of a Topological Phase*, Science **344**, 280 (2014).

[227] S.-K. Jian, Y.-F. Jiang, and H. Yao, *Emergent Spacetime Supersymmetry in 3D Weyl Semimetals and 2D Dirac Semimetals*, Phys. Rev. Lett. **114**, 237001 (2015).

[228] P. Ponte and S.-S. Lee, *Emergence of supersymmetry on the surface of three-dimensional topological insulators*, New J. Phys. **16**, 013044 (2014).